UNIVERSITY OF MICHIGAN
NOV 11 1953
ENGINEERING LIBRARY

JOURNAL OF THE AERONAUTICAL SCIENCES

VOLUME 20 NOVEMBER, 1953 NUMBER 11

CONTENTS

Interactions Between Wholly Laminar or Wholly Turbulent Boundary Layers and Shock Waves Strong Enough to Cause Separation.....G. E. GADD 729

Some Basic Concepts for Analyzing Dynamic Flight-Test Data.....H. KLEIN AND R. SEDNEY 740

A Simplified Method to Obtain the Load Distribution Corresponding to the Ackeret Region for Wings Having Arbitrary Source Distribution at Supersonic Speeds.....JULIAN H. KAINER 749

Airflow About Cone-Cylinders with Curved Shock Waves.....V. E. BERGDOLT 751

Two-Dimensional Unsymmetric Flow Patterns at Mach Number 1.....GOTTFRIED GUDERLEY AND HIDEO YOSHIHARA 757

Similarity Theory of Isotropic Turbulence.....J. C. ROTTA 769

Ludwig Prandtl, 1875–1953—Necrology..... 779

Readers' Forum: "On Laminar Boundary Layer over a Rotating Blade," by H. S. Tan; "On the Evaluation of the Function $f_\lambda(M, \bar{\omega})$," by G. Zartarian and H. M. Voss; "Spanwise and Chordwise Loadings for Rectangular Wings of Aspect Ratio near Unity," by William R. Laidlaw; "A Note on Poisson's Ratio," by Morris Feigen; "Two-Dimensional Correction of the Outlet Angle in Cascade Flow," by N. Scholz; "Mean Skin-Friction Coefficients for Biconvex Airfoils in Supersonic Flow," by J. Christopher Boison; "On Theories of Plasticity and the Plastic Stability of Cruciform Sections," by P. P. Bijlaard and H. A. B. Wiseman; "Note on the Prandtl Number for Dissociated Air," by C. Frederick Hansen; "A Double-Diaphragm Shock Tube to Produce Transient High Mach Number Flows," by Harry Bernstein; "A Note on the Contribution of Higher Mode Resonance to Bending in the Teetering Rotor Blade," by R. M. Carison and D. R. Jacoby; "Differentiation of Experimental Data by Means of Higher Order Finite-Difference Formulas," by Chi-Teh Wang and Daniel F. DeSanto; "Note on Model Effective Span for Wind-Tunnel Wall Corrections," by Alan Pope; "Hypersonic Viscous Flow over an Inclined Wedge," by Lester Lees; "On Strong Interaction for the Hypersonic Boundary Layer on an Inclined Wedge," by Shih-I Pai; "Effect of a Turbojet Engine on the Dynamic Stability of an Aircraft," by Hans C. Vetter; "Note on Nonstationary Slender-Body Theory," by J. D. Cole; "Remarks on 'Shock-Wave Effects on the Laminar Skin Friction of an Insulated Flat Plate at Hypersonic Speeds,'" by M. Z. v. Krzywoblocki.....780–800

Published by
INSTITUTE OF THE AERONAUTICAL SCIENCES, INC.

JOURNAL OF THE AERONAUTICAL SCIENCES

Editor: HUGH L. DRYDEN, *Director, NACA*

Associate Editor: ROBERT R. DEXTER *Managing Editor:* BERNEICE H. JARCK

Editorial Committee

Aerodynamics

Francis Clauser
Howard Emmons
Antonio Ferri
Alexander Flax
R. Paul Harrington
R. T. Jones
Carl Kaplan
H. W. Liepmann
C. C. Lin
H. F. Ludloff
Harold Luskin
John R. Markham
Clark B. Millikan
Shatswell Ober
W. Bailey Oswald
Allen E. Puckett
Elliott G. Reid
H. J. E. Reid
Russell Robinson
G. B. Schubauer
W. R. Sears
John Stack
Theodore von Kármán

Air Transport

Charles Froesch
J. A. Herlihy
R. D. Kelly
Otto E. Kirchner
Jerome Lederer
John C. Leslie
R. Dixon Speas

Flight Testing

W. K. Ebel
R. R. Gilruth
Melvin N. Gough
E. G. Stout

Structures and Materials

W. B. Bleakney
E. W. Conlon
L. H. Donnell
E. C. Hartmann
N. J. Hoff
Samuel Levy
E. E. Lundquist
Alfred S. Niles
W. Ramberg
F. R. Shanley
H. W. Sibert
C. R. Strang
S. Timoshenko
H. S. Tsien
Chi-Teh Wang

Rotating Wing Aircraft

F. B. Gustafson
K. H. Hohenemser
Bartram Kelley
R. B. Maloy
Ralph McClarren
R. H. Miller
R. H. Prewitt
Igor I. Sikorsky

Vibration and Flutter

Lee Arnold
M. A. Biot
R. L. Bisplinghoff
William Bollay
Chieh-Chien Chang
I. E. Garrick
Martin Goland
J. P. Den Hartog

Aircraft Design

W. E. Beall
W. K. Ebel
Hall L. Hibbard
Richard Hutton
C. L. Johnson
A. A. Kartveli
C. J. McCarthy
Fred E. Weick
Robert J. Woods

Electronics in Aviation

K. C. Black
E. F. Herzog
David S. Little
D. K. Martin
George Rappaport
Paul Rosenberg
L. M. Sherer

Physiologic Problems

H. G. Armstrong
Louis H. Bauer
Robert J. Benford
Eugene Du Bois
W. Randolph Lovelace, II
Ross A. MacFarland

Fuels and Oils

D. P. Barnard
J. H. Doolittle
Graham Edgar
R. T. Goodwin
S. D. Heron
A. M. Rothrock

Flight Propulsion

George W. Brady
Frank W. Caldwell
L. S. Hobbs
E. E. Johnson
Joseph Keenan
R. P. Kroon
Hans Reissner
Abe Silverstein
C. Fayette Taylor
E. S. Taylor
P. Taylor
E. S. Thompson
H. S. Tsien

Instruments

Allan G. Binnie
J. R. Bradburn
Charles H. Colvin
C. S. Draper
S. G. Eskin
O. E. Esval
H. W. Holzapfel
W. L. Howland
George H. Purcell
C. F. Savage
O. Hugo Schuck
C. L. Seward, Jr.
L. D. Statham
R. C. Sylvander
D. K. Warner

Meteorology

C. F. Brooks
D. M. Little
E. J. Minser
F. W. Reichelderfer
H. C. Willett

SUBSCRIPTION RATES

JOURNAL OF THE AERONAUTICAL SCIENCES, Published Monthly.—United States and Possessions: 1 Year, $12.00; Single Copies, $1.50. Foreign Countries Including Canada (American Currency Rates): 1 Year, $13.00; Single Copies, $1.50.

AERONAUTICAL ENGINEERING REVIEW, Published Monthly.—United States and Possessions: 1 Year, $3.00; Single Copies, $0.50. Foreign Countries Including Canada (American Currency Rates): 1 Year, $3.50; Single Copies, $0.50.

Notices of change of address should be sent to the Institute at least 30 days prior to actual change of address.

Manuscripts for publication, proofs, and all correspondence should be addressed to the Editorial Office of the JOURNAL.

Correspondence regarding subscriptions may be addressed to Publication Office, 20th and Northampton Sts., Easton, Pa., or to the Editorial Office of the JOURNAL OF THE AERONAUTICAL SCIENCES, 2 East 64th Street, New York 21, New York.

Copyright, 1953, by the Institute of the Aeronautical Sciences, Inc.

Entered as Second Class Matter at the Post Office, Easton, Pa., May 1, 1937. Acceptance for mailing at a special rate of Postage provided for in the Act of August 24, 1912. Authorized April 29, 1937.

JOURNAL OF THE AERONAUTICAL SCIENCES

VOLUME 20 NOVEMBER, 1953 NUMBER 11

Interactions Between Wholly Laminar or Wholly Turbulent Boundary Layers and Shock Waves Strong Enough to Cause Separation*

G. E. GADD†

National Physical Laboratory, Teddington, England

SUMMARY

A qualitative discussion is presented covering both wholly laminar and wholly turbulent cases (i.e., where transition occurs upstream of the region of interaction). Relations are obtained for the pressures at separation with laminar and turbulent boundary layers. Semiempirical relations permitting the rapid calculation of the overall characteristics of turbulent interactions are also obtained.

LIST OF SYMBOLS

x = distance from leading edge measured parallel to wall
y = distance from wall measured normal to wall
u = mean x-component velocity in boundary layer
U = x-component velocity at edge of boundary layer
u' = fluctuating x-component velocity
v = mean y-component velocity
v' = fluctuating y-component velocity
p = mean pressure
ρ = mean density
ρ_1 = density at edge of boundary layer
ρ' = fluctuating density
μ = viscosity
μ_1 = viscosity at edge of boundary layer
γ = ratio of specific heat at constant pressure to specific heat at constant volume: assumed to equal 1.4
ω = viscosity temperature relation index ($\mu \alpha T^{\omega}$, where T is absolute temperature)
σ = Prandtl Number ($\mu c_p/k$, where c_p is specific heat at constant pressure and k is thermal conductivity)
M = Mach Number at edge of boundary layer
R_x = Reynolds Number, $\rho_{10} U_0 x/\mu_{10}$
δ = boundary-layer total thickness
δ_z = δ for zero pressure gradient laminar boundary layer
δ^* = displacement thickness $\int_0^{\delta} \left(1 - \frac{\rho u}{\rho_1 U}\right) dy$
δ_z^* = δ^* for zero pressure gradient laminar boundary layer
θ = momentum thickness $\int_0^{\delta} \frac{\rho u}{\rho_1 U} \left(1 - \frac{u}{U}\right) dy$
λ = parameter in assumed velocity profile for laminar boundary layer [see Eqs. (4)]
n = as λ
τ = friction stress
ψ = angle between edge of boundary layer and local mean flow stream lines

The suffices F, 0, R, s refer to the positions F, 0, R, s of Figs. 2 and 3 [see Section (2)].

(1) INTRODUCTION

THIS PAPER IS CONCERNED WITH the two-dimensional interaction between the boundary layer on a flat plate and an incident oblique shock wave strong enough to cause separation. The configuration envisaged is as in Fig. 1, and it is assumed that the boundary layer is either wholly laminar or wholly turbulent—i.e., that transition does not occur in the region of interaction.

Wholly laminar cases are physically similar to wholly turbulent ones, and in Section (2) a qualitative interpretation for both conditions is presented.

In Section (3) a relation is obtained for the pressure at the separation point with laminar boundary layers.

Received June 26, 1953.

* The work described above was carried out in the Aerodynamics Division of the National Physical Laboratory, and it is published on the recommendation of the Aeronautical Research Council and by permission of the Director of the Laboratory. The author desires to acknowledge the comments and suggestions he received from Dr. D. W. Holder.

† Scientific Officer.

FIGS. 1-3.

FIG. 1.

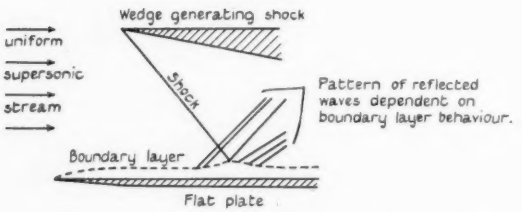

The general configuration of the interactions discussed.

FIG. 2.

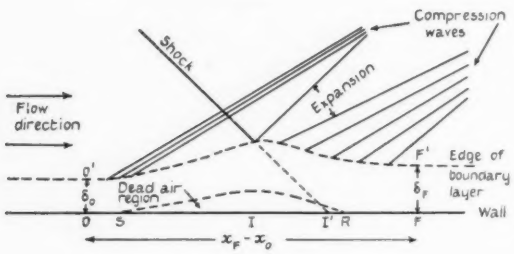

Details of the flow in the region of interaction

FIG. 3.

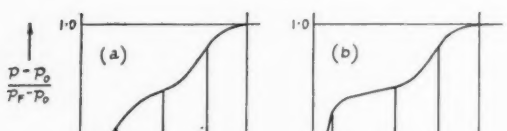

Shapes of pressure distribution at the wall typical with (a) laminar (b) turbulent boundary layers.

By a similar but much cruder method, an expression for the pressure at separation in wholly turbulent cases is derived in Section (4). Semiempirical relations are also obtained permitting the rapid calculation of the overall effects produced in a turbulent boundary layer when the shock is strong enough to cause a large extent of separated flow. Similar relations could have been obtained in Section (3) for wholly laminar cases with separation, but this was not considered worth while, since the obtaining of such cases experimentally is fairly difficult so that they are in a sense more academic. Moreover, semiempirical methods can only make a limited contribution to the theoretical understanding of any problem, so that their application to laminar cases, for which an adequate theoretical treatment may well be feasible, seems less justifiable than applying them to turbulent cases, where some admixture of empiricism is probably almost inevitable.

The method of Section (4) for turbulent boundary layers do not explicitly deal with all the relevant factors. Thus, while it is shown in the qualitative discussion of Section (2) that the turning of the flow toward the wall which occurs in the immediate vicinity of the shock is an important factor, the methods of Section (4) take no explicit account of it. They account for it implicitly in an empirical constant. Such a procedure is possible because interactions between turbulent boundary layers on flat plates and incident oblique shock waves represent a fairly restricted class of conditions even with varying shock strength and Mach Numbers.

(2) Qualitative Discussion

The following discussion is in part based on the analysis of Section (3) below and also partly on reference 1. It is consistent with the experimental results of reference 2 but not entirely so with those of reference 3.†

When a sufficiently strong oblique shock wave is incident upon the boundary layer on a flat plate, as in Fig. 2, it causes both the pressure to increase and the boundary layer to thicken and separate upstream of it. The thickening of the boundary layer generates a band of compression waves that determine the pressure distribution acting on the boundary layer upstream of the shock, and this pressure distribution in turn governs the rate of thickening of the boundary layer. The two processes must adjust themselves to be in equilibrium, so that the pressure distribution upstream of a point I_1 where a shock impinges on a boundary layer would presumably remain unaltered if the shock were increased in strength and simultaneously moved downstream to some point I_2 such that the separation point did not move. Hence, the ratio of the pressure at separation to the undisturbed free stream pressure should be a function of Mach Number and Reynolds Number only, independent of shock strength.

The shock is reflected locally where it strikes the boundary layer as an expansion just as it would be if it impinged on a constant pressure boundary. This is because without the expansion there would be a discontinuous jump in pressure which the separated boundary layer could not withstand. The flow at the edge of the boundary is turned in toward the wall by the shock-expansion system, downstream of which accordingly there is a further pressure rise as the flow turns back approximately parallel to the wall.

† When comparing these two sets of experimental results, one should bear in mind the fact that the boundary layer thickness as defined in reference 3 is not the same as the thickness of the boundary layer as it appears in a schlieren photograph. The latter thickness is probably roughly the same as the thickness of the zone in which the friction tangential stresses on surfaces normal to the local isobars are appreciable, and it is this zone which is defined as the boundary layer in the present paper. The edge of the boundary layer so defined is almost coincident with the local mean flow stream lines.

The pressure distribution at the wall is as in Fig. 3. There is a relatively steep (for turbulent boundary layers very steep) initial rise of pressure up to the separation position s. Downstream of s for some distance there is a "dead air" region next to the wall.† Where this dead air region is thin, it can sustain an appreciable adverse pressure gradient largely because of the friction forces acting on it. Where the dead air region is thick, however, the rate of change of friction stress normal to the wall must become small in the dead air region, and the boundary layer will be unable to withstand a large adverse pressure gradient. Now the dead air region increases rapidly in thickness downstream of s because the edge of the boundary layer is deflected away from the wall at a considerable angle. Accordingly, the pressure gradient soon falls off downstream of s. At I, the point where the incident shock strikes the boundary layer and is reflected locally as an expansion, the external flow is turned in toward the wall, and the dead air region begins to reduce in thickness and to become capable of sustaining a larger adverse pressure gradient. Hence, the pressure gradient again begins to rise until the reattachment point R is reached.

In the case of turbulent boundary layers, mass acceleration effects may play a significant part in the equilibrium of the so-called dead air region. Where the dead air region is reducing in thickness, as near reattachment, the mass acceleration forces will balance part of the pressure gradient forces, all of which accordingly will not have to be met by the friction forces. On the other hand, where the dead air region is increasing in thickness, the mass acceleration effects will be such that friction will have to meet more than the pressure gradient forces. This may explain why, with turbulent boundary layers, the pressure increase between the shock and reattachment is much greater than that between separation and the shock, whereas there is much less difference with laminar layers where mass acceleration effects in the dead air region are probably less important.

Downstream of the reattachment point R the boundary-layer profile begins to approach the zero pressure gradient form, and the pressure gradient once more falls off. The pressure asymptotes to the peak pressure p_F, which is reached shortly downstream of R at F. The ratio of this peak pressure to the original free-stream pressure is approximately the same as if there were no boundary layer present, when the incident shock would simply be reflected as another single shock as in Fig. 4, a pattern known as "regular reflection."

† The dead air region is defined as being of thickness $t(x)$, where

$$\int_0^t \rho u \, dy = 0$$

The velocities in the dead air region, though not large, are not zero, since there is reversed flow near to the wall and forward flow further out.

FIGS 4-7.

FIG. 4

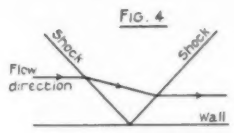

Regular reflection.

FIG 5

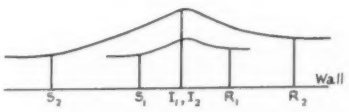

The edge of the boundary layer with shocks 1 and 2 where shock 2 is stronger than shock 1.

FIG 6

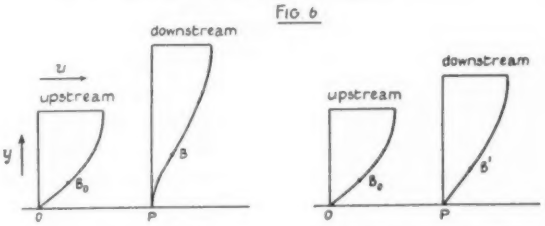

(a) With pressure rise (b) At constant pressure

Velocity profiles with laminar boundary layers

FIG 7

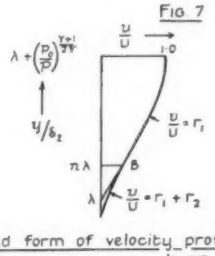

Assumed form of velocity profile for laminar boundary layer.

With the help of shock tables it is easy to calculate the regular reflection pressure rise. This is approximately equal to the actual pressure rise because the waves reflected from the boundary layer must have the overall effect of turning the external flow deflected through the incident shock back approximately parallel to the wall, just as the single reflected shock does when there is no boundary layer present, and though the change of entropy in the external flow is slightly different in the two systems, this makes little difference to the pressures reached.

The fact that an increase of shock strength moves the separation point upstream may be interpreted physically as follows: At I, the position where the shock strikes the edge of the boundary layer (see Figs. 2 and 3), the pressure is little affected by the distance of the separation point s upstream of I, provided sI is not too small, because the pressure gradient becomes small between s and I some distance downstream of s. Hence,

just downstream of I, where the incident shock is reflected locally as an expansion as at a constant pressure boundary, the external flow will be more steeply inclined toward the wall if the shock strength is increased. With increase of shock strength, it is unlikely that the boundary layer will be able to withstand any increase of pressure gradient between I and the reattachment point R, so that the curvature of the external flow stream lines between I and R cannot increase. The boundary-layer thickness at R will probably increase with increase of shock strength, while the external flow direction at R will remain nearly parallel to the wall because the pressure at R is near to the maximum. In order, therefore, for the external flow to accommodate itself to the change of direction between I and R without violating the conditions imposed by the boundary layer, the thickness of the boundary layer at I must be greater when the shock strength is greater, as in Fig. 5. This requires the separation point to move farther upstream of the shock.

The possibility that mass acceleration effects may play a more important role in the equilibrium of the so-called dead air region with turbulent boundary layers than with laminar has been pointed out. Nevertheless, in broad outline the laminar and turbulent cases are physically similar, and the principal difference lies in the fact that to produce comparable effects shock strengths some five to ten times greater are required for turbulent cases than for laminar ones.† Also, of course, a condition for attaining wholly laminar flow is that the Reynolds Number should be extremely low, while it must be relatively high for turbulent flow.

(3) Boundary Layers Laminar over the Whole Region of Interaction

An approximate method of predicting the behavior of the laminar boundary layer is developed. It is a variant of an unpublished method for incompressible flow due to B. S. Stratford. Besides being easier to apply than the Pohlhausen method, it is probably more accurate for cases where small pressure increases with sharp pressure gradients occur after a considerable length with zero pressure gradient. The method gives grounds for the physical interpretation presented in Section (2) above, and by its use a fairly simple expression for the pressure ratio at separation is obtained.

(3.1) The Method of Analysis

The following approximate method of analysis is applicable to cases where a boundary layer, after growing for a distance x_0 with constant pressure p_0, experiences pressure increases small compared with p_0 in a distance not greater than, say, $x_0/2$.

In the region where the pressure (which is assumed not to vary through the thickness of the boundary layer in the direction normal to the wall‡) is equal to p_0, the velocity profiles are assumed to be of the form

$$\frac{u}{U_0} = \sin\,(\pi/2)(y/\delta_z) \tag{1}$$

If $\omega = \sigma = 1$ and there is no heat transfer to the wall, so that

$$\rho = \frac{\rho_{10}p}{p_0\left[1 + \left(1 - \frac{u^2}{U_0^2}\right)\frac{\gamma - 1}{2}M_0^2\right]}$$

$$\mu = \mu_{10}\left[1 + \left(1 - \frac{u^2}{U_0^2}\right)\frac{\gamma - 1}{2}M_0^2\right]$$

the displacement thickness with zero pressure gradient is

$$\delta_z{}^* = \delta_z\left[1 - \frac{2\tan^{-1}\left[\left(\frac{\gamma - 1}{2}\right)^{1/2}M_0\right]}{\pi\,[(\gamma - 1)/2]^{1/2}\,M_0}\right]$$

But from reference 4

$$\delta_z{}^* = 1.721[1 + 0.693(\gamma - 1)M_0^2](x/\sqrt{R_x}) \tag{2}$$

where R_x is the Reynolds Number, $\rho_{10}U_0x/\mu_{10}$. Hence,

$$\delta_z = \frac{1.721\,[1 + 0.693(\gamma - 1)M_0^2]x}{\left[1 - \frac{0.636\tan^{-1}\left[\left(\frac{\gamma - 1}{2}\right)^{1/2}M_0\right]}{[(\gamma - 1)/2]^{1/2}\,M_0}\right]\sqrt{R_x}} \tag{3}$$

Where the pressure differs from p_0, the approximate form of the velocity profiles can be deduced as follows: In Fig. 6a the velocity profiles at two points 0 and P are sketched. 0 is the point downstream of which the pressure begins to increase above p_0. The points B_0 and B are on the same stream line, and B is in the region of the point of inflexion of the profile at P. If the pressure gradient between 0 and P were very steep, the pressure gradient forces acting on the fluid in the outer part of the boundary [layer] would be much greater than the viscous forces, which could accordingly be ignored. Hence, the outer profile at P could be derived from that at 0 by the application of Bernouilli's equation and continuity considerations. Only the total change of pressure between 0 and P would be relevant; the way in which the pressure varied with x would not matter so long as the pressure gradient were everywhere sufficiently steep. If, however, the pressure gradient between 0 and P is not steep, it is not legitimate to ignore the viscosity effects, but with a little modification the method can take account of these approximately. Fig. 6b shows the velocity profiles as they would be if the

† The shock strength is defined as the ratio of the pressure rise through the shock to the pressure upstream of the shock.

‡ This assumption is probably not seriously in error for laminar layers except in the immediate neighborhood of the shock.

pressure remained equal to p_0; B' is on the same stream line as B_0. (The profile at 0 is, of course, the same as in Fig. 6a.) Outside of B in Fig. 6a the profile does not differ greatly from that outside of B' in Fig. 6b, so the viscous forces acting between 0 and P on the stream lines passing outside of B_0 at 0 are little different in the two cases. It seems plausible to treat the effects of viscosity and pressure gradient as separable and to assume that the profile outside of B at the point P, where the pressure is p, is approximately the same as if the profile outside of B' in Fig. 6b were suddenly subjected to the pressure rise $p - p_0$. On these assumptions inviscid fluid theory indicates that outside of B the profile is of the form

$$\frac{u}{U} = \sin\frac{\pi}{2}\left(\frac{p}{p_0}\right)^{(\gamma+1)/2\gamma}\left(\frac{y}{\delta_z} - \lambda\right)$$

where δ_z is given by Eq. (3), with x the distance of P from the leading edge of the boundary layer, and λ is an arbitrary constant dependent on the distance that the "outer" profile at P is displaced from the wall. For the complete profile at P, to satisfy the conditions that the velocity should be zero at the wall and that the velocity and its first two derivatives with respect to y should be continuous through the thickness of the boundary layer, it is assumed that

$$\left.\begin{aligned} \frac{u}{U} &= r_1, \qquad \text{for } n\lambda < \frac{y}{\delta_z} < \lambda + \left(\frac{p_0}{p}\right)^{(\gamma+1)/2\gamma} \\ &= r_1 + r_2, \quad \text{for } 0 < \frac{y}{\delta_z} < n\lambda \end{aligned}\right\} \tag{4}$$

where

$$r_1 \equiv \sin\frac{\pi}{2}\left(\frac{p}{p_0}\right)^{(\gamma+1)/2\gamma}\left(\frac{y}{\delta_z} - \lambda\right)$$

$$r_2 \equiv \left[1 - \frac{y}{n\lambda\delta_z}\right]^3 \sin\frac{\pi}{2}\left(\frac{p}{p_0}\right)^{(\gamma+1)/2\gamma}\lambda$$

(see Fig. 7). The outer edge of the boundary layer is at

$$y/\delta_z = \lambda + (p_0/p)^{(\gamma+1)/2\gamma}$$

and the position $y/\delta_z = n\lambda$ is the point B. Between this point B and the wall there must be the same quantity of fluid flow as between B_0 and the wall at 0 and, hence, the same as between B' and the wall in Fig. 6b. If

$$\frac{\pi^2}{16}\lambda^2(n-2) = \frac{\left(1 + \frac{\gamma-1}{2}M_0^2\right)(p - p_0)}{\gamma M_0^2 p_0} \tag{5}$$

this continuity requirement is approximately met provided that $(p - p_0)/p_0$ and λ are small so that $1 < p/p_0 < 1.2$, say, and $\cos(\pi/2)\lambda \approx 1 - (\pi^2\lambda^2/4)$. Finally, near the wall the pressure gradient must be balanced by the viscous stresses—i.e.,

$$dp/dx = \mu(\partial^2 u/\partial y^2)$$

Hence,

$$\frac{dp}{dx} = \frac{3\pi\mu_{10}U_0}{n^2\lambda\delta_z^2}\left(1 + \frac{\gamma-1}{2}M_0^2\right) \tag{6}$$

Eqs. (4) to (6) determine the velocity profile in terms of the pressure and the pressure gradient. The pressure is related to the displacement thickness of the boundary layer. If $(n-2)\lambda < 0.25$, say, the displacement thickness can be shown from Eqs. (4) to be approximately equal to

$$\delta^* = \delta_z^* + \delta_z\lambda \tag{7}$$

where δ_z^* and δ_z are given by Eqs. (2) and (3). Since the pressure changes are assumed to be small, the angle of deflection of α of the external flow from the free-stream direction parallel to the wall is related to the pressure by the equation

$$\alpha = \sqrt{M_0^2 - 1}(p - p_0)/\gamma M_0^2 p_0$$

upstream of the shock. Where there are sharp longitudinal pressure gradients α is, in fact, somewhat indefinite, since the divergence of the stream lines in the external flow is of the same order as that within the boundary layer; but it is assumed that with a flat wall

$$\alpha = (d\delta^*/dx) - (d\delta_z^*/dx)$$

Hence, upstream of the shock

$$\frac{d}{dx}(\delta^* - \delta_2^*) = \frac{\sqrt{M_0^2 - 1}(p - p_0)}{\gamma M_0^2 p_0} \tag{8}$$

In the above analysis the division of the boundary layer into an inner viscous flow and outer inviscid flow corresponds closely to the exact mathematical analysis for small perturbations in reference 5. Moreover Eqs. (5)–(8) above can be solved for the logarithmic decrement with x of a small disturbance, and results nearly the same as those of reference 5 are obtained.

(3.2) The Interrelation Between the Pressure, Pressure Gradient, and Velocity Profile

The physical interpretation presented in Section (2) above is partly based on the following facts deduced from Eqs. (5) and (6):

Eqs. (5) and (6) show that for a given n the pressure gradient is inversely proportional to the square root of $(p - p_0)/p_0$. This suggests that the pressure gradient in the region of the reattachment point is at any rate unlikely to increase greatly with increase of shock strength, although Eqs. (5) and (6) are not really applicable for pressure ratios so great as occur in practice at reattachment.

Eq. (5) shows that n must be greater than 2. It also implies that for a given pressure $n^2\lambda$ is a minimum when $n = 8/3$. When n is 3, so that the velocity gradient with respect to y is zero at the wall and the profile is of the type which occurs at a separation or reattachment point, $n^2\lambda$ is little different from the minimum. If, however, n is close to 2, corresponding to a well-

separated profile, or is large, corresponding to a profile not much different from the zero pressure gradient case, $n^2\lambda$ can be considerably larger than the minimum value. (However, the theory would break down if n were assumed to be extremely large or close to 2 with $(p - p_0) \div p_0$ not very small.) From Eq. (6) it follows that the pressure gradient is near to the maximum for a given pressure at the separation or reattachment condition but is considerably smaller when n is near 2 or is large. In physical terms, when the profile is of the separation type, as in Fig. 8b, $\partial^2 u/\partial y^2$ at the wall is bigger than when there is a thick dead air region, as in Fig. 8c, or when the profile is near to the zero pressure gradient form, as in Fig. 8a. It should be noted that the pressure gradient can be large when the boundary layer is separated provided the dead air region is not too thick; in fact, the maximum pressure gradient for a given pressure occurs when $n = 8/3$—i.e., when there is a certain amount of backflow.

(3.3) The Pressure at Separation

The pressure does not begin to change appreciably from p_0 until downstream of the point 0. Hence, by Eq. (8),

$$\frac{d}{dx}(\delta^* - \delta_z^*) = \frac{\sqrt{M_0^2 - 1}(p_s - p_0)}{\gamma M_0^2 p_0}$$

at s, and

$$(d/dx)(\delta^* - \delta_z^*) = 0$$

at 0. Accordingly, if $(\delta^* - \delta_z^*)$ can be assumed to vary roughly parabolically with x in the interval $0s$, the length $0s$,

$$x_s - x_0 \approx \frac{(\delta^* - \delta_z^*)_s - (\delta^* - \delta_z^*)_0}{\frac{1}{2}\left[\frac{d}{dx}(\delta^* - \delta_z^*)\right]_s} = \frac{2\delta_{zs}\lambda_s \gamma M_0^2 p_0}{\sqrt{M_0^2 - 1}(p_s - p_0)}$$

by Eq. (7). Also, since the pressure gradient is small at 0 and the pressure varies roughly parabolically with x in the interval $0s$,

$$p_s - p_0 \approx \frac{1}{2}\left(\frac{dp}{dx}\right)_s (x_s - x_0) = \frac{\pi\mu_{10}U_0\left(1 + \frac{\gamma - 1}{2}M_0^2\right)\gamma M_0^2 p_0}{3\delta_{zs}\sqrt{M_0^2 - 1}(p_s - p_0)}$$

by Eq. (6) and the fact that $n = 3$ at the separation point s. Hence,

$$\frac{p_s - p_0}{p_0} = \frac{0.780\gamma M_0^2}{[(M_0^2 - 1)R_{xs}]^{1/4}}\left[\frac{\left(1 + \frac{\gamma - 1}{2}M_0^2\right)\left(1 - \frac{0.636\tan^{-1}\left[\left(\frac{\gamma - 1}{2}\right)^{1/2}M_0\right]}{[(\gamma - 1)/2]^{1/2}M_0}\right)}{1 + 0.693(\gamma - 1)M_0^2}\right]^{1/2}$$

by Eq. (3) and the fact that $\mu_{10}U_0/\gamma M_0^2 p_0 = x_s/R_{xs}$. The values for $(p_s - p_0)/p_0$ calculated by means of this relation for the cases $\gamma = 1.4$, $R_{xs} = 0.25 \times 10^6$, and $M_0 = 1.5$, 2, 3, and 4 are 0.065, 0.095, 0.175, and 0.272, respectively. The first three results are not far from the experimental values,[2] but the figure for $M_0 = 4$ is probably too high. This may be due to the fact that the zero pressure gradient velocity profile departs considerably from the assumed form, Eq. (1), at the higher Mach Numbers. It would have been practicable to have used the actual zero pressure gradient profile instead of Eq. (1), but the analysis would have been considerably more complicated.

(4) Boundary Layers Turbulent over the Whole Region of Interaction

A method, similar to but much cruder than the analysis given in Section (3) for laminar cases, is first presented for the pressure at separation in Section (4.1). Semiempirical relations are then obtained covering the overall characteristics of interactions for shocks so strong that the distance between F, the peak pressure position, and 0 is several times greater than the distance between s and 0 (see Figs. 2 and 3b). The distance $x_F - x_0$ between F and 0 and the thickness δ_F of the boundary layer at F are regarded as the primary unknown parameters of the interaction to be determined in terms of the boundary-layer thickness δ_0 at 0, the peak pressure p_F, and the free-stream Mach Number M_0. The position of 0 relative to the shock does not enter into the equations, but, when comparing with experimental data on the distance between 0 and I or between 0 and I', it is assumed that $0I$ is about $(1/2)\times(x_F - x_0)$ and $0I'$ about $(2/3)(x_F - x_0)$.

(4.1) The Separation Pressure

In incompressible flow and also at a Mach Number of 2.5,[6] a good fit to the turbulent zero pressure gradient velocity profile is given by the relation

$$u/U = (y/\delta)^{1/7}$$

which is here assumed to obtain for all Mach Numbers up to, say, 4. Thus, at the position 0,

$$u/U_0 = (y/\delta_0)^{1/7}$$

This profile, sketched in Fig. 9, has a "shoulder" at $u/U_0 \approx 0.6$. Experiments show that the bulk of the pressure rise to the separation point takes place steeply, so it is reasonable to suppose that in this pressure rise region the pressure gradient forces on the fluid are considerably greater than the friction forces except near the wall. If this is so, the changes that the pressure increase causes in the velocities in the outer part of the boundary layer can be calculated approximately by the application of Bernouilli's equation, on the assumption that the total temperature is constant across the boundary layer. Consider a pressure increase Δp just sufficient to bring to rest without friction the fluid at the shoulder $u/U_0 = 0.6$ of the profile at 0. At 0 there is only a small flow of fluid between the $u/U_0 = 0.6$ position and the wall, so for pressure increases less than Δp it is perhaps unlikely that there can be any thick dead air region near the wall. On the other hand, for pressure increases greater than Δp all the relatively high velocity fluid at the shoulder of the profile at 0 will be brought to rest, and there will be a thick dead air region. Hence, it is plausible to assume that Δp is roughly equal to the increase of pressure at the separation point—i.e., that the pressure p_s at the separation point s is given approximately by

$$\frac{p_s}{p_0} = \left[\frac{1 + \frac{\gamma - 1}{2} M_0^2}{1 + 0.64 \frac{\gamma - 1}{2} M_0^2}\right]^{\gamma/(\gamma-1)} \qquad (9)$$

At Mach Numbers of 1.5, 2, 3, and 4 this ratio assumes the values 1.52, 1.84, 2.51, and 3.08, respectively, which are close to the experimental values except for the $M_0 = 4$ case where the experimental value is rather lower.[2] This approximate experimental verification is really the chief justification of Eq. (9), which is not based on satisfactory theoretical grounds. An analysis on the lines of that given in Section (3) above on laminar boundary layers, taking a more adequate account of the fluid at the wall, would be preferable. This was not attempted, however, because of uncertainties as to the relation between the turbulent friction stress and the shape of the velocity profile.

(4.2) *The Reattaching Boundary Layer*

It is assumed that at the reattachment point R (see Fig. 2), u/U_R and $\overline{u'v'}/U_R^2$ are invariant functions of y/δ_R, where U_R is the velocity at the edge of the boundary layer, δ_R is the thickness of the boundary layer, and u' and v' are the fluctuating velocity components parallel and perpendicular to the wall.

FIGS. 8-10.

FIG. 8

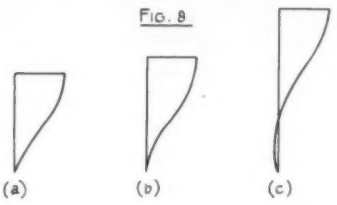

Laminar boundary layer velocity profiles with different curvatures at the wall.

FIG. 9.

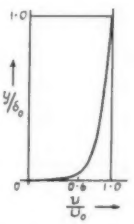

Turbulent zero pressure gradient velocity profile
$\frac{u}{U_0} = \left(\frac{y}{\delta_0}\right)^{1/7}$

FIG 10

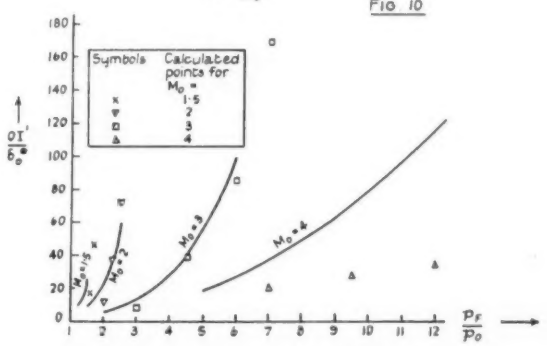

Upstream distance $0I' \div \delta_0^*$ for turbulent boundary layers: experimental curves compared with calculated values of $\frac{1}{3}(x_R - x_0)/\delta_0^*$

This assumption seems plausible for the following reasons:

(1) The zero pressure gradient profile does not vary appreciably from the form

$$u/U = (y/\delta)^{1/7}$$

at least up to Mach Numbers of 2.5,[6] so it is reasonable to suppose that the profile of u at reattachment is not greatly affected by Mach Number.

(2) It is shown in the Appendix that the distribution of $\overline{u'v'}/U^2$ with y/δ does not vary greatly with Mach Number in the zero pressure gradient case except where sharp gradients of the mean density occur. This result is, moreover, to be expected because where the mean density gradient is small something like von Kármán's incompressible flow "similarity hypothesis," relating the turbulent fluctuations to the lower derivatives of

the mean u-velocity, should be applicable. Since the reattachment u-profile will probably be roughly linear with y, there will not be any sharp gradients of mean density at the reattachment point such as there are close to the wall in the zero pressure gradient boundary layer. Hence, it is reasonable to suppose that at the reattachment point, $\overline{u'v'}/U_R^2$ will be a function of y/δ_R only independent of Mach Number.

If there is no heat transfer to the wall and the Prandtl Number does not differ greatly from 1, the total temperature will not vary much through the boundary layer, and the density near the wall at the reattachment point will be given approximately by

$$\rho = \rho_{10} p_R / \{1 + [(\gamma - 1)/2] M_0^2\} p_0$$

where ρ_{10} is the free-stream density and p_R is the pressure at the wall at R. Now the friction stress τ is equal to $-\rho\overline{u'v'}$, so that near the wall at the reattachment point $(1/p_0)(\partial\tau/\partial y)$ will, according to the foregoing assumption, be proportional to

$$\frac{\rho_{10} p_R U_R^2}{\left(1 + \frac{\gamma - 1}{2} M_0^2\right) p_0^2 \delta_R} = \frac{\gamma M_0^2 p_R U_R^2}{\left(1 + \frac{\gamma - 1}{2} M_0^2\right) p_0 U_0^2 \delta_R}$$

since $\rho_{10}/p_0 = \gamma M_0^2/U_0^2$.

From the boundary-layer equations, it follows that, at the reattachment point, $(1/p_0)(\partial\tau/\partial y)$ near the wall is equal to $(1/p_0)(dp/dx)$. At R, $(1/p_0)(dp/dx)$ is roughly proportional to

$$(p_F - p_s)/p_0(x_F - x_0)$$

Also p_R, U_R, and δ_R are not very different from p_F, U_F, and δ_F, respectively. Hence,

$$\frac{p_F - p_s}{p_0(x_F - x_0)} = \frac{k\gamma M_0^2 p_F U_F^2}{\left(1 + \frac{\gamma - 1}{2} M_0^2\right) p_0 U_0^2 \delta_F}$$

where k is a constant independent of Mach Number. It is found that this relation fits the experimental facts approximately if $k = 0.01$. Thus, on semiempirical grounds,

$$\frac{\delta_F}{x_F - x_0} = \frac{0.01\gamma M_0^2 p_F U_F^2}{\left(1 + \frac{\gamma - 1}{2} M_0^2\right)(p_F - p_s) U_0^2} \qquad (10)$$

In this equation the right-hand side can be evaluated, since p_s is given by Eq. (9) and velocities at the edge of the boundary layer such as U_F, can be calculated roughly in terms of the pressures at the wall† from the isentropic relation

$$\frac{U^2}{U_0^2} = 1 - \frac{(p/p_0)^{(\gamma-1)/\gamma} - 1}{[(\gamma - 1)/2] M_0^2} \qquad (11)$$

† At the peak pressure position F, the pressure at the edge of the boundary layer will probably not differ greatly from that at the wall, although nearer the shock there is probably a considerable variation of pressure across the boundary layer.

(4.3) Continuity Consideratians

In Eq. (10) there are essentially two unknowns, δ_F and $(x_F - x_0)$, so another relation between them is required. This is obtained from the continuity condition,

$$\text{flow across } FF' - \text{flow across } 00' = \text{flow across } 0'F'$$

(see Fig. 2).

The flow across FF' is calculated in terms of δ_F on the assumption that at F

$$u/U_F = (y/\delta_F)^{1/2}$$

This is a profile somewhat "fuller" than the probable profile at the reattachment point R, where the profile will probably be roughly of the form

$$u/U_R = (y/\delta_R)^{1/n}$$

with n between 1 and 2 and nearer to 1. For a profile of this sort is found to occur at a separation point in incompressible flow—see, for example, reference 7. The profile at F must be somewhat fuller than that at R because ultimately, of course, the profile returns to the $(y/\delta)^{1/7}$ form. However, this ultimate form is probably not reached until a distance of the order of $10\delta_F$ downstream of R. For otherwise, unless there were an exceptionally high rate of entrainment of the external flow at the edge of the boundary layer, continuity requirements would cause the boundary layer to diminish considerably in thickness downstream of R, and experiments show that no such reduction in thickness occurs. Hence, it is reasonable to assume that

$$u/U_F = (y/\delta_F)^{1/2}$$

at F, which is only a short distance downstream of R. From this assumption and the assumption that at F the pressure and total temperature are constant across the boundary layer, it follows that

$$\text{flow across } FF' = \int_{\substack{0 \\ \text{at } F}}^{\delta_F} \rho u \, dy = Q_F \rho_{10} U_0 \delta_F$$

where

$$\left.\begin{aligned} Q_F &= \frac{2 p_F U_0}{p_0 U_F (\gamma - 1) M_0^2}\left[A \log \frac{A + 1}{A - 1} - 2\right] \\ A &\equiv \left[\frac{1 + \frac{\gamma - 1}{2} M_0^2}{\frac{U_F^2}{U_0^2}\frac{\gamma - 1}{2} M_0^2}\right]^{1/2} \end{aligned}\right\} \qquad (12)$$

At 0 the velocity profile is assumed to be of the form

$$u/U_0 = (y/\delta_0)^{1/7}$$

if

$$\text{flow across } 00' = \int_{\substack{0 \\ \text{at } 0}}^{\delta_0} \rho u \, dy = Q_0 \rho_{10} U_0 \delta_0$$

it is possible to calculate an expression for Q_0 similar to Eq. (12) for Q_F. However, the expression involves the difference of nearly equal quantities, and it is easier to use the relation

$$Q_0 = 1 - (\delta_1^*/\delta_0) \tag{13}$$

where δ_0^* is the displacement thickness and values of δ_0^*/δ_0 as a function of M_0 are given in references 8 and 9 and reproduced in Table 1.

Finally, an expression for the rate of entrainment of flow across the edge of the boundary layer between 0 and F is needed. In a zero pressure gradient boundary layer, the edge of the boundary layer is inclined to the wall at an angle $d\delta/dx$, while the mean-flow stream lines at the edge of the boundary layer are inclined at an angle $d\delta^*/dx$ to the wall. Hence, there is an angle of entrainment; ψ = angle between the edge of the boundary layer and the local mean-flow stream lines = $(d\delta/dx) - (d\delta^*/dx)$ with zero pressure gradient. Now references 6 and 10 show that, for the zero pressure gradient boundary layer, δ^* is approximately given by

$$\delta^* = \frac{0.0475\,(1 + 0.35M_1^2)x_t}{\left(1 + 0.88\,\frac{\gamma - 1}{2}M_0^2\right)^{0.44} R_t^{1/5}}$$

where x_t is the x-distance from the (fictitious) leading edge of the "equivalent fully turbulent flat plate" and R_t is the Reynolds Number based on x_t and the free-stream density and velocity. Hence ψ can be calculated from the data of Table 1, and in Table 2 values of ψ are presented for various Mach Numbers and Reynolds Numbers. It can be seen that over a wide range of these variables ψ for the zero pressure gradient boundary layer is the region of 0.010. Between the positions 0 and F, ψ should be considerably higher than this, because the presence of a dead air region near the wall will presumably increase the general scale of the turbulence. The case should be intermediate between that of the zero pressure gradient boundary layer and the boundary of a two-dimensional jet emerging into still air. For this latter case in incompressible flow $\psi = 0.083$ on the side of the jet.[11] It is assumed here that the mean value of ψ between 0 and F is 0.025. This is not very different from the value $\psi = 0.03$ assumed in reference 12 for a separated turbulent boundary layer. (In reference 12 the concept of the mixing at the edge of the boundary layer is used in a more fundamental way than it is used here and is related to the changes in the boundary layer profile. However, the method, though of greater theoretical interest than the present semiempirical method is more complicated analytically.) It is further assumed here that the mean value of $\rho_1 U$ between 0 and F is $1/2(\rho_{1s}U_s + \rho_{1F}U_F)$, where the densities ρ_1 at the edge of the boundary layer are given roughly in terms of the pressures at the wall by the isentropic flow relation

$$\rho_1/\rho_{10} = (p/p_0)^{1/\gamma} \tag{14}$$

and velocities U are given roughly by Eq. (11).

Hence, the flow across $0'F'$ is approximately equal to

$$0.025\,[(\rho_{1s}U_s + \rho_{1F}U_F)/2]\,(x_F - x_0)$$

and continuity therefore requires that

$$Q_F\delta_F - Q_0\delta_0 = 0.025\left(\frac{\rho_{1s}U_s + \rho_{1F}U_F}{2\rho_{10}U_0}\right)(x_F - x_0) \tag{15}$$

Table 1

$\frac{\delta_0^*}{\delta_0}$ for $u/U_0 = (y/\delta_0)^{1/7}$

M_0	0	1	2	3	4
δ_0^*/δ_0	0.13	0.16	0.24	0.33	0.42

Table 2

ψ for Zero Pressure Gradient Boundary Layer at Various Reynolds Numbers R_t

R_t \ M	0	1	2	3	4
10^6	0.0167	0.0158	0.0148	0.0133	0.0123
$5\cdot10^6$	0.0121	0.0114	0.0107	0.0096	0.0090
10^7	0.0106	0.0100	0.0094	0.0084	0.0078

(7) Results

From Eqs. (9)–(15) it is easy to calculate δ_F and $x_F - x_0$ in terms of δ_0 (and, hence, by Table 1, δ_0^*), p_F/p_0, and M_0. The results of several such calculations are presented in Table 3.

It is assumed in comparing with experiment that the upstream distance measured from 0 to the point I' where the plane of the shock meets the plate is $(2/3)(x_F - x_0)$. (This assumption is found to fit closely the experimental facts.) Fig. 10 shows the calculated points plotted for comparison with the experimental curves of upstream distance $0I'$ divided by δ_0^* against p_F/p_0 for the values 1.5, 2, 3, and 4 of M_0.[2] It can be seen that the agreement is good apart from the $M_0 = 4$ case. Comparison with schlieren photographs of the flow shows that the theory predicts δ_F for $M_0 = 4$ to be smaller than it really is, $x_F - x_0$ is also underestimated, but the ratio $\delta_F/(x_F - x_0)$ is not far wrong. Hence, the errors seem to arise from Eq. (15) and not from Eq. (10).

Table 3

Calculated Results

M_0	1.5	1.5	2.0	2.0	2.0	3.0	3.0	3.0	3.0	4.0	4.0	4.0
p_F/p_0	1.60	1.70	2.00	2.25	2.50	3.0	4.5	6.0	7.0	7.0	9.5	12.0
δ_F/δ_0	1.4	1.7	1.2	1.5	1.8	0.9	1.3	2.0	3.4	0.9	1.0	1.0
$(x_F - x_0)/\delta_0$	5	13	4	13	25	4	19	42	84	13	17	21
$(x_F - x_0)/\delta_0^*$	25	70	18	56	106	13	58	127	254	30	40	50
$(2/3)(x_F - x_0)/\delta_0^*$	17	47	12	37	72	9	39	85	169	20	27	34

Appendix.—The Distribution of $\overline{u'v'}$ in a Zero Pressure Gradient Turbulent Boundary Layer

The equations of continuity, motion, and energy for the zero pressure gradient boundary layer are assumed to be

$$\frac{\partial(\rho u)}{\partial x} + \frac{\partial(\rho v)}{\partial y} + \frac{\partial(\overline{\rho' v'})}{\partial y} = 0 \tag{16}$$

$$\rho u \frac{\partial u}{\partial x} + \rho v \frac{\partial u}{\partial y} = -\frac{\partial}{\partial y}(\rho \overline{u'v'}) - \overline{\rho' v'} \frac{\partial u}{\partial y} \tag{17}$$

$$\rho = \rho_1 \Big/ \left[1 + \left(1 - \frac{u^2}{U^2}\right)\frac{\gamma - 1}{2} M^2\right] \tag{18}$$

where quantities with dashes are fluctuating components. It is assumed on empirical grounds[6] that

$$u/U = (y/\delta)^{1/7} \tag{19}$$

Table 4

M	0	1	2	3	4
n	2	2.3	3.3	4.3	5.4

Table 5

$-\overline{u'v'}/U^2(d\delta/dx)$ at Various u/U in Zero Pressure Gradient Boundary layer

u/U \ M	0	1	2	3	4
1.0	0.0	0	0	0	0
0.9	0.0594	0.0588	0.0571	0.0550	0.0550
0.8	0.0840	0.0849	0.0875	0.0915	0.0970
0.7	0.0933	0.0966	0.1047	0.1150	0.1269
0	0.0972	0.1092	0.1380	0.1725	0.207

Table 6

M	0	1	2	3	4
$\left(\frac{d\delta}{dx}\right)\Big/\left(\frac{d\delta_i^*}{dx}\right)$	8	7.98	8.07	8.30	8.80

From Eqs. (16), (18), and (19), it follows that

$$v = U(d\delta/dx)(u/U)^8 E - (\overline{\rho' v'}/\rho)$$

where

$$E \equiv \left(\frac{U}{u}\right)^8 \left[1 + \left(1 - \frac{u^2}{U^2}\right)\frac{\gamma - 1}{2} M^2\right] \int_0^{u/U} \frac{1 + (1 + s^2)\dfrac{\gamma - 1}{2} M^2}{\left[1 + (1 - s^2)\dfrac{\gamma - 1}{2} M^2\right]^2} s^7\, d$$

E varies monotonically between 1/8 at the wall and δ^*/δ at the edge of the boundary layer. Eq. (17) becomes

$$(\partial/\partial y)(\rho \overline{u'v'}) = (\rho u^2/7\delta)(d\delta/dx)(1 - E)$$

so that

$$\overline{u'v'} = -\left[1 + \left(1 - \frac{u^2}{U^2}\right)\frac{\gamma - 1}{2} M^2\right] U^2 \frac{d\delta}{dx} \int_{u/U}^1 \frac{s^8(1 - E)\, ds}{1 + (1 - s^2)\dfrac{\gamma - 1}{2} M^2}$$

The factor

$$(1 - E)/\{1 + (1 - s^2)[(\gamma - 1)/2]M^2\}$$

occurring in the integral assumes the values $7/8\{1 + [(\gamma - 1)/2]M^2\}$ at the wall and $1 - (\delta^*/\delta)$ at the edge of the boundary layer. It can therefore be replaced by the approximation

$$\left[7/8\left(1 + \frac{\gamma - 1}{2} M^2\right)\right] + \left\{1 - \frac{\delta^*}{\delta} - \left[7/8\left(1 + \frac{\gamma - 1}{2} M^2\right)\right]\right\} s^n$$

Hence,

$$-\frac{\overline{u'v'}}{U^2 \dfrac{d\delta}{dx}} \approx \left[1 + \left(1 - \frac{u^2}{U^2}\right)\frac{\gamma - 1}{2} M^2\right] \left\{ \frac{7\left[1 - \left(\dfrac{u}{U}\right)^9\right]}{72\left(1 + \dfrac{\gamma - 1}{2} M^2\right)} + \frac{\left[1 - \dfrac{\delta^*}{\delta} - \dfrac{7}{8\left(1 - \dfrac{\gamma - 1}{2} M^2\right)}\right]\left[1 - \left(\dfrac{u}{U}\right)^{(n+9)}\right]}{n + 9} \right\}$$

where the constant n is chosen to give the correct value of $\overline{u'v'}$ at the wall. Here the friction stress

$$\tau = \frac{-\rho_1 \overline{u'v'}}{1 + \frac{\gamma - 1}{2} M^2} = \rho_1 U^2 \frac{d\theta}{dx} = \rho_1 U^2 \frac{d\delta}{dx} \frac{\theta}{\delta}$$

where θ is the momentum thickness. Hence,

$$n = \frac{1 - (\delta^*/\delta) - 9(\theta/\delta)}{(\theta/\delta) - (7/72\{1 + [(\gamma - 1)/2]M^2\})}$$

The ratios δ^*/δ and θ/δ are given as functions of M in references 8 and 9, so that n can be calculated. The resulting values for Mach Numbers up to 4 are given in Table 4. Hence, the quantity $r \equiv -\overline{u'v'}/U^2(d\delta/dx)$ can be calculated for various values of the velocity ratio u/U and Mach Number M, and results are presented in Table 5.

It can be seen that in the outer part of the boundary layer r does not vary much with M, though it varies a great deal near the wall. The gradient $d\delta/dx$ of boundary-layer total thickness also varies little with Mach Number; the gradient $d\delta^*/dx$ of displacement thickness increases, but $(d\delta^*/dx)/(d\delta/dx)$ also increases. According to references 6 and 10,

$$\delta^* = \frac{0.0475\ (1 + 0.35M^2)x_t}{\{1 + 0.88[(\gamma - 1)/2]M^2\}^{0.44} R_t^{1/5}}$$

where x_t is the x-distance from the (fictitious) leading edge of the "equivalent fully turbulent flat plate" and R_t is the Reynolds Number based on x_t and the free-stream density and velocity. Hence,

$$\frac{d\delta^*}{dx} \Big/ \frac{d\delta_i^*}{dx} = \frac{1 + 0.35M^2}{\{1 + 0.88[(\gamma - 1)/2]M^2\}^{0.44}}$$

where δ_i^* is the displacement thickness in incompressible flow at the same Reynolds Number R_t. By the use of Table 1, $(d\delta/dx)/(d\delta_i^*/dx)$ can be calculated, and the values are given in Table 6. It can be seen that there is little change up to Mach Number of 4. Hence, the rough constancy of r in the outer part of the boundary layer means that the distribution of $\overline{u'v'}/U^2$ with y/δ for zero pressure gradient boundary layers with the same Reynolds Number R_t does not vary greatly with Mach Number except near the wall, where there are large gradients in the mean density at the higher Mach Numbers.

References

[1] Lees, L., *Interaction Between the Laminar Boundary Layer over a Plane Surface and an Incident Oblique Shock Wave*, Aero. Eng. Lab. Rep. No. 143 (Princeton), 1949.

[2] Gadd, G. E., Holder, D. W., and Regan, J. D., *The Interaction of an Oblique Shock Wave with the Boundary Layer on a Flat Plate. Part II, Interim Note on the Results for M = 1.5, 2, 3, and 4*, British A.R.C. 15,591 (unpublished), 1953.

[3] Cope, W. F., *The Measurement of Skin Friction in a Turbulent Boundary Layer at a Mach Number of 2.5, Including the Effect of a Shock Wave*, Proc. Roy. Soc. A, Vol. 215, p. 84, 1952.

[4] Young, A. D., *Skin Friction in Compressible Flow*, The Aeronautical Quarterly, Vol. 1, 1949.

[5] Lighthill, M. J., *On Boundary Layers and Upstream Influence; II, Supersonic Flows Without Separation* (to be published), 1953.

[6] Monaghan, R. J., and Johnson, J. E., *The Measurement of Heat Transfer and Skin Friction at Supersonic Speeds. Part II, Boundary Layer Measurements on a Flat Plate at M = 2.5 and Zero Heat Transfer*, British A.R.C., C.P.64, 1949.

[7] Schubauer, G. B., and Klebanoff, P. S., *Investigation of Separation of the Turbulent Boundary Layer*, NACA Rep. No. 1030, 1949.

[8] Cope, W. F., *Notes and Graphs for Boundary Layer Calculations in Compressible Flow*, British A.R.C., C.P.89, 1951.

[9] Eckert, H. U., *Characteristics of the Turbulent Boundary Layer on a Flat Plate in Compressible Flow from Measurements of Friction in Pipes*, Journal of the Aeronautical Sciences, Vol. 17, No. 9, p. 573, September, 1950.

[10] Monaghan, R. J., *Comparison Between Experimental Measurements and a Suggested Formula for the Variation of Turbulent Skin Friction in Compressible Flow*, British A.R.C., C.P.45, 1950.

[11] Durand, W. F. (Ed.), *Aerodynamic Theory*, Vol. III, Division G, Section 25; Julius Springer, Berlin, 1935.

[12] Crocco, L., and Lees, L., *A Mixing Theory for the Interaction Between Dissipative Flows and Nearly Isentropic Streams*, Journal of the Aeronautical Sciences, Vol. 19, No. 10, p. 649, October, 1952.

Some Basic Concepts for Analyzing Dynamic Flight-Test Data

H. KLEIN* AND R. SEDNEY†
Douglas Aircraft Company, Inc.

ABSTRACT

The problem considered here is that of finding, through the use of observed data, the coefficients of the differential equations that describe a dynamic system. This problem occurs in the determination of the aerodynamic stability derivatives of an airplane or missile from flight-test data. There is a maximum number of coefficients which may be determined. A method is given for finding this number, and conditions are given under which the maximum number is obtained. These results are summarized in a working rule and are applied to two examples. It is shown that the free oscillation type of flight testing can never yield all the coefficients. Suitable forcing functions are described which do permit all coefficients to be evaluated.

INTRODUCTION

THE USUAL PROBLEM IN DYNAMICS is the following: Given the forces acting on a system, find the resulting motion of the system. The solution to this problem is obtained by setting up and solving a set of differential equations subject to given initial conditions. This will be called the direct problem. The inverse problem would then consist of finding the internal forces acting within a system given the motion of the system. The solution to the inverse problem would require, in effect, constructing the equations of motion, given the solution of these equations. The type of problem considered in this paper may be called a semi-inverse problem, since the form of the equations of motion is assumed given. This means that in every equation each term involving the generalized coordinates, their derivatives, and the forcing functions is given except for an unknown multiplicative constant. The solution to the semi-inverse problem consists of finding these unknown constants, the constant coefficients in the equations of motion.

The importance of the semi-inverse problem in aeronautics lies in its application to dynamic flight testing. These tests are normally accomplished by subjecting the aircraft to a disturbance (usually a control deflection) and measuring the resulting motion. The object of such testing is the determination of the aerodynamic forces and moments, or their effects, which are conventionally represented by stability derivatives, transfer functions, or indicial responses. The stability derivatives are the coefficients of the differential equations describing the motion of the aircraft. The transfer functions are the responses to a sinusoidal input. The indicial responses are the responses to a step function input. The convenience of each of these descriptions of a dynamic system depends upon what use is to be made of the results. Table 1 gives a comparison of certain features of these descriptions from the point of view of the problem of flight testing for aerodynamic data.

Because of the desirability to an aerodynamicist of knowing the coefficients of the differential equations, the work described in this paper was undertaken.

This paper considers the theoretical aspects of the flight-testing problem exclusively from the point of view of obtaining the coefficients of the differential equations. These coefficients are found by solving sets of linear algebraic equations. It is shown that it may be impossible to find all coefficients and that there exists an upper limit to the number that can be found. A method for finding this number is given, and three conditions are stated which must be satisfied in order to find this maximum number of coefficients. The results are summarized in a working rule whose application is demonstrated by two examples. A method is pointed out for increasing the number of coefficients which may be determined.

For the theoretical considerations in this paper, it is assumed throughout that the equations of motion are

TABLE 1
Comparison of Descriptions of Dynamic Systems

Consideration	Type of Description: Transfer functions or indicial responses	Type of Description: Coefficients of differential equations
Test conditions	Time history must be taken in a period in which steady-state conditions exist at beginning and end of period	Time history may be taken in any period of time. Steady-state conditions need not exist at beginning or end of period
Application to nonlinear problems	Can be applied only to linear systems	Can be used in linear and nonlinear systems
Usefulness of results	Results are useful for synthesis of control systems. Responses can only be computed for some input variables—e.g., gust responses cannot be computed from measured responses to controls	Results are useful for checking aerodynamic design calculations. Responses for any kind of input (gust, control, etc.) may be computed by well-known methods

Presented at the Aircraft Design Session, Twenty-First Annual Meeting, IAS, New York, January 26–29, 1953.

* Aerodynamics Engineer, Santa Monica Division.
† Aerodynamicist, Santa Monica Division.

linear with constant coefficients. Equations of this type result from the linearization of the exact equations of motion. However, in certain cases linearization may not be justified. In those cases the method of analysis discussed here can be applied to the following more general types of equation of motion. If the equation consists wholly of terms that are composed of an unknown coefficient times a known function of time, these coefficients may be obtained as the solution to the semi-inverse problem. This known function of time may appear naturally in the problem, as for example, the dynamic pressure; or it may be a nonlinear function of the generalized coordinates that would occur if the linearization process is not valid. To determine the maximum number of coefficients that may be found in the solution to the semi-inverse problem for cases in which the more general types of equations occur, the same method of analysis given here is applicable. However, two of the three conditions that are found to ensure a unique solution cannot be applied to a system that is described by nonlinear equations. Throughout the discussion it is also assumed that the data giving the time history of the generalized coordinates, their derivatives, and the forcing functions are free from experimental error. For any practical experiment this will not be the case. The problem of developing a suitable averaging process and other questions related to handling inaccurate data are being studied and will be considered in a later paper.

The idea of determining coefficients in the equations of motion from experimental time histories is not new. A limitation on the number of coefficients which may be determined was pointed out by Greenberg[1] for a two degree of freedom system. The present paper considers systems with an arbitrary number of degrees of freedom. A summary of the status of this problem has been given by Milliken.[2] Previous work on this problem is separated into two categories. The first category, "Equations of Motion," is essentially what is called here the semi-inverse problem. The various methods of approach listed differ only in the details of the necessary calculations. The second category, "Response Curve Fitting," is a collection of methods using various devices to extract from the data certain combinations of the differential equation coefficients. These combinations are called transfer coefficients in reference 1. These methods are usually applied to the case of a system with two degrees of freedom.

Attempts have been made to generalize the response curve fitting techniques to a system with more degrees of freedom by using the concept of transfer functions.[3] There are inherent difficulties in obtaining the transfer coefficients for a system with more than two degrees of freedom. First, there is a practical difficulty since a set of nonlinear algebraic equations must be solved. Second, there is a theoretical difficulty, since the transfer coefficients may satisfy one or more functional relations that can apparently be discovered only by trial-and-error methods. Obtaining the differential equation coefficients—i.e., the stability derivatives—from the transfer coefficients is also difficult, because in the general case another set of nonlinear algebraic equations must be solved. Furthermore, the transfer function concept can only be used for a system described by linear, constant coefficient differential equations. Evidently the transfer function concept, which is useful for other purposes, is not well adapted to the solution of the semi-inverse problem with several degrees of freedom.

With regard to the notation employed, it was not practical to use conventional aerodynamic notation when discussing the general problem. The coefficients, a_{ij}, can represent stability derivatives and the inertia properties of an airplane or missile. The correspondence will be apparent by referring to the section on examples. The arrangement of the paper is such that, if one is interested only in applying the results to specific examples, the section on "Practical Application and Examples" can be read at once.

Theory

One Degree of Freedom Case

The semi-inverse problem for a simple example will now be discussed in detail. This will illustrate the principles involved in the general problem and the methods to be used, while avoiding extensive calculations. Problems of greater generality will be considered in the next section.

A linear spring-mass-damper system executing free vibrations is the example to be discussed. Data giving the displacement, velocity, and acceleration of the mass as functions of time are measured directly or computed from measured data by integration or differentiation. This system is assumed to be described by a second-order, linear, constant coefficient differential equation. It is assumed that all three terms are present in this equation—i.e., the coefficients of the mass, damping, and spring terms are not zero. If all three terms are not present in the equation that actually describes the system, this will be discovered in the calculations.

If x denotes the displacement of the mass, the equation of motion assumed is

$$a_1\ddot{x} + a_2\dot{x} + a_3x = 0$$

and the problem is to determine a_1, a_2, and a_3. Not all three of these constants can be found because of the homogeneity of the equation. The trivial solution,

$$a_1 = a_2 = a_3 = 0$$

is excluded. But it would seem possible to solve for two of the coefficients in terms of the third or equivalently solve for the ratios of two of the coefficients to the third one. For example, suppose it is decided to solve for the ratios a_1/a_2 and a_3/a_2. The above equation would be written

$$(a_1/a_2)\ddot{x} + (a_3/a_2)x = -\dot{x}$$

Select two values of time, t_1 and t_2, and substitute the corresponding known values of x, $\dot{x}$, $\ddot{x}$ in this equation, giving

$$(a_1/a_2)\ddot{x}(t_1) + (a_3/a_2)x(t_1) = -\dot{x}(t_1)$$

$$(a_1/a_2)\ddot{x}(t_2) + (a_3/a_2)\,x(t_2) = -\dot{x}(t_2)$$

If the determinant

$$|X| = \begin{vmatrix} \ddot{x}(t_1) & x(t_1) \\ \ddot{x}(t_2) & x(t_2) \end{vmatrix}$$

is not zero, then it is possible to solve for the ratios uniquely.

The condition of a nonzero determinant is necessary and sufficient for a unique solution, but there is no assurance that it is possible to choose t_1 and t_2 such that $|X| \neq 0$. There are three situations that will cause $|X|$ to vanish. First of all, an unfortunate choice of the two values of time will give a zero determinant; for example, if t_1 and t_2 are such that $x(t_1) = x(t_2) = 0$. But this can be circumvented by choosing other values of time.

Second, as mentioned above, the assumed form of the equation of motion may be wrong. Suppose, in that case, that a_1 and a_3 are solved for in terms of a_2, but the physical system is actually one without damping—i.e., $a_2 = 0$. Then $|X| = 0$ for any t_1 and t_2. Again this difficulty is not serious, since it is known then that $a_2 = 0$ and the ratio a_1/a_3 can be found. The data thus still give two of the coefficients of the system. On the other hand, suppose that the assumption of nonzero mass, a_1, is false. Then the equation of motion would be of first order, and it would be possible to solve for no two coefficients. This is so because the solution would be

$$x = ce^{\lambda t}$$

where c is an arbitrary constant and λ is the ratio, $-(a_3/a_2)$, and the three possible second-order determinants from the matrix

$$\begin{bmatrix} \ddot{x}(t_1) & \dot{x}(t_1) & x(t_1) \\ \ddot{x}(t_2) & \dot{x}(t_2) & x(t_2) \end{bmatrix}$$

would all be zero for any t_1 and t_2. In this case it is possible to solve for only one coefficient in terms of two others, one of which is zero. The difference between the cases $a_1 = 0$ and $a_2 = 0$ is that the first reduces the order of the equation while the second does not. The case $a_1 = 0$ is more crucial, since all determinants of the above matrix are zero. This second situation shows that the assumed form of the equation of motion determines what coefficients may be solved for and whether the expected maximum number can be solved for. An equivalent way of expressing this latter conclusion, which is more convenient for multiple degree of freedom systems, is: If the order of the true characteristic equation describing the system is greater than, or equal to, the order of the characteristic equation describing the assumed system, then the maximum possible number of ratios can be obtained from the data provided certain other conditions are met.

There is a third situation that will make it impossible to solve uniquely for two ratios. It is known that the general solution of the second-order differential equation is

$$x = c_1e^{\lambda_1 t} + c_2e^{\lambda_2 t}$$

and that the initial conditions determine c_1 and c_2. The roots of the characteristic equation, λ_1 and λ_2, may be real, imaginary, or complex. Consider first that λ_1 and λ_2 are real. Further, suppose the initial conditions are such that $c_2 = 0$. Then the solution is simply

$$x = c_1e^{\lambda_1 t}$$

Again, all of the possible second-order determinants of the coefficients arising in solving for two ratios will be zero. Note that the above solution for x satisfies any number of distinct second-order differential equations, all with the same initial conditions so that the semi-inverse problem would not have a unique solution in this case. If λ_1 and λ_2 are pure imaginary, this implies that $a_2 = 0$, which has already been considered. If λ_1 and λ_2 are complex with nonzero real part, then all of the three possible second-order determinants are nonzero. The conclusions concerning this third situation can be summarized as follows: To be able to obtain two (the maximum possible number) of the coefficients of the system in terms of a third, the initial conditions must be such that all modes are excited.

In summary, the results for this example show that to be able to solve for a maximum of two coefficients of the given system from the data alone, the following three conditions are necessary and sufficient.

(1) A fortunate choice of values of t is made.

(2) The order of the true characteristic equation is greater than or equal to the order of the assumed characteristic equation.*

(3) The initial conditions are such that all modes are excited in the motion.

These three conditions are of importance to any attempted solution of the semi-inverse problem. However, it should be noted that it cannot be determined whether or not they are satisfied except by evaluating the determinants. In practice the first condition will not be troublesome, since for actual data some averaging process should be used. This, in effect will nullify an accidental choice of unfortunate times. It is possible that the second condition might be violated in the study of airplane or missile dynamics. However, there will usually be sufficient knowledge of the physical

* The "correct" values of the coefficients can be found only if the orders of the assumed and true characteristic equations are equal.

system so that it would be known how to change the assumed form of the equations of motion. The third condition presents a dilemma, since, to determine whether all the modes are excited or even what the modes are, the coefficients of the system must be known. However, from all possible types of initial conditions, only a relatively small number will force one or more of the arbitrary constants to vanish. Thus the probability that condition three is violated is extremely small.

For this simple example, two was the maximum number of coefficients of the differential equation that could be obtained from the data. To be able to discuss more complicated examples, a systematic way of finding the maximum number of coefficients is needed. The maximum number of coefficients that can be solved for is determined by the rank of a matrix. The kth row of this matrix consists of the quantities x, $\dot{x}$, and $\ddot{x}$ evaluated at a time t_k. The rank of this matrix is the number of coefficients that may be solved for in terms of other coefficients. Evidently the rank must be less than three. The maximum possible rank is two, though from the previous discussion it may be less than two.

A systematic way of deducing the maximum possible rank of a matrix is offered by the geometrical concept of vectors. This concept will be introduced by applying it to the above example. Let the three coefficients of the differential equation, a_1, a_2, and a_3, be the components of a vector $\boldsymbol{A}$, and let $\ddot{x}$, $\dot{x}$, x be the components of a vector $\boldsymbol{X} = \boldsymbol{X}(t)$. Let

$$\boldsymbol{X}_k = \boldsymbol{X}(t_k)$$

In this notation the equation of motion is then

$$\boldsymbol{A} \cdot \boldsymbol{X} = 0$$

Thus the fixed vector $\boldsymbol{A}$ is perpendicular to the $\boldsymbol{X}$ vector at all times so that all vectors $\boldsymbol{X}_k$ lie in the plane perpendicular to $\boldsymbol{A}$. The end point of $\boldsymbol{X}$ traces out a curve in this fixed plane, as shown in Fig. 1.

The concept of the linear independence of vectors will be used in the following discussion. The n vectors $\boldsymbol{X}_j$ for $j = 1, 2, \ldots, n$ are linearly independent if it is impossible to find n scalars, $c_1, c_2, \ldots c_n$, where at least one is not equal to zero, such that

$$c_1\boldsymbol{X}_1 + c_2\boldsymbol{X}_2 + \ldots + c_n\boldsymbol{X}_n = 0$$

It can be shown that, for vectors lying in a plane, at most two are linearly independent. For vectors in three-dimensional space, at most three are linearly independent, so that any vector may be expressed as a linear combination of three linearly independent vectors.

The rank of the matrix defined above is equal to the number of linearly independent rows—i.e., the maximum number of linearly independent $\boldsymbol{X}_k$ vectors.[4] Since all $\boldsymbol{X}_k$ lie in a plane, there are at most two linearly independent $\boldsymbol{X}_k$ vectors.

The same result can be obtained analytically as follows: In a three-dimensional space there are at most three linearly independent vectors. Since $\boldsymbol{A}$ must be one of these (any two vectors that are perpendicular are linearly independent) there can be at most two linearly independent $\boldsymbol{X}_k$ vectors. Thus the maximum possible rank of the matrix is two.

The above methods will now be applied to more general physical systems.

Multiple Degrees of Freedom Case:

Consider first the free vibrations of an n degree of freedom physical system. Let the generalized coordinates be $x_1, \ldots x_n$. For an "ordinary" system the equations of motion will be

$$\left.\begin{aligned} &a_{11}\ddot{x}_1 + \ldots + a_{1n}\ddot{x}_n + a_{1,\,n+1}\dot{x}_1 + \ldots + a_{1,\,2n}\dot{x}_n + a_{1,\,2n+1}x_1 + \ldots + a_{1,\,3n}x_n = 0 \\ &\quad\cdot \\ &\quad\cdot \\ &\quad\cdot \\ &a_{n1}\ddot{x}_1 + \ldots + a_{nn}\ddot{x}_n + \quad\cdot\quad\cdot\quad\cdot\quad + a_{n,\,3n}x_n = 0 \end{aligned}\right\} \tag{1}$$

The term "ordinary" is used to emphasize the fact that it is possible to have higher order derivatives in the equations of motion of certain physical systems. This is true, for example, if downwash lag effects are completely considered. However, the presence of such terms introduces no essential changes in the discussion. Define the following sets of numbers as vectors in a vector space of $3n$ dimensions:

$$\boldsymbol{A}_i\colon\ (a_{i1}, a_{i2}, \ldots, a_{i,\,3n}) \tag{2}$$

$$\boldsymbol{X}\colon\ (\ddot{x}_1, \ldots \ddot{x}_n, \dot{x}_1, \ldots \dot{x}_n, x_1 \ldots x_n) \tag{3}$$

and $\boldsymbol{X}_k = \boldsymbol{X}(t_k)$. Then the equations of motion, Eqs. (1), can be written as

$$\boldsymbol{A}_i \cdot \boldsymbol{X} = 0 \qquad (i = 1, 2, \ldots, n)$$

There are n fixed (but unknown) vectors $\boldsymbol{A}_i$. The determination of the components of $\boldsymbol{A}_i$ is the semi-inverse problem. These n vectors are linearly independent

because the equations of motion are linearly independent. Therefore, in the $3n$-space, there are at most $2n$ linearly independent vectors X_k. Call the matrix, which has for its kth row the components of X_k, the X matrix. The rank of this matrix is at most $2n$. This means that from each equation of motion at most $2n$ of the a_{ij} can be solved for in terms of the remaining n. This is a generalization of the conclusion reached in studying the one degree of freedom case.

In order to be able to solve for this maximum number, the previously stated conditions 1, 2, and 3 must be satisfied. That these conditions are necessary and sufficient in order to obtain the maximum number of a_{ij} from the data will be demonstrated by examples. It is obvious that condition 1 must be satisfied, but, since some averaging process should be used with real data, in practice it is of no great concern. To illustrate why conditions 2 and 3 must be satisfied for multiple degrees of freedom, assume that the physical system is represented by Eq. (1) for $n = 2$.

$$a_{11}\ddot{x}_1 + a_{12}\ddot{x}_2 + a_{13}\dot{x}_1 + a_{14}\dot{x}_2 + a_{15}x_1 + a_{16}x_2 = 0$$

$$a_{21}\ddot{x}_1 + a_{22}\ddot{x}_2 + a_{23}\dot{x}_1 + a_{24}\dot{x}_2 + a_{25}x_1 + a_{26}x_2 = 0$$

According to the rule for determining the maximum number of coefficients that can be found, it is possible to solve for at most four of these in terms of the remaining two in each equation. But suppose that for the actual physical system

$$\begin{vmatrix} a_{11} & a_{12} \\ a_{21} & a_{22} \end{vmatrix} = 0 \qquad (4)$$

and that the characteristic equation is of degree three. Then x_1 and x_2 are linear combinations of three exponentials. It can be shown that the X matrix for this example cannot have rank four. In fact it is at most of rank three, and thus only three of the a_{ij} can be solved for in terms of the remaining three in each equation. Similar considerations hold for the n degree of freedom case.

To show why condition 3 must be satisfied, some further calculations are necessary. It is no longer assumed that Eq. (4) is satisfied. Assuming that the roots of the characteristic equation, λ_p, for $p = 1, 2, 3, 4$ are distinct, it can be shown that

$$x_1 = \sum_{p=1}^{4} c_p e^{\lambda_p t}$$

$$x_2 = \sum_{p=1}^{4} c_p K_p e^{\lambda_p t}$$

where the c_p are arbitrary constants and the K_p are constants involving the a_{ij}. Suppose it is desired to solve for a_{1j} and a_{2j} for $j = 3, 4, 5, 6$. Pick four values of time t_k and denote the matrix, whose kth row is

$$\dot{x}_1(t_k)\dot{x}_2(t_k)x_1(t_k)x_2(t_k)$$

by Y. Define the matrix

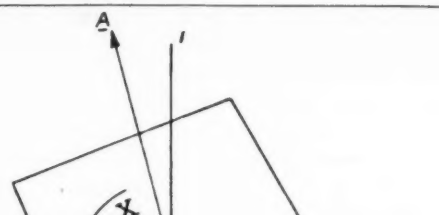

FIG. 1.

$$e = (e^{\lambda_p t_k}) \qquad (p, k = 1, 2, 3, 4)$$

where k denotes the row and p the column, and the matrix

$$\Lambda = \begin{bmatrix} \lambda_1 & K_1\lambda_1 & 1 & K_1 \\ \lambda_2 & K_2\lambda_2 & 1 & K_2 \\ \lambda_3 & K_3\lambda_3 & 1 & K_3 \\ \lambda_4 & K_4\lambda_4 & 1 & K_4 \end{bmatrix}$$

Then it can be shown that

$$Y = e \begin{bmatrix} c_1 & 0 & 0 & 0 \\ 0 & c_2 & 0 & 0 \\ 0 & 0 & c_3 & 0 \\ 0 & 0 & 0 & c_4 \end{bmatrix} \Lambda$$

To solve for the desired a_{ij}, Y must be nonsingular—i.e., of rank 4. If condition 1 is satisfied, e is nonsingular, and it can be shown that Λ is nonsingular. Then the rank of Y is equal to the number of nonzero c_p. The rank of Y is four if all modes are present in the solution—i.e., if all $c_p \neq 0$. These results can be generalized to any number of degrees of freedom.

Returning to the multiple degree of freedom problem, it must be emphasized that, when it is decided that the rank of X is $2n$, this means that there is at least one determinant of order $2n$ in X which is not zero. Therefore it cannot be said that any set of $2n$ of the a_{ij} can be solved for in each equation. It may happen that only certain sets of $2n$ coefficients may be solved for in terms of the remaining n.

In determining the maximum number of a_{ij} that can be obtained from the data, the number of degrees of freedom and the dimension of the suitable vector space must be known. The former would be known in any given problem. For the general n degree of freedom system the latter has been taken to be $3n$. However this requires some discussion. Suppose that $a_{i,\,3n} = 0$ for all i so that x_n does not appear in any equation. Should the appropriate vector space be one of dimension $3n$ or $3n$-1? Either of these can be chosen if a

certain precaution is taken. If a $3n$-1 space is chosen, then by following the same reasoning as above it would be deduced that, at most, $2n$-1 of the a_{ij} can be solved for in terms of the remaining n from each equation of motion. If a $3n$-space is decided upon (by keeping in the equations a literal term for $a_{i,\,3n}x_n$), it is found that, at most, $2n$ of the a_{ij} can be solved for in terms of the remaining n from each equation of motion. However, included in the set of $2n$ of the a_{ij} must be $a_{i,\,3n}$. Otherwise the coefficient matrix would be singular. Thus there is no contradiction in the arbitrary choice of dimension of the space. The same amount of information is obtained in both cases—$2n$-1 of the nonzero coefficients and the result that $a_{i,\,3n} = 0$. It is not difficult to prove the statement that $a_{i,\,3n}$ must be included in the unknowns solved for when a $3n$-space is chosen. However, only an illustrative example will be given here.

Consider a two degree of freedom system with no damping.

$$a_{11}\ddot{x}_1 + a_{12}\ddot{x}_2 + a_{13}x_1 = 0$$

$$a_{21}\ddot{x}_1 + a_{22}\ddot{x}_2 + a_{23}x_1 = 0$$

where x_2 does not appear in either equation. A solution to the equations is

$$x_1 = c_3 \sin \omega t + c_4 \cos \omega t$$

$$x_2 = b_1 + b_2 t + b_3 \sin \omega t + b_4 \cos \omega t$$

If the appropriate vector space is taken to be a 3-space, only one of the a_{ij} can be found in terms of the other two from each equation. But suppose a 4-space is decided upon (by carrying along a term $a_{i4}x_2$ in each equation), with the result that two of the a_{ij} can be solved for in terms of the remaining two from each equation of motion. This is possible if at least one second-order determinant from the matrix

$$\begin{vmatrix} \ddot{x}_1(t_1) & \ddot{x}_2(t_1) & x_1(t_1) & x_2(t_1) \\ \ddot{x}_1(t_2) & \ddot{x}_2(t_2) & x_1(t_2) & x_2(t_2) \end{vmatrix}$$

is nonzero. It can be shown that the following relation holds between the constants appearing in the expressions for x_1 and x_2.

$$b_3/c_3 = b_4/c_4$$

Using this fact and the expressions for x_1 and x_2 given above, it can be shown that the only nonzero determinants from the matrix are those that include the last column from the matrix. This means that, to solve for two a_{ij} in each equation of motion, a_{i4} must be one of these. It will be found that $a_{i4} = 0$.

In discussing practical applications of the foregoing theory, which will be done in the next section, it happens that some of the a_{ij} are zero or accurately known in advance. There is a large variety of cases to be considered, but all of these have been reduced to a simple working rule that is stated in the next section. In essence this rule says the following: If conditions 1, 2, and 3 are satisfied so that the maximum number of a_{ij} may be obtained, contained in this maximum number may be some a_{ij} that are already known (zero or nonzero). This occurs regardless of the chosen dimension of the space.

Next consider the case of an n degree of freedom system undergoing forced vibrations. The system of Eqs. (1) will be modified only by the presence of terms on the right-hand sides. Suppose the forcing function for the ith equation is $b_i\delta$, where δ is given experimentally and the b_i are either known or unknown. Unknown b_i arise in the case of a control deflection in airplane dynamics where the control effectiveness may be unknown. To reduce this case to the type considered previously first redefine $\boldsymbol{A}_i$ and $\boldsymbol{X}$ as

$$\boldsymbol{A}_i\text{:}\quad (a_{i1}, \ldots, a_{i,\,3n}, b_i)$$

$$\boldsymbol{X}\text{:}\quad (\ddot{x}_1, \ldots x_n, -\delta)$$

Now the appropriate space is of dimension $3n + 1$. There are $n\boldsymbol{A}$ vectors and thus at most $3n + 1 - n = 2n + 1$ linearly independent $\boldsymbol{X}$ vectors can be found. The number of independent $\boldsymbol{X}$ vectors was shown to be the number of coefficients that may be solved for in each equation. Therefore from each equation at most $2n + 1$ of the a_{ij} and b_i can be solved for in terms of the remaining n. If all the b_i were known, a total of n more of the unknown a_{ij} could be found than in the case of free vibrations.

The next question to be considered is: If all the a_{ij} are unknown, can an experiment be devised so that it is possible to determine all the a_{ij}? The answer to this question is an affirmative one, at least in theory.

By having forcing functions of the form $b_i\delta$, the dimension of the appropriate space was increased by one, and it was possible to solve for a total of n more of the a_{ij}. Therefore, further ways of increasing the dimension of the vector space will be sought. This must be done with some care. For example, it is not possible to write the forcing functions $b_i\delta$ as $(1/2)b_i\delta + (1/2)b_i\delta$ and conclude that the appropriate vector space is of dimension $3n + 2$.

To make certain that the dimension of the vector space is increased, the concept of the direct sum of vector spaces will be used. The definition and a discussion of this concept is given in reference 5. However, it is possible to gain an intuitive feeling for this concept which is sufficient for the purpose of this paper. Let Y represent a vector space of dimension r. Then Y is completely specified if r linearly independent vectors from Y are given, since any other vector in Y is a linear combination of the given vectors. These r vectors are said to span Y. Let the vectors be $\boldsymbol{Y}_1, \ldots, \boldsymbol{Y}_r$ where

$$\boldsymbol{Y}_i = (y_{i1}, \ldots, y_{ir})$$

in component form. It is convenient to represent this set of vectors as a matrix

$$\begin{bmatrix} y_{11} & \cdots & y_{1r} \\ y_{21} & \cdots & y_{2r} \\ \cdot & & \\ \cdot & & \\ \cdot & & \\ y_{r1} & \cdots & y_{rr} \end{bmatrix}$$

Suppose another vector space, Z, of dimension s is given—i.e., s linearly independent vectors $\boldsymbol{Z}_1, \ldots \boldsymbol{Z}_s$ are given. Let the vectors in component form be represented by the matrix

$$\begin{bmatrix} Z_{11} & \cdots & Z_{1s} \\ Z_{21} & \cdots & Z_{2s} \\ \cdot & & \cdot \\ \cdot & & \cdot \\ \cdot & & \cdot \\ Z_{s1} & \cdots & Z_{ss} \end{bmatrix}$$

Now define the matrix

$$\begin{bmatrix} y_{11} & \cdots & y_{1r} & 0 & \cdots & 0 \\ \cdot & & \cdot & \cdot & & \cdot \\ \cdot & & \cdot & \cdot & & \cdot \\ \cdot & & \cdot & \cdot & & \cdot \\ y_{r1} & \cdots & y_{rr} & 0 & \cdots & 0 \\ 0 & \cdots & 0 & Z_{11} & \cdots & Z_{1s} \\ \cdot & & \cdot & \cdot & & \cdot \\ \cdot & & \cdot & \cdot & & \cdot \\ \cdot & & \cdot & \cdot & & \cdot \\ 0 & \cdots & 0 & Z_{s1} & \cdots & Z_{ss} \end{bmatrix}$$

It can be proved that these $r + s$ vectors with $r + s$ components are linearly independent. Therefore they span a vector space of dimension $r + s$. This vector space is called the direct sum of Y and Z, which is represented by the symbol

$$Y \oplus Z$$

The result that will be used in the following discussion is. The direct sum of two vector spaces is a vector space whose dimension is the sum of the dimensions of the two spaces.

The following result will be proved. Given n linearly independent functions of t, say $\delta_1, \ldots, \delta_n$, and n linearly independent vectors $\boldsymbol{B}_i$

$$\boldsymbol{B}_i: \quad (b_{i1}, \ldots, b_{in})$$

where the b_{ij} are known. If the equations of motion of a physical system are

$$\boldsymbol{A}_i \cdot \boldsymbol{X} = F_i \tag{5}$$

where

$$F_i = b_{i1}\delta_1 + \ldots + b_{in}\delta_n$$

with $\boldsymbol{A}_i$ and $\boldsymbol{X}$ defined as in Eqs. (2) and (3), then the maximum number of a_{ij} which can be determined is $3n$ from each equation of motion. Note that the components of $\boldsymbol{X}$ as defined in Eq. (3) are now obtained from the solutions to the system Eq. (5). This maximum number can be determined if conditions 1, 2, and 3 are satisfied.

Denote the original $3n$-space by A and the n-space spanned by $\boldsymbol{B}_i$ by B. The vector space defined by the direct sum of A and B

$$S = A \oplus B$$

is a $4n$ dimensional vector space. The space S can be spanned by the n $\boldsymbol{B}_i$ vectors, which are now written as

$$\boldsymbol{B}_i: \quad (0, \ldots 0, b_{i1}, \ldots, b_{in})$$

with the first $3n$ components zero, the n $\boldsymbol{A}_i$ vectors, and $2n$ $\boldsymbol{X}_k$ vectors

$$\boldsymbol{A}_i: \quad (a_{i1}, \ldots a_{i,\,3n}, 0, \ldots, 0)$$

$$\boldsymbol{X}_k: \quad [\dot{x}_1(t_k), \ldots, x_n(t_k), 0, \ldots 0]$$

with the last n components zero.

However, a different set of $4n$ linearly independent vectors that span the space is desired. Define in S the vectors

$$\Delta_k: \quad [0, \ldots, 0, \delta_1(t_k), \ldots, \delta_n(t_k)]$$

with the first $3n$ components zero. The $\boldsymbol{\Delta}_k$ lie wholly within B, which is spanned by the $\boldsymbol{B}_i$. Therefore, each $\boldsymbol{\Delta}_k$ must be a linear combination of the $\boldsymbol{B}_i$. It can be shown that this is possible if the set of functions $\delta_1, \ldots, \delta_n$ form a linearly independent set. Let

$$\boldsymbol{A}_i' = \boldsymbol{A}_i + \boldsymbol{B}_i \qquad (i = 1, \ldots, n)$$

These n vectors are linearly independent. Then it is possible to choose a maximum of $3n$ other linearly independent vectors to span S. For these, take

$$\boldsymbol{X}_k' = \boldsymbol{X}_k - \boldsymbol{\Delta}_k \qquad (k = 1, \ldots, 3n)$$

The $\boldsymbol{A}_i'$ are linearly independent of the $\boldsymbol{X}_k'$, since

$$\boldsymbol{A}_i' \cdot \boldsymbol{X}_k' = 0$$

Since $3n$ is clearly the maximum possible number of linearly independent vectors $\boldsymbol{X}_k'$, the maximum possible number of a_{ij} which can be determined is $3n$ from each equation.

Therefore it has been shown that to completely determine the physical system, n essentially distinct forcing functions, F_i are needed. Since this is in effect what was proved, it might be argued that there was no point in introducing the function δ_i. This was done because in the applications to airplane dynamics it is often impossible to separate the forcing functions into specific degrees of freedom. For example, an elevator deflection or gust will produce both a lift and a moment.

A possible way of introducing additional forcing functions is to attach rockets to the airplane or missile at various points. Then the δ_i may be in the nature of short pulses and idealized to impulses. If the idealized impulses are defined to be linearly independent when they occur at different times, then the above results still hold.

Applications and Examples

Working Rule

The result of the foregoing theory may be summarized for convenience into a working rule. This rule, which presupposes certain stated requirements for the data used, allows one to predict which coefficients may be solved for, in principle. In practice, inaccuracies in the data may cause large inaccuracies in the results, but this problem is not considered here. The following previously stated conditions are assumed satisfied:

(1) A fortunate choice of values of t is made.

(2) The order of the true characteristic equation is greater than, or equal to, the order of the assumed characteristic equation.

(3) All modes are excited in the motion.

The rule states that in each equation the number of unknown coefficients which can be determined plus the number of known coefficients which may be checked are equal to the total number of measured quantities less the number of equations. This is restated below in terms of symbols. The following quantities are defined:

n = number of equations describing system

m = number of nonzero column vectors in coefficient matrix

m_i = number of nonzero coefficients in ith equation

p_i = number of coefficients not known in advance in ith equation

d_i = number of coefficients in ith equation that may be *determined*

c_i = number of coefficients (zero or nonzero) in ith equation known in advance and which may be *checked*

u_i = number of coefficients in ith equation that remain *unknown*

The rule for finding d_i, c_i, and u_i may be stated as follows: If $p_i \leqq (m - n)$ and $m_i > p_i$, then $d_i = p_i$. If $p_i \leqq (m - n)$ and $m_i = p_i$, then $d_i = p_i - 1$. If $p_i > (m - n)$, then $d_i = (m - n)$. In any event,

$$c_i = (m - n) - d_i$$

$$u_i = (p_i - d_i)$$

Solving for Coefficients

Devising a method of solving for the coefficients, after having decided (by the foregoing working rule) which coefficients are to be solved for, is a separate problem. In addition, the preceding discussion has not considered the effect of inaccuracy in the data. In order to minimize the effect of such inaccuracies upon the calculated coefficients, it is evidently desirable to adopt some procedure that averages over a great number of times. The selection of the "best" averaging procedure is a formidable task, which is not examined here.

Examples, Airplane Longitudinal Motion

In order to illustrate the application of the working rule, two cases of the airplane longitudinal equations of motion are considered. The matrix of coefficients of

TABLE 2

$(m - n) = (4 - 2) = 2$

$\ddot{\alpha}$	$\ddot{\theta}$	$\dot{\alpha}$	$\dot{\theta}$	α	θ	Non-zero m_i	Not Given p_i	Determined d_i	Checked c_i	Unknown u_i
0	0	1	−1	$\frac{C_{L\alpha}}{2}$	0	3	1	1	1	0
0	$-h$	$C_{m_{\dot{\alpha}}}$	$C_{m_{\dot{\theta}}}$	C_{m_α}	0	4	4	2	0	2

TABLE 3

$(m - n) = (5 - 2) = 3$

$\ddot{\alpha}$	$\ddot{\theta}$	$\dot{\alpha}$	$\dot{\theta}$	α	θ	δ_e	Non-zero m_i	Not Given p_i	Determined d_i	Checked c_i	Unknown u_i
0	0	1	−1	$\frac{C_{L\alpha}}{2}$	0	0	3	1	1	2	0
0	$-h$	$C_{m_{\dot{\alpha}}}$	$C_{m_{\dot{\theta}}}$	C_{m_α}	0	$C_{m_{\delta_e}}$	5	5	3	0	2

TABLE 4

$(m - n) = (10 - 4) = 6$

$\ddot{\theta}$	$\ddot{\delta}_e$	$\dot{u}$	$\dot{\alpha}$	$\dot{\theta}$	$\dot{\delta}_e$	u	α	θ	δ_e	Non-zero m_i	Not Given p_i	Determined d_i	Checked c_i	Unknown u_i
0	0	1	0	0	0	C_D	$\frac{C_{D\alpha} - C_L}{2}$	$\frac{C_L}{2}$	0	4	3	3	3	0
0	0	0	1	−1	0	C_L	$\frac{C_{L\alpha}}{2}$	0	0	4	2	2	4	0
$-h$	0	0	$C_{m_{\dot{\alpha}}}$	$C_{m_{\dot{\theta}}}$	$C_{m_{\dot{\delta}_e}}$	C_{m_u}	C_{m_α}	0	$C_{m_{\delta_e}}$	7	7	6	0	1
$-l_1$	$-(l_1 + h_2)$	0	$-h_1$	$(C_{h_{\dot{\theta}}} + h_1)$	$C_{h_{\dot{\delta}_e}}$	C_{h_u}	C_{h_α}	0	$C_{h_{\delta_e}}$	8	8	6	0	2

All symbols are taken from reference 6

the equations of motion are taken from reference 6 in both cases.

(1) *Short-Period Motion Only.*—The equations of motion for this case are given nondimensionally in reference 6 on page 403. The degrees of freedom are plunging, α, and pitching, θ.

$$\dot{\alpha} - \dot{\theta} + (C_{L\alpha}/2)\alpha = 0$$

$$-h\ddot{\theta} + C_{m\dot{\alpha}}\dot{\alpha} + C_{m\dot{\theta}}\dot{\theta} + C_{m\alpha}\alpha = 0$$

where all symbols are defined in reference 6. Rewriting the coefficient matrix and applying the working rule gives Table 2.

For the example in Table 2, it may be noted that in each equation d_i coefficients may be determined in terms of u_i other unknown coefficients. For example, $C_{L\alpha}$ may be found outright, whereas two of h, $C_{m\dot{\alpha}}$, $C_{m\dot{\theta}}$, and $C_{m\alpha}$ may be found in terms of the remaining two. Notice also that adding a moment due to elevator deflection would alter the situation, as shown in Table 3. Thus, the addition of a forcing function permits checking one more coefficient from the first equation and finding one more in the second.

(2) *Longitudinal Motion Stick-Free.*—The equations for this fairly general case of longitudinal motion with four degrees of freedom are given in reference 6 on page 392. The degrees of freedom considered are axial velocity, u; plunging, α; pitching, θ; and elevator position, δ_e. The coefficient matrix from these equations is given in Table 4.

From Table 4 it is clear that in the first row, the three coefficients C_D, $(C_D - C_{L\alpha})/2$, and $C_L/2$ may be found. Also three zeros may be checked. In the second row, both C_L and $C_{L\alpha}/2$ may be found and four known coefficients may be checked. The C_L values from the first and second row will agree exactly only if the data are perfect. In the third row, six of the seven coefficients may be found in terms of the seventh. In the fourth row six of the eight coefficients may be found in terms of the remaining two. If two linearly independent known forcing functions were introduced (e.g., rockets at two points fired at separate times), then u_i would be zero for all equations and all coefficients could be determined.

References

[1] Greenberg, H., *A Survey of Methods for Determining Stability of an Airplane from Dynamic Flight Measurements*, NACA TN No. 2340, April, 1951.

[2] Milliken, William, Jr., *Dynamic Stability and Control Research;* Proceedings, Anglo-American Aeronautical Conference, RAeS-IAS, Brighton, England, September 4–7, 1951.

[3] Swanson, R. S., and Mastrocola, N., *Preliminary Report on Methods for Determining Dynamic Stability Parameters from Free-Flight Tests*, Technical Report No. 58, U.S. NAMTC, Point Mugu, Calif., September, 1949.

[4] Frazer, R. A., Duncan, W. J., and Collar, A. R., *Elementary Matrices*, p. 18; Cambridge University Press, New York, 1938.

[5] Halmos, P. R., *Finite Dimensional Vector Spaces;* Princeton University Press, Princeton, N.J., 1948.

[6] Perkins, C. D., and Hage, R. E., *Airplane Performance Stability and Control;* John Wiley & Sons, Inc., New York, 1949.

Suggestion for Binding
Issues of the Journal of the Aeronautical Sciences

Arrangements have been made so that our readers may have their issues of the JOURNAL bound carefully and economically in our authorized binding. Simply write for details to:

AIRE
P.O. Box 776
Highland Park, Illinois

A Simplified Method to Obtain the Load Distribution Corresponding to the Ackeret Region for Wings Having Arbitrary Source Distribution at Supersonic Speeds

JULIAN H. KAINER*
Ryan Aeronautical Company

SUMMARY

A simplified approach to the loading on swept and triangular wings of planar and nonplanar form at supersonic speeds was presented[1, 2] which required the potential in the region between the supersonic leading edge and the leading-edge disturbance wave. It is the purpose herein to indicate a simple means of obtaining these potentials and to justify the method with mathematical and physical reasoning. The process involved is inspection.

INTRODUCTION

SEVERAL THEORETICAL STUDIES[1, 2] have been completed as a result of the current interest in the supersonic loading distributions due to aeroelastic and/or twist and camber effects on swept and triangular wings. The means of applying the quasi-conical solutions[1, 2] to the construction of the span loading on swept wings, in particular, requires a knowledge of the loading in the region bounded by the supersonic leading edge and the disturbance waves emanating from the root and tip chords. Hereinafter this region will be referred to as the Ackeret region, since it corresponds to a swept wing of infinite span. Experience has shown that the desired solutions are obtained by inspection of the existing solutions for the flow within the root and/or tip Mach cones.

SYMBOLS

V	= free-stream velocity
M	= free-stream Mach Number
β	= $\sqrt{M^2 - 1}$
(x, y, z)	= Cartesian coordinates
P	= a point inside a Mach cone
P_1	= a point outside a Mach cone
u, v, w	= perturbations and/or components of velocity in the (x, y, z) directions, respectively
ϕ or Φ	= velocity potential
(ξ, η) or (ξ_i, η_i)	= Cartesian coordinates of a source disturbance
I_P or I_{P_1}	= source strength of a point inside or outside the Mach cone, respectively
R, R_1	= area within the fore-cone of a point P or P_1, respectively
θ_1	= arc cos $[(1 - mt)/(m - t)]$
θ_2	= arc cos $[(1 + mt)/(m + t)]$
θ_3	= arc cosh $(1/t)$
t	= $\beta y/x$
ϵ	= wing apex angle
m	= $\beta \tan \epsilon$

Received May 5, 1953.
* Aerodynamics Engineer.

ANALYSIS

Theorem

Given the potential for a point $P(x, y)$ within the after-cone of the leading-edge disturbance at 0, the potential for any point P_1 on the wing exterior to the leading-edge disturbance is obtained by retaining only the pure real expressions when P is replaced by P_1.

Proof

Let u, v, and w be the perturbation velocities in the x, y, and z directions, respectively. Furthermore, define the pure real potential ϕ (or Φ),

$$\phi = \oint (u\,dx + v\,dy + w\,dz) \tag{1}$$

Puckett[3] has shown that in the plane of the wing the potential at a point $P(x, y)$ is represented by a summation of all sources, (ξ_i, η_i) located within the fore-cone R of the point P; hence,

$$\Phi_P \equiv \int_R \int \frac{I_P\,d\xi\,d\eta}{\sqrt{(x_P - \xi_i)^2 - \beta^2(y_P - \eta_i)^2}} \tag{2}$$

where (x, y) represents the Cartesian coordinates of a point within the leading Mach cone, (ξ_i, η_i) are the Cartesian coordinates of source disturbances in R, and I_P is the source strength at (x, y).

Then, by definition, the potential at a point $P_1(x_{P_1}, y_{P_1})$ exterior to the leading-edge Mach cone is defined similar to Eq. (3) as

$$\Phi_{P_1} \equiv \int_{R_1} \int \frac{I_{P_1}\,d\xi\,d\eta}{\sqrt{(x_{P_1} - \xi_i)^2 - \beta^2(y_{P_1} - \eta_i)^2}} \tag{3}$$

Eq. (2) is now expanded as follows:

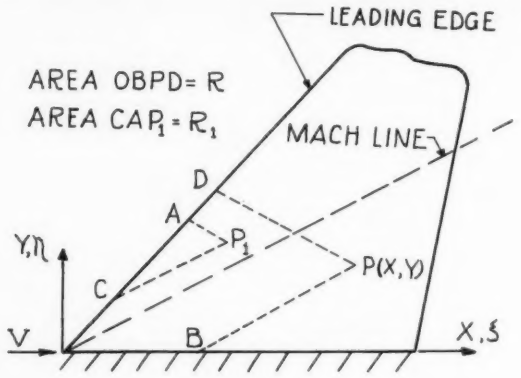

Fig. 1. Typical configuration.

$$\phi_P = \Phi_P \equiv \int_R\int \frac{I_P\, d\xi\, d\eta}{\sqrt{(x_P - \xi_i)^2 - \beta^2(y_P - \eta_i)^2}} \tag{2}$$

$$= \int_{R_1}\int \frac{I_P\, d\xi\, d\eta}{\sqrt{(x_P - \xi_i)^2 - \beta^2(y_P - \eta_i)^2}} + \int_{R\,-\,R_1}\int \frac{I_P\, d\xi\, d\eta}{\sqrt{(x_P - \xi_i)^2 - \beta^2(y_P - \eta_i)^2}} \tag{4}$$

where all expressions under the integrals are pure real since $(x_P - \xi_i) \geq \beta(y_P - \eta_i)$.

The potential at $P_1(x_{P_1}, y_{P_1})$ is obtained by changing proper subscripts in Eq. (4), thus

$$\phi_{P_1} = \int_{R_1}\int \frac{I_{P_1}\, d\xi\, d\eta}{\sqrt{(x_{P_1} - \xi_i)^2 - \beta^2(y_{P_1} - \eta_i)^2}} + \int_{R\,-\,R_1}\int \frac{I_{P_1}\, d\xi\, d\eta}{\sqrt{(x_{P_1} - \xi_i')^2 - \beta^2(y_{P1} - \eta_i')^2}} \tag{5}$$

where (ξ_i, η_i) are sources located in R_1 (area CAP_1) and (ξ_i', η_i') are sources located in R-R_1, where $(x_{P_1} - \xi_i') \leq \beta(y_{P_1} - \eta_i')$.

By examination it is noted that the expression immediately to the right of the equality signs in Eq. (5) is identically the expression Φ_{P_1} defined in Eq. (3); hence,

$$\phi_{P_1} = \Phi_{P_1} + \int_{R\,-\,R_1}\int \frac{I_{P_1}\, d\xi\, d\eta}{\sqrt{(x_{P_1} - \xi_i') - \beta^2(y_{P_1} - \eta_i')^2}} \tag{6}$$

Since $(x_{P_1} - \xi_i') \leq \beta(y_{P_1} - \eta_i')$, Eq. (6) may be written in the form of the complex potential,

$$\phi_{P_1} = \Phi_{P_1} - i\int_{R\,-\,R_1}\int \frac{I_{P_1}\, d\xi\, d\eta}{\sqrt{\beta^2(y_{P_1} - \eta_i')^2 - (x_{P_1} - \xi_i')^2}} \tag{7}$$

By physical identity,

$$\phi_{P_1} \equiv \Phi_{P_1} \tag{8}$$

so the only mathematical means of expressing the potential at P_1 from the expression for ϕ_{P_1} derived from Eq. (7) is that

$$\phi_{P_1} = \text{real part } \Phi_P \tag{9}$$

In order to secure physical consistency for the expression just derived, it is necessary to prove only that the imaginary potential has no physical contribution to the potential at P_1. This is immediately apparent upon consideration of the manner in which the disturbances in a uniform supersonic stream are propagated (see, for example, Puckett[3]). A disturbance located at (x, y) in a uniform supersonic flow creates a stationary conical wave front in which the effects of the disturbances are felt. Hence, a point in a source field is disturbed only by those sources that lie within the fore-cone of the point in question. It may be shown geometrically that the imaginary function corresponds to the source distribution (ξ_i', η_i') in the field $(R - R_1)$ that does not lie within the fore-cone of $P_1(x_{P_1}, y_{P_1})$. Therefore, it may be implied that the imaginary functions appearing in ϕ_{P_1} = function of Φ_P do not contribute to the velocity potential at P_1. This constitutes a physical proof for the mathematical derivation that the potential in the Ackeret region may be obtained by retaining only the real part of the three-dimensional potential.

The form of the loading functions[1, 2] within the Mach cone is quasi-conical—i.e.,

$$\phi = x^i\phi(t) \tag{10}$$

where the conical functions $\phi(t)$ consist of various combinations of polynomials in m and t multiplied by the various antitrigonometric functions (i.e., θ_1 and θ_2), various inverse hyperbolic functions (i.e., θ_3), and various irrational functions in t.[1, 2] In the Ackeret region $(1 \leq t \leq m)$ all the above functions become complex, the real part of which is zero with the exception of θ_1, which becomes equal to π. Hence, $\phi(t)$ reduces simply to that polynomial in (m, t) which is the coefficient of θ_1 with θ_1 replaced by π.

References

[1] Kainer, Julian H., *Equations for the Loading on Triangular Wings Having Supersonic Leading and Trailing Edges Due to Various Basic Twist Distributions*, Journal of the Aeronautical Sciences, Vol. 20, No. 7, pp. 469–476, July, 1953.

[2] Kainer, Julian H., and Kazan, Elliott, *Equations for the Potential, Pressure, and Span Load Distributions on Swept Wings Having Supersonic Leading Edges Due to Various Basic Twist Distributions With Application to the Aeroelastic Problem*, Proposed Republic Aviation Corp. Report No. EAR 280.

[3] Puckett, Allen E., *Supersonic Wave Drag of Thin Airfoils*, Journal of the Aeronautical Sciences, Vol. 13, No. 9, pp. 475–484, September, 1946.

Airflow About Cone-Cylinders with Curved Shock Waves

V. E. BERGDOLT

Ballistics Research Laboratories, Aberdeen Proving Ground

ABSTRACT

Flows about 35° cone-cylinders in free flight at Mach Numbers ranging from the régime of detached shocks to the region where completely supersonic Taylor-Maccoll flow has been established have been investigated with interferometric techniques. Measured fringe shifts from the interferograms, density distributions, and the corresponding pressures have been compared with theoretical predictions and wind-tunnel data. Good agreement has been found with theory and other experiments.

(I) INTRODUCTION

THE FLOW ABOUT an infinite solid cone traveling through air at supersonic velocity has been determined mathematically, with certain assumptions, by Taylor and Maccoll[1] and others.[2] Depending on the free-stream Mach Number, there are three possible types of solutions: The flow behind the shock wave can be completely subsonic, subsonic on the cone and supersonic behind the shock, or wholly supersonic. The limits for these flow régimes are tabulated by Kopal[2] as functions of Mach Number and cone angle.

For the cone-cylinder or any practical model with a finite cone, only the completely supersonic flow can be realized. Partially subsonic Taylor-Maccoll flow cannot occur on a finite cone because the influence of the change in model contour would be propagated upstream through the subsonic flow along the cone, thereby disrupting the conical nature of the flow. However, the shock wave remains attached down to the minimum Mach Number for Taylor-Maccoll flow but now is curved because of the influence of the corner. Below this Mach Number, the shock is detached. It was the purpose of this program to investigate by interferometric techniques flows over cone-cylinders in free flight from the region of detached shocks to the establishment of completely supersonic Taylor-Maccoll flow.

In a supersonic wind tunnel at the California Institute of Technology, Mac Kinnon[3] determined pressure distributions over the surface of 35° (semiangle) cone-cylinder models. His test Mach Numbers ranged from 1.49 for a detached shock wave to 1.997, where the flow is theoretically completely supersonic. In the present work, geometrically similar projectiles were fired at approximately the same Mach Numbers in order to make comparisons between the wind-tunnel and interferometric data.

For the 35° cone, the theoretical limits of the three flow régimes are at Mach Numbers 1.681, 1.769, and 1.911. The wind-tunnel tests were at Mach Numbers 1.49 for a detached shock wave, 1.636 for a detached shock just before attachment, 1.694 for completely subsonic flow behind the shock wave, 1.86 for mixed subsonic and supersonic flow, and 1.997 for completely supersonic flow. The projectile models were fired at Mach Numbers of 1.49, 1.64, 1.69, 1.87, and 2.03.

(II) EXPERIMENTAL DETAILS

The models were brass cone-cylinders incorporating a rotating band for spin stabilization and having a 35° semicone angle, Fig. 1. They were launched from a caliber 0.30 rifle in the enclosed Model Firing Range.[4,12] A velocity-measuring system consisting of photocell triggering beams and a 1.6 mc. electronic counter gave velocity for each round fired. Interferograms, of which Fig. 2 at $M = 1.49$ is typical, were obtained with a 2-in. Mach-Zehnder interferometer and a rotating mirror camera system. The light source was a B-H6 mercury tube flashed by the discharge of a 0.07-microfarad condenser charged to 13,000 volts and used in conjunction with a carbon-bisulfide liquid prism monochromator. This source has an effective duration of approximately 5 microsec. during which the projectiles move about 3 mm., but the projectile image is stopped on the film with the rotating mirror. The monochromator was adjusted to have a pass band of approximately 55Å. in the region of the 4,358Å. mercury line. This gave 150 good fringes across the interferometer field.

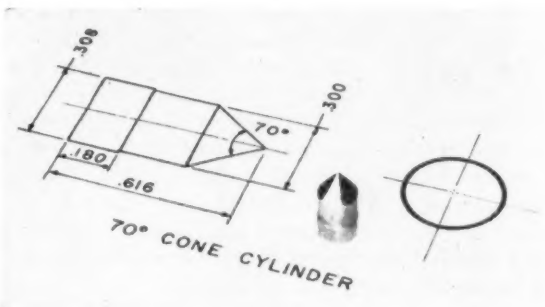

FIG. 1.

Received March 25, 1953.

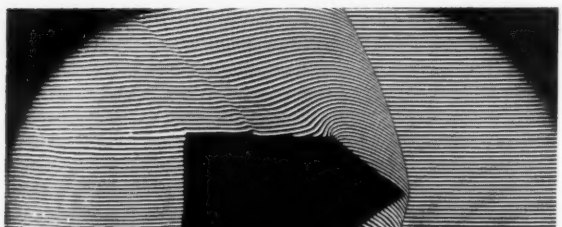

FIG. 2.

(III) DATA REDUCTION

From fringe shifts measured on the interferogram, the air density can be computed throughout an axisymmetric disturbance such as that generated by the cone-cylinder model.[5, 9] When this flow is observed by a Mach-Zehnder interferometer, the fringe shift at the point (y, z) on the film is related to the ratio of disturbed to free-stream density ρ/ρ_1 by

$$\delta_{(y,\,z)} = \frac{2K\rho_1}{\lambda} \int_y^{r_N} \frac{[(\rho_{(r,\,z)}/\rho_1) - 1]}{\sqrt{r^2 - y^2}}\, r\, dr \qquad (1)$$

where (y, z) are cartesian coordinates with the z axis on the axis of symmetry, K is the Gladstone-Dale constant (i.e., the ratio of increments of index of refraction to increments of density), λ is the vacuum wave length of the monochromatic light source, and $y = r_N$ at the shock on the trace z = constant. The solution of this Abel integral equation is

$$\frac{\rho_{(r,\,z)}}{\rho_1} = 1 - \frac{K\rho_1}{\pi\lambda} \int_y^{r_N} \frac{\partial\delta_{(r,\,z)}/\partial r}{\sqrt{r^2 - y^2}}\, dr \qquad (2)$$

For numerical work this can be manipulated into the form

$$\frac{\rho_{(r,\,z)}}{\rho_1} = 1 - \frac{2\lambda}{\pi K\rho_1} \sum_{j=i}^{N-1} \frac{\delta_{j+1} - \delta_j}{\sqrt{r_{j+1}^2 - r_i^2} + \sqrt{r_j^2 - r_i^2}} \qquad (3)$$

where $r = r_j$ $(j = 1, \ldots, N)$ is a monotone sequence of values on the relevant part of the trace, $y = r_i$, and $\delta_j = \delta_{(r_j,\,z)}$.

Fringe locations on the interferograms, Fig. 2, were measured with a Carl Zeiss toolmaker's microscope.

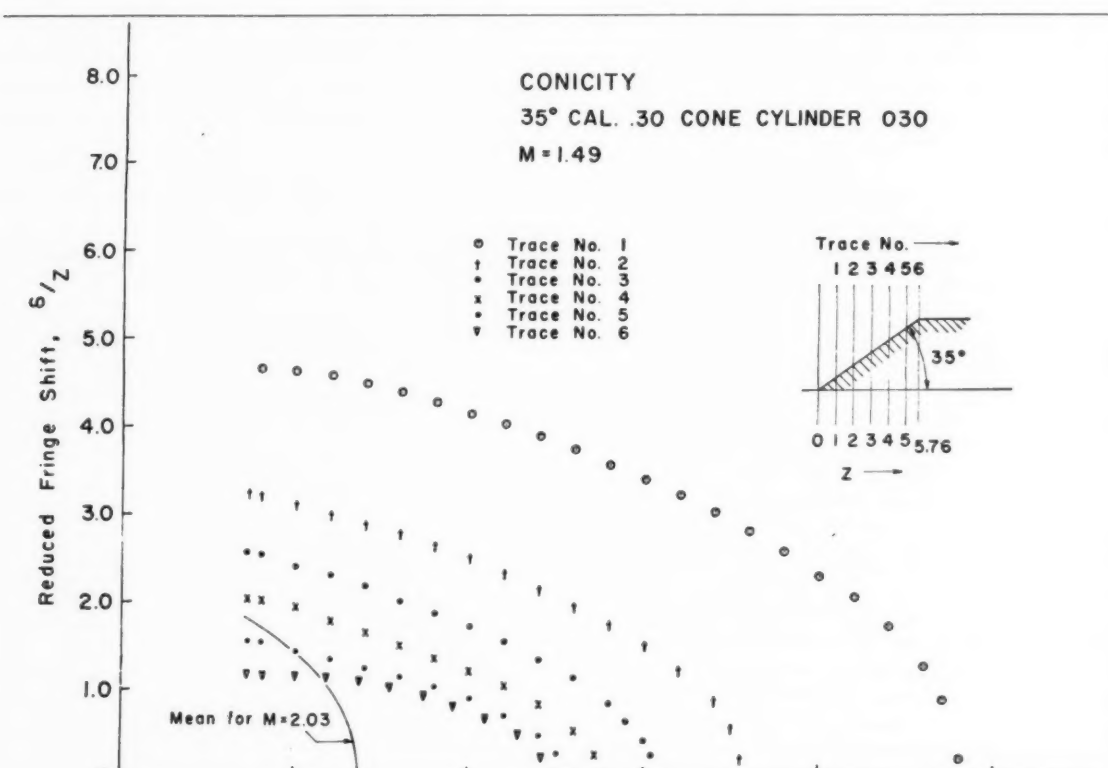

FIG. 3.

Fringe shift values δ_j were obtained along traces z = constant perpendicular to the flow axis at multiples of 1 mm. from the projectile tip, Fig. 3. The calculation of density from fringe shifts is a lengthy operation, involving the determination of as many as 3,500 values for an accurate reduction of an interferogram. The actual computation has been performed on the ENIAC, a machine well adapted for such work. A detailed description of the interferometric data reduction process is given in reference 9.

From a knowledge of the density ratio ρ/ρ_1, the pressure, the temperature, and the velocity can be determined by well-known relations from compressible-flow theory.[6] In the present investigation, ratios of surface pressure along the model to the free-stream stagnation pressure were required. Now

$$p/p_{10} = (p/p_{20})\ (p_{20}/p_{10}) \tag{4}$$

where p denotes static pressure and where subscript 0 refers to stagnation values; 1, to upstream conditions; and 2, to the downstream side of the shock.

$$p/p_{20} = (\rho/\rho_{20})^{\gamma} \tag{5}$$

where p_{20} and ρ_{20} are constant on segments of stream lines between successive shocks. Also,

$$\rho/\rho_{20} = (\rho/\rho_1)\ (\rho_1/\rho_{10})\ (\rho_{10}/\rho_{20}) \tag{6}$$

By isentropic flow relations,

$$\rho_1/\rho_{10} = [1 + (1/2)\ (\gamma - 1)\ M_1^2]^{-1/(\gamma-1)} \tag{7}$$

where M_1 is the Mach Number of the undisturbed stream. Finally, by shock conditions,

$$\frac{p_{20}}{p_{10}} = \frac{\rho_{20}}{\rho_{10}} = \left[\frac{(\gamma + 1)\ M_1^2 \sin^2 \sigma}{(\gamma - 1)\ M_1^2 \sin^2 \sigma + 2}\right]^{\gamma/(\gamma-1)} \times \left[\frac{\gamma + 1}{2\gamma M_1^2 \sin^2 \sigma - (\gamma - 1)}\right]^{1/(\gamma-1)} \tag{8}$$

where σ is the shock-wave angle. Values for Eq. (7) are tabulated as functions of M_1 and for Eq. (8) as functions of $M_1 \sin \sigma$ by Emmons[7] and in reference 11. It will be assumed that the model profile is a stream line along which these formulas are applicable.

(IV) Experimental Results

(A) Conicity

For the Taylor-Maccoll or conical-flow model in the region bounded by the cone and the shock wave, velocity components, density, and pressure do not vary along straight lines emanating from the vertex of the cone. It follows that, if the fringe shift δ is measured as a function of radial distance Y along traces perpendicular to the cone axis at various values of z from the tip, then the points $(Y/z,\ \delta/z)$ should fall on a single curve.[8] The degree to which these points produce a single curve is a measure of the conicity or approach to conical flow.

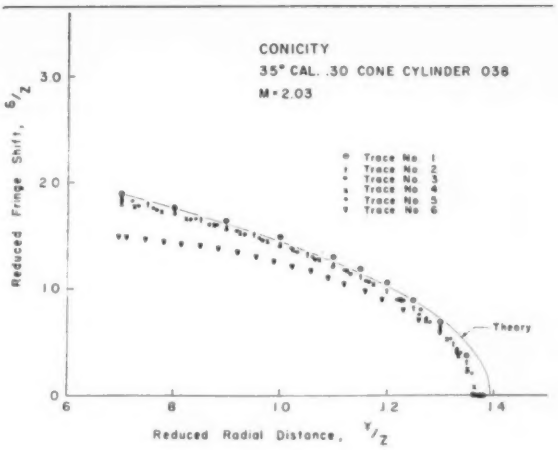

FIG. 4.

Figs. 3 and 4 show the development of conicity, ranging from the widely scattered data for definitely nonconical flow at $M = 1.49$ to approximately conical flow at $M = 2.03$. The radial distance Y is measured from the cone axis, and the traces terminate at the shock wave where the fringe shift becomes zero. Appreciable convergence has occurred when the shock wave becomes attached, but there is no pronounced tendency toward conicity until the limit for completely supersonic Taylor-Maccoll flow is approached. The plot for $M = 2.03$ shows good convergence and agreement with theory, except for the last trace which appears to reflect some influence of the corner.

(B) Isopycnals

For the pressure distribution along the model surface, it would suffice on each trace to find the density only at the body. It is desirable to have the density over a substantial part of the trace in order to detect errors in the calculation. If these are isolated points, which is the usual case, the density values are graphically smoothed to eliminate the errors. The calculation time is not increased appreciably if the entire trace is computed, so all reductions are carried through to produce the complete density field, Figs. 5 and 6.

The conical-flow region for the cone-cylinder model is bounded by the cone surface, the shock wave, and the characteristic from the shoulder. Beyond this characteristic is a region of expansion produced by the flow turning the corner. If Taylor-Maccoll flow exists within the conical region, the isopycnals should theoretically be straight lines emanating from the cone vertex. Fig. 6 shows this general radial pattern in the conical region, to within the experimental error, and the expansion that occurs around the corner. At the Mach Numbers below the supersonic régime, the radial pattern changes to one where the isopycnals gradually loop back to the cone surface with no appearance of conicity. For these cases with the curved shock

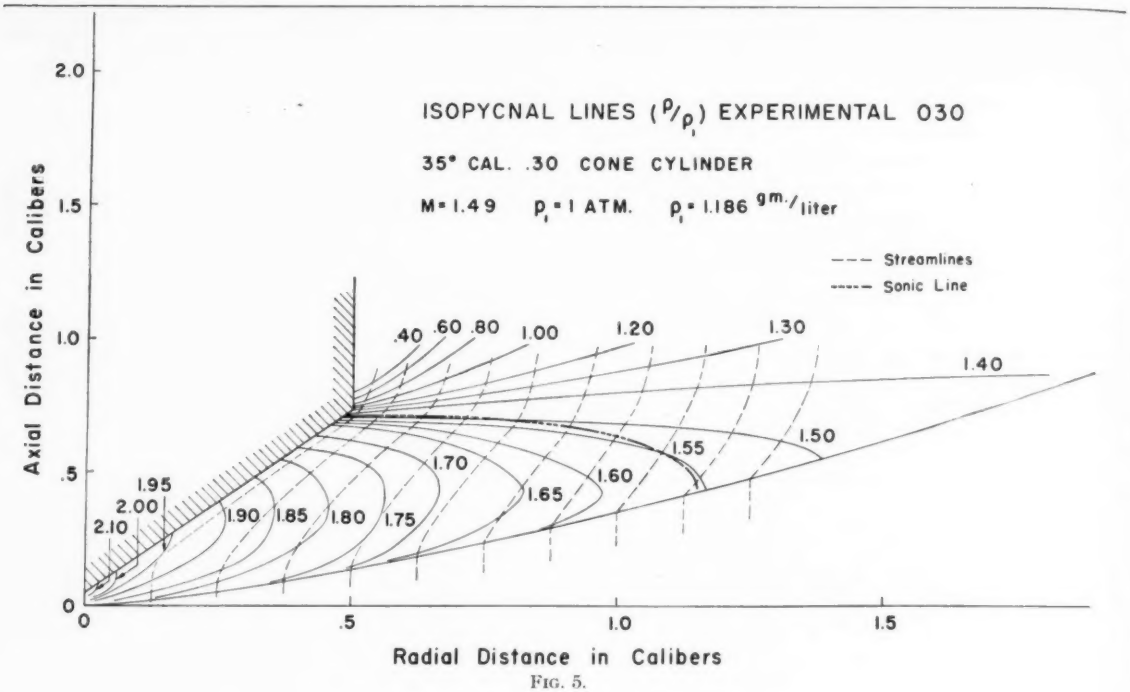
ISOPYCNAL LINES (ρ/ρ_i) EXPERIMENTAL 030
35° CAL. .30 CONE CYLINDER
M = 1.49 p_i = 1 ATM. ρ_i = 1.186 gm./liter
Streamlines
Sonic Line
Axial Distance in Calibers
Radial Distance in Calibers
.40 .60 .80 1.00 1.20 1.30 1.40 1.50 1.55 1.60 1.65 1.70 1.75 1.80 1.85 1.90 1.95 2.00 2.10
0 .5 1.0 1.5 2.0

FIG. 5.

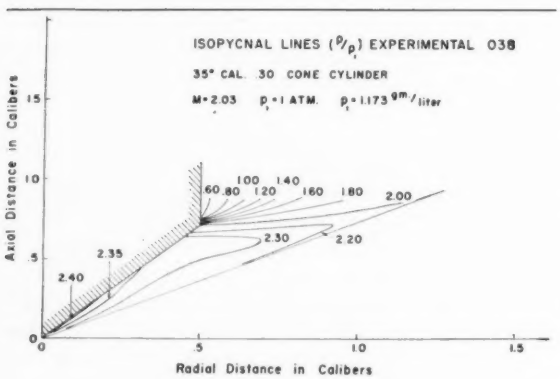
ISOPYCNAL LINES (ρ/ρ_i) EXPERIMENTAL 038
35° CAL. 30 CONE CYLINDER
M = 2.03 p_i = 1 ATM. ρ_i = 1.173 gm./liter
Axial Distance in Calibers
Radial Distance in Calibers
.60 .80 1.00 1.20 1.40 1.60 1.80 2.00 2.20 2.30 2.35 2.40
0 .5 1.0 1.5

FIG. 6.

wave, it is expected that the flow will attain sonic velocity at the corner and that the expansion region will develop as in the supersonic case. This expansion is shown in all the isopycnals, as well as an early expansion that occurs ahead of the corner. This effect is discussed in the following section. The high-density gradient associated with the corner expansion results in a high fringe shift gradient, which can be seen on the interferograms.

For conical flow, the density along the cone should be constant, since the surface defines a straight line from the cone vertex. At Mach Number 2.03, Fig. 6, the density is not actually constant. Because of practical limitations in the construction of the models, the tip is not perfectly sharp so that the flow encounters a truncated or rounded cone which means a detached shock wave. The detachment is so slight that it is obscured by the relatively wide fringes. There are reduction errors[9] and probably yaw effects contributing to the departure from constant density. These effects are manifest in the slightly increased density near the tip, which has also been observed independently by Ladenburg.[5]

Of immediate interest is the location of the sonic line in the subsonic flow cases. Along the stream lines, the velocity and pressure are specifically related to the density by suitable forms of Eqs. (5) and (7). Since the stagnation values of density vary from one stream line to another, it is necessary to have the system of stream lines in the flow. These stream lines can be found from the density by a semigraphical method[10] based on the equation of continuity for a stream tube bounded by two stream lines. In Fig. 5 the stream lines and the sonic line have been superimposed upon the isopycnals. The sonic line intersects the cone just ahead of the corner at a slant height of 0.98 from the vertex. On the pressure distribution plot of Fig. 7, the sonic value intersects the 031 curve at an X/S of 0.97.

The reduction of the interferometric data to densities is based on the assumption of zero yaw. This condition is usually not realized, although projectiles can be fired with yaws of 20 to 40 min. Interferograms are considered suitable for reduction if the yaw is approximately half a degree or less. The two halves of the

flow then are not identical and are considered as two separate flows, each representing an axisymmetric model. If the interferogram of Fig. 2 is studied, it is evident that the accuracy of film measurement differs for the two halves, since the fringe pattern is more favorable on the top side. The difference in fringe shift values is such as to prevent averaging the two sides. In Figs. 7 to 9 the actual divergence of the two halves can be seen for the pressure distributions.

(C) *Pressures*

The general transition of the flow from the detached shock wave to the supersonic condition is shown in the pressure distributions of Figs. 7 to 9. For Mach Number 1.49, the shock wave is detached, and there is no resemblance to the constant pressure distribution for Taylor-Maccoll flow. At the cone vertex the value is that for the stagnation pressure behind a normal shock. The rapid drop in the pressure curves indicates the rapid increase of velocity necessary for the flow to attain the predicted sonic velocity at the corner. Since the flow is theoretically sonic at the corner, there should be a Prandtl-Meyer expansion here. The experimental values appear to be in good agreement with the predicted expansion, but the expansion begins ahead of the corner and the sonic point likewise moves ahead. This might be expected, since it is conjec-

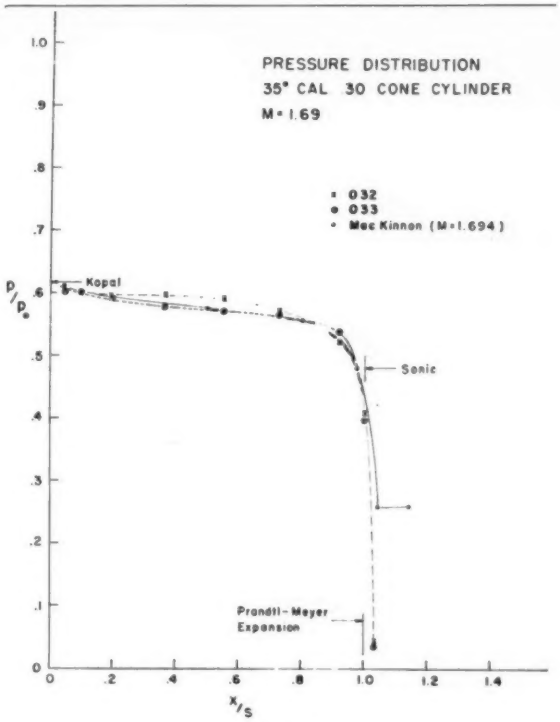

FIG. 8.

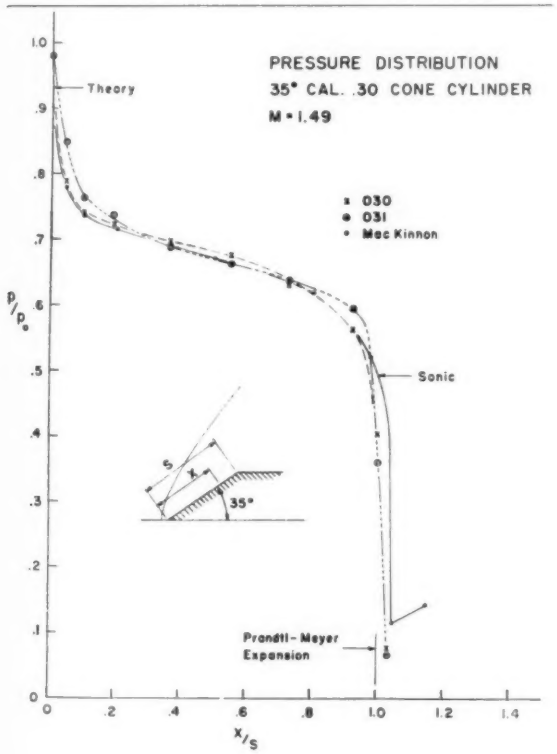

FIG. 7.

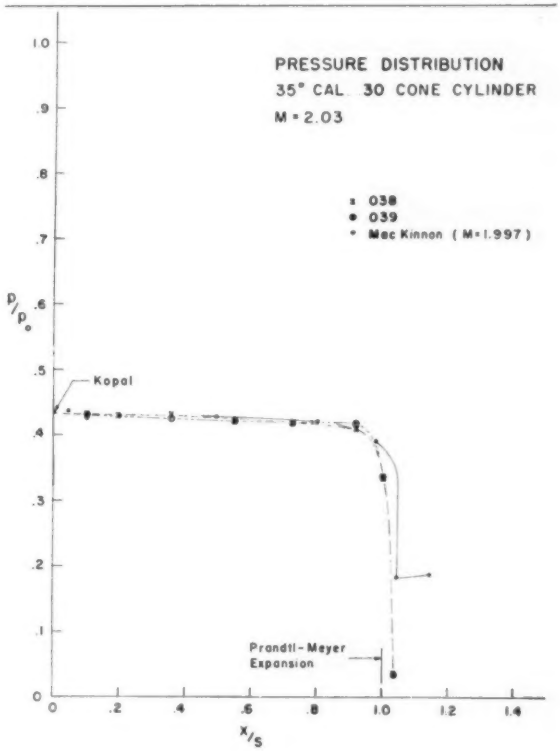

FIG. 9.

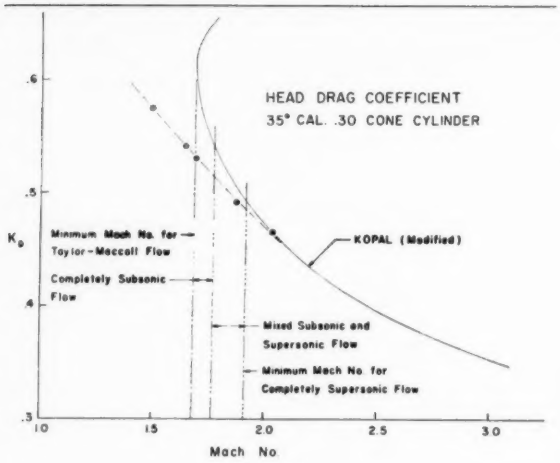

FIG. 10.

tured that the boundary layer builds up along the cone and rounds off the corner, so that the corner seems to move forward and the flow does not actually follow the cone-cylinder profile. The early expansion of the flow at the corner was observed in all the cases.

The character of the pressure distribution changes when the shock wave becomes attached, Fig. 8. The pressures encountered near the tip are reduced, since the tip is no longer a stagnation point, and the curves begin to assume the relatively flat appearance that is associated with the Taylor-Maccoll flow model. As the Mach Number increases toward the minimum for completely supersonic flow, the theoretical value for the cone surface pressure is approached. At Mach Number 2.03, Fig. 9, the flow should be completely supersonic along the cone, and the experimental results show that the pressure is virtually constant. There appears to be good agreement at all Mach Numbers with Mac Kinnon's results, as well as with the predictions of theory.

(D) *Head-Drag Coefficient*

The head drag on the model is a function of the pressure distribution over the cone surface. A form of head-drag coefficient is

$$K_D = \frac{D}{\rho_1 d^2 v^2} = \frac{\pi p_0}{2\rho_1 v^2} \int_0^1 \frac{p}{p_0} \left(\frac{X}{S}\right) d\left(\frac{X}{S}\right) = \frac{\pi}{2\gamma M_1^2} \left(1 + \frac{M_1^2}{5}\right)^{\gamma/(\gamma+1)} \int_0^1 \frac{p}{p_0} \left(\frac{X}{S}\right) d\left(\frac{X}{S}\right) \quad (9)$$

The five values shown in Fig. 10 were computed by this definition. For Taylor-Maccoll flow, Kopal[2] uses the usual definition based on excess pressure, $p_s - p_1$, to obtain

$$K_{D\text{Kopal}} = \left(\frac{p_s}{p_1} - 1\right) \frac{a_1^2}{\gamma v^2} = \left(\frac{p_s}{p_1} - 1\right) \frac{1}{\gamma M_1^2} \quad (10)$$

where p_s is the constant pressure along the cone surface. With the constant cone surface pressure, the relation between the two definitions becomes

$$K_D = (\pi/4)\ [K_{D\text{Kopal}} + (1/\gamma M_1^2)] \quad (11)$$

The Kopal (modified) curve was plotted from Eq. (11).

Below the completely supersonic régime, Fig. 10, the experimental values do not agree with theory, of course. However, the curve fairs smoothly into the theoretical plot in the supersonic régime. The failure of the two curves to be tangent at the supersonic flow limit is probably due to the pronounced rounding off of the pressure distribution curves near the model corner, which causes a reduction in the drag coefficient. In this particular case it should be remarked that extrapolation along the tangent to the theoretical curve at the completely supersonic limit will lead to values of K_D which are too high.

REFERENCES

[1] Taylor, G. I., and Maccoll, J. W., Proc. Roy. Soc., Vol. A139, pp. 278–311, 1933.

[2] Kopal, *Tables of Supersonic Flow of Air Around Cones*, Technical Report No. 1, Massachusetts Institute of Technology, 1947.

[3] Mac Kinnon, N. A., *Flow Field Around a Finite Cone With Shock*, Thesis, California Institute of Technology, 1949.

[4] Bergdolt, V. E., Greenwald, A. J., and Sleator, D. B., *A Pressurized Range for Small Caliber Projectiles*, BRLM Report No. 548, Aberdeen Proving Ground, May, 1951.

[5] Ladenburg, R., Winckler, J., and Van Voorhis, C. C., *Interferometric Studies of Faster than Sound Phenomena*, Part I, Phys. Rev., Vol. 73, p. 1359, 1948.

[6] Sauer, R., *Introduction to Gas Dynamics;* J. W. Edwards, Ann Arbor, Mich., 1947.

[7] Emmons, H. W., *Gas Dynamics Tables for Air;* Dover Publications, New York, 1947.

[8] Giese, J. H., Bennett, F. D., and Bergdolt, V. E., *A Simple Interferometric Test for Conical Flow*, J. Appl. Phys., Vol. 21, pp. 1226–1231, 1950.

[9] Bennett, F. D., Carter, W. C., and Bergdolt, V. E., *Interferometric Analysis of Airflow About Projectiles in Free Flight*, J. Appl. Phys., Vol. 23, pp. 453–469, 1952.

[10] Wood, G. P., and Gooderum, P. B., *Method of Determining Initial Tangents of Contours of Flow Variables Behind a Curved, Axially Symmetric Shock Wave*, NACA TN No. 2411, 1951.

[11] *Notes and Tables for Use in the Analysis of Supersonic Flow*, NACA TN No. 1428, December, 1947; *An Expansion of Tables 11 and 111 of NACA TN No. 1428*, BRL TN No. 482, July, 1951.

[12] Bergdolt, V. E., Greenwald, A. J., and Sleator, D. B., *The Model Range, A Pressurized Range for Small Caliber Projectiles in Free Flight*, Phys. Rev., Vol. 76, p. 879, 1949.

Two-Dimensional Unsymmetric Flow Patterns at Mach Number 1

GOTTFRIED GUDERLEY* AND HIDEO YOSHIHARA†
Wright Air Development Center

ABSTRACT

Two-dimensional unsymmetric flow patterns at Mach Number 1 are discussed by means of the hodograph representation. As an example, the flow over a wedge profile is investigated and the pressure distribution and the lift curve slope are computed. The results indicate that the value of the lift curve slope at Mach Number 1 is much lower than what would be expected by an extrapolation from the purely supersonic results.

INTRODUCTION

THE FLOW PATTERNS with the free-stream Mach Number 1 considered previously are all symmetric with respect to an axis parallel to the free-stream direction. In the present paper we shall extend these considerations to unsymmetric flows; in particular, we shall investigate the dissymmetry introduced by placing a symmetric wedge at an angle of attack.

The investigation will be carried out in the hodograph plane. Here the point that represents the free-stream velocity will be singular. This singularity has been discussed for symmetric flow patterns, but in the present case it must be re-examined.

Knowing the properties of this singular point, one can formulate the desired boundary value problem. In order to obtain the general character of unsymmetric flows, we shall first discuss the case of a body with a rounded nose, since a profile with a pointed leading edge (for example, a wedge) will have additional complications at an angle of attack because of a local supersonic region arising at the nose. The presence of this region is not a typical characteristic for a general profile with an angle of attack, and it adds the difficulty that the boundary value problem cannot be formulated because of the complexity of the flow over the sharp nose. On the other hand, a profile with a rounded leading edge gives rise to a difficult boundary condition in the hodograph plane when the profile is prescribed in the physical plane. To overcome this difficulty, we shall consider the flow over the body to be known for a given configuration—for example, at zero angle of attack. (This flow may be computed indirectly starting from the hodograph plane.) We then ask for the change of this flow due to a small angle of attack. In this case, the boundary conditions can be linearized to a convenient form. By these investigations, the general characteristics of an unsymmetric flow can be found. It will be seen in particular that the flow pattern is entirely determined by its boundary conditions—that is, no arbitrariness arises as in the case of incompressible flows where one required the Kutta condition to insure uniqueness.

The actual computations are carried out for a wedge profile; in this regard the present paper may be considered as a continuation of reference 1. The effect of the local supersonic region which must be expected at the nose will be shown to give a negligible contribution to the lift for sufficiently small angles of attack. Under these circumstances the wedge has the advantage that the boundary value problem in the hodograph plane can be formulated and solved with comparative ease. One will finally obtain the change of the pressure distribution over the wedge due to the angle of attack. In this way the slope of the lift curve and the location of the center of pressure may be found.

SECTION (I)—BASIC RELATIONS

Let us introduce the following symbols: x and y are the cartesian coordinates in the physical plane; w and θ, the magnitude and inclination of the velocity vector; p and ρ, the pressure and density of the gas; a, the velocity of sound; Ψ, the stream function; Φ, Legendre's transformed potential; and κ, the ratio of specific heats. The asterisk (*) will denote the conditions of the sonic state.

The flow is assumed to be such that the usual transonic approximations are valid (see reference 2). Under these conditions, the hodograph equations for the stream function and Legendre's potential may be simplified to

$$\Psi_{\eta\eta} - \eta\,\Psi_{\theta\theta} = 0 \tag{1}$$

$$\Phi_{\eta\eta} - \eta\,\Phi_{\theta\theta} = 0 \tag{2}$$

where

$$\eta = (\kappa + 1)^{1/3}\,[(w - w^*)/w^*] \tag{3}$$

Eqs. (1) and (2) are of the form investigated by Tricomi.[3] In the subsequent sections, we shall refer to either of them as the Tricomi equation.

The transformation equations from the hodograph plane to the physical plane assume an especially simple form in terms of the Legendre potential; one has

$$x = (\kappa + 1)^{1/3} \cdot \frac{1}{w^*} \cdot \Phi_\eta(\eta, \theta) \tag{4}$$

Received March 12, 1953.

* Aeronautical Research Laboratory.
† Wind Tunnel Branch, Aircraft Laboratory.

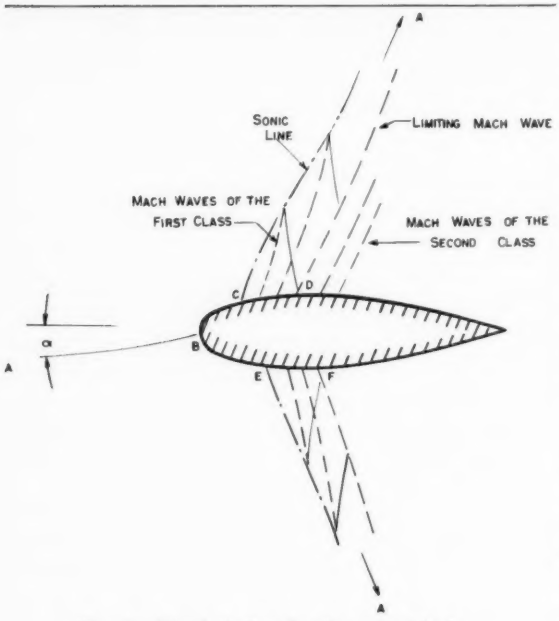

FIG. 1. Physical plane for the general body.

$$y = (1/w^*) \cdot \Phi_\theta \, (\eta, \theta)$$

Here the subscripts denote partial differentiations.

The corresponding expressions in terms of the stream function may be obtained by using the relation

$$\Psi = \rho^* \cdot \Phi_\theta \tag{5}$$

For the supersonic region, the characteristics and the compatibility relations are given by

$$\theta \mp (2/3)\eta^{3/2} = \text{const.} \tag{6a}$$

$$d(\Phi_\eta) - \eta \cdot (d\eta/d\theta) \cdot d(\Phi_\theta) = 0 \tag{6b}$$

In the physical plane, the direction of the Mach waves will be

$$dy/dx = \pm \, (\kappa + 1)^{-1/2} \cdot \eta^{-1/2} \tag{7}$$

Here the signs must be used consistently with those in Eq. (6a).

Consistent with our approximation, the pressure coefficient, C_p, is expressed in the form

$$C_p = (p - p^*)/(\rho^* w^{*2}/2) = -2(\kappa + 1)^{-1/2} \cdot \eta \tag{8}$$

SECTION (II)—THE FLOW OVER A SYMMETRIC BODY WITH A ROUNDED NOSE

(*A*) *The Hodograph*

The general flow configuration to be expected for a body with a rounded nose is shown in Fig. 1 with the corresponding hodograph plane shown in Fig. 2. Since all stream lines must originate far upstream of the profile with the free-stream conditions, they must all have their origin at the single point A in the hodograph plane representing the free-stream velocity. This point will, therefore, be a singular point for the stream function; we shall call it the free-stream singularity.

Let us trace the course of the zero stream line in order to orient ourselves in the hodograph plane. It starts at point A and proceeds toward the profile with decreasing velocity. It reaches the body at the stagnation point at B where the stream line branches. The course of these branches is then shown by the shaded lines. Along the upper branch, the velocity will now increase until at some point C the sonic velocity is reached. The velocity will then become supersonic along the segment of the zero stream line given by CD. One has a similar behavior along the lower branch.

Of the Mach waves starting from the body, one will have two classes; the first class is composed of those that reach the sonic line at a finite distance from the body, while those of the second never reach the sonic line (see Fig. 1). The distinction between these two classes is made in order to determine the portion of the supersonic region which influences the subsonic flow. It is clear that the subsonic flow cannot be completely determined by specifying only the contour of the body up to the sonic line. The segment of the profile from which the Mach waves of the first class originate must also be given, since a perturbation of this portion of the contour will propagate along the Mach waves of the first class to the sonic line and thus influence the subsonic flow. On the other hand, perturbations traveling along the Mach waves of the second class will never reach the sonic line and will not affect the subsonic flow. We must accordingly prescribe the contour of the profile downstream to the point from which the last Mach wave of the first class starts. This wave will have a special significance in our discussions, and we shall label it as the limiting Mach wave. Thus, in Fig. 2, we have shown the zero stream line only to points D and F. The limiting Mach waves are the characteristics AD and AF.

The continuation of the flow downstream of the limiting Mach wave may be computed independently by a purely supersonic method—for example, by the method of characteristics. Of course, the required initial conditions will be furnished by the solution for the flow at the limiting Mach wave, while the necessary boundary conditions are furnished by prescribing the remaining contour of the body. Incidentally, for a closed body, this portion of the flow will occur on several Riemann sheets in the hodograph plane.

(*B*) *The Free-Stream Singularity*

There exist particular solutions of Tricomi's equation which are singular at one point of the sonic line.[2] In the present section, we shall determine which of these particular solutions is suitable to represent the free-stream singularity mentioned in the previous section. For the stream function we use the hypothesis

$$\Psi_{ns} = \rho^* |\eta|^{n_s} \cdot f(\zeta, n_s) \tag{9}$$

where

$$\zeta = 9\theta^2/4\eta^3 \tag{10}$$

and for the Legendre potential

$$\Phi_{np} = |\eta|^{n_p} f(\zeta, n_p) \tag{11}$$

Here n is a constant with the subscripts s and p denoting whether the n refers to the stream function or to the potential. The function $f(\zeta, n)$ must fulfill the hypergeometric differential equation

$$\zeta(\zeta - 1) \cdot f'' + \left[\frac{2}{3}(2 - n)\zeta - \frac{1}{2}\right] \cdot f' + \frac{1}{9} n(n - 1) f = 0 \tag{12}$$

Because of Eq. (5), $\Psi = \rho^* \cdot \Phi_\theta$, particular solutions in terms of Ψ and Φ are closely connected. We have especially the relations

$$n_s = n_p - (3/2)$$

$$f(\zeta, n_s) = \frac{3(4n_p - 5)}{2n_p(n_p - 1)} \cdot |\zeta|^{1/2} \cdot f'(\zeta, n_p) \operatorname{sign}(\eta \cdot \theta) \tag{13}$$

where the symbol, sign $\eta \cdot \theta$, means a factor one with the sign of $\eta \cdot \theta$. Because of these relations, we may confine our subsequent considerations to only the stream function.

Before we proceed to determine the parameter n, let us first discuss the solutions of the hypergeometric equation, Eq. (12). The singular points of the equation are located at the values of ζ of 0, 1, and ∞. About each of these singular points there are two linearly independent power series solutions. For each value of ζ, we find a line in the η, θ-plane since $\zeta = (9\theta^2)/(4\eta^3)$. Therefore, about each of these lines there will be two linearly independent series solutions of the hypergeometric equation. If we choose the representation about one of the lines, then we must, from physical reasoning, determine the coefficients of the two linearly independent particular solutions about each of the other lines such that the stream function and its first derivatives are continuous in the entire region under consideration.

The choice of the solution f must be dictated from physical reasoning. It is clear that the singular points at $\zeta = 0$ and $\zeta = \infty$ are due solely to the form of the independent variable ζ; the singularity at $\zeta = 1$, on the other hand, is essential. In Fig. 2, if we take the origin of the hodograph plane at point A, the lines $\zeta = 1$ will represent the limiting Mach waves mentioned in a previous section. It is therefore logical that the selection of the correct representation of the function f be made by examining the series solution about this line. In the vicinity of this value of ζ, one of the linearly independent solutions of Eq. (12), denoted by $u_3(\zeta, n)$, is given by a power series in $(\zeta - 1)$ while the other, denoted by $v_3(\zeta, n)$, is given by a power series multiplied by a factor $(\zeta - 1)^{(4n+1)/6}$. Accordingly, the expression for Ψ formed with the portion u_3 is regular along the characteristics $\zeta = 1$, while that with v_3 will tend to infinity for negative values of n, the negative values of n being necessary to produce a singularity at the free stream point. The presence of a portion of the solution with v_3 will cause the characteristics $\zeta = 1$ to map to infinity in the physical plane. [See Eqs. (4) and (5) giving the transformation.] Since the characteristics $\zeta = 1$ correspond to the limiting Mach waves, we are naturally interested only in such cases for which the limiting Mach waves are not mapped completely to infinity in the physical plane.

With these remarks the permissible values of n may now be found. According to the previous discussion, we stipulate that the function $f(\zeta, n)$ must be given by $u_3(\zeta, n)$ along the limiting Mach waves AD and AF of Fig. 2. It is found that a solution $f(\zeta, n)$ for an arbitrary value of n which is represented along AD by $u_3(\zeta, n)$ is given along the other characteristic AF by a linear combination of u_3 and v_3, where the coefficients are functions of n (see reference 2). The condition that the coefficient of v_3 vanishes along AF will give a set of permissible values of n; we have $n_s = -1 - (3/2)k$, where $k = 0, 1, 2, \ldots$.

If we now investigate the physical plane resulting from the particular solutions with these values of n_s, we will find that a single-valued physical plane will result only for values of n_s equal to $-5/2$ and -1. We may therefore eliminate all but these values of n_s. Of these, the singularity produced by the particular solution for $n_s = -5/2$ is familiar; it is this that was used to represent the behavior of the flow at a far distance from the airfoil for the case of zero angle of attack. The par-

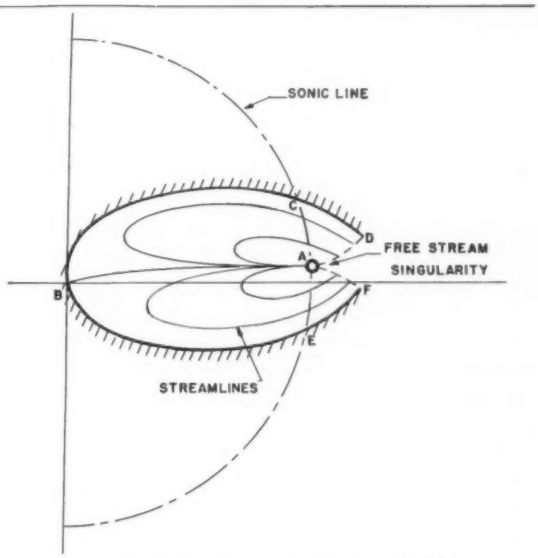

FIG. 2. Hodograph plane for the general body.

ticular solution with $n_s = -1$ taken by itself does not give a flow that is of interest at present. It may, however, still be used superimposed to the particular solution with $n_s = -5/2$, since, near the free-stream point, the latter particular solution will predominate. Therefore, the free-stream singularity can be represented by the expression

$$c_1 \cdot \Psi_{-(5/2)} + c_2 \cdot \Psi_{-1} \tag{14}$$

where c_1 and c_2 are *two* arbitrary constants and Ψ_{n_s} is defined in Eq. (9).

The corresponding representation for the free-stream singularity in terms of the Legendre potential may be found by using the relationship between n_s and n_p as given by Eq. (13). We have, therefore, $n_p = -1$ and $^1/_2$. The particular solution with $n_p = {}^1/_2$, however, is no longer singular at the free-stream point in the sense of Tricomi's existence and uniqueness proofs.[3] Consequently, in terms of the Legendre potential, the free-stream singularity is represented by only one singular particular solution, Φ_{-1}. Thus, there is but *one* arbitrary constant in this representation.

(C) *Boundary Value Problem for the General Profile*

As mentioned previously, the problem for a profile with a rounded nose will give a better insight into the mathematical and physical questions of unsymmetric flows, but it will assume a rather difficult form in the hodograph plane. For this reason, we must restrict our considerations to perturbations of a known flow. In this way, a linear boundary value problem will be obtained. We shall assume that the flow over a certain symmetric profile is known, and we want to find the influence of a small angle of attack. For this purpose, it is convenient to keep the position of the body fixed in space and to rotate the free-stream direction. In the hodograph, the free-stream singularity will then be shifted from the point ($\eta = 0, \theta = 0$) to the point ($\eta = 0, \theta = \alpha$), where α is the angle of attack. In order to obtain separately the change of the flow pattern due to the angle of attack, we ask which hodograph solution must be superimposed to the hodograph representation of the original flow with $\alpha = 0$ such that the flow with an angle of attack is obtained.

We must therefore subtract from the original solution, an expression $\Phi_{-1}(\eta, \theta)$ [see Eq. (11)], which contains the free-stream singularity for zero angle of attack, and then add another expression, $\Phi_{-1}(\eta, \theta - \alpha)$, which has the same singularity at the point ($\eta = 0, \theta = \alpha$). The coefficient with which this latter particular solution is multiplied, however, must be considered as a function of α, the angle of attack. We have, therefore, for the particular solution that performs the shift of the free-stream singularity, the expression

$$\varphi = \Phi_{-1}(\eta, \theta) - [1 + k(\alpha)]\, \Phi_{-1}(\eta, \theta - \alpha) \tag{15}$$

where $k(\alpha)$ is some function of α and φ is the Legendre potential which represents the change of the free-stream singularity due to the angle of attack. For sufficiently small angles of attack, the second term in Eq. (15) may be expanded with respect to α, with the result

$$\varphi = -k(\alpha) \cdot \Phi_{-1}(\eta, \theta) + [1 + k(\alpha)] \cdot \Phi_{-1,\theta} \cdot \alpha + 0(\alpha^2)$$

This expression describes the flow at a far distance from the body due to the angle of attack; it must therefore be antisymmetric in α. The term Φ_{-1} is an even function of θ; consequently, in order for the above expression to have the correct symmetry, we must take $k(\alpha)$ proportional to α^2. We have, therefore, as the terms of lowest order in α,

$$\varphi = \alpha \cdot \Phi_{-1,\theta}$$

This, according to Eq. (13), is equivalent to

$$\varphi = -(4/9)\alpha \cdot \Phi_{-(5/2)} \tag{16}$$

The boundary condition for the problem due to the angle of attack may be found as follows: The profile in the physical plane is first described in the parametric form

$$x = p_1(\theta) \cdot w^{*-1} (\kappa + 1)^{1/2}$$
$$y = p_2(\theta) \cdot w^{*-1}$$

where p_1 and p_2 depend upon the profile shape. Using Eq. (4), one then obtains

$$\left.\begin{aligned} \bar{\Phi}_\eta(\bar{\Pi}, \theta) &= p_1(\theta) \\ \bar{\Phi}_\theta(\bar{\Pi}, \theta) &= p_2(\theta) \end{aligned}\right\} \tag{17}$$

Here $\bar{\Phi}$ is Legendre's potential, and $\eta = \bar{\Pi}(\theta)$ is the hodograph of the profile, both for the case of zero angle of attack. [The fact that the function $\bar{\Pi}(\theta)$ is an unknown function will prevent us from considering the general case; we have assumed here that it is a given function.] By the change of the free-stream direction, the Legendre potential will be perturbed from $\bar{\Phi}$ to $\bar{\Phi} + \varphi$, where φ is due to the angle of attack. The hodograph of the body will also be changed from $\bar{\Pi}$ to $\bar{\Pi} + \bar{\eta}$. In order for the profile to be fixed in the physical plane, we must have, therefore,

$$\bar{\Phi}_\eta(\bar{\Pi} + \bar{\eta}, \theta) + \varphi_\eta(\bar{\Pi} + \bar{\eta}, \theta) = p_1(\theta)$$
$$\bar{\Phi}_\theta(\bar{\Pi} + \bar{\eta}, \theta) + \varphi_\eta(\bar{\Pi} + \bar{\eta}, \theta) = p_2(\theta)$$

For sufficiently small angles of attack, we may expand these expressions with respect to $\bar{\eta}$, and using Eq. (17), we obtain, as the terms of lowest order,

$$\bar{\eta}\, \bar{\Phi}_{\eta\eta}(\bar{\Pi}, \theta) + \varphi_\eta(\bar{\Pi}, \theta) = 0$$
$$\bar{\eta}\, \bar{\Phi}_{\eta\theta}(\bar{\Pi}, \theta) + \varphi_\theta(\bar{\Pi}, \theta) = 0$$

If we eliminate $\bar{\eta}$ between these two equations, we have

$$\varphi_\eta(\bar{\Pi}, \theta) - \left(\frac{\bar{\Phi}_{\eta\eta}(\bar{\Pi}, \theta)}{\bar{\Phi}_{\eta\theta}(\bar{\Pi}, \theta)}\right) \cdot \varphi_\theta(\bar{\Pi}, \theta) = 0 \tag{18}$$

Moreover, the contour $\eta = \bar{\Pi}(\theta)$ is a stream line; we

have, therefore, according to Eq. (5),

$$\bar{\Phi}_\theta(\bar{\Pi}, \theta) = 0$$

or differentiating

$$\bar{\Phi}_{\theta\theta}(\bar{\Pi}, \theta) + (d\bar{\Pi}/d\theta)\cdot\bar{\Phi}_{\eta\theta}(\bar{\Pi}, \theta) = 0$$

By using this relation and the Tricomi equation

$$\bar{\Phi}_{\eta\eta}(\bar{\Pi}, \theta) - \bar{\Pi}\cdot\bar{\Phi}_{\theta\theta}(\bar{\Pi}, \theta) = 0$$

one may rewrite Eq. (18) to

$$\varphi_\eta(\bar{\Pi}, \theta) + \bar{\Pi}\cdot(d\bar{\Pi}/d\theta)\cdot\varphi_\theta(\bar{\Pi}, \theta) = 0 \qquad (19)$$

This is now the boundary condition that must be fulfilled by the potential φ due to the angle of attack. It is to be fulfilled along the original hodograph of the body $\eta = \bar{\Pi}(\theta)$ for zero angle of attack.

The particular solution, $\Phi_{-(5/2)}$ [see Eq. (16)], which gives the required free-stream singularity will not generally fulfill the boundary condition (19) at the body. Therefore, one must superimpose additional regular particular solutions so as to correct the boundary conditions. The boundary value problem for determining the required regular portion of the solution is of a type that has not been investigated thoroughly. A few remarks, however, regarding the plausibility of existence and uniqueness of this type of problem have been given in reference 4. (Here, this type of problem has been called the boundary value problem of the second type because of its similarity to the problem of the second type in the potential theory.) According to these remarks, it appears that such problems do not possess a solution (at least no physically useful solution) unless the boundary values fulfill an additional condition. This condition will in general determine the expression $k(\alpha)$ in Eq. (15) which, in the present case of a symmetric body, was determined by consideration of symmetry.

Section (III)—The Wedge Profile

(A) *The Boundary Value Problem in the Hodograph Plane*

For the actual computations, a wedge profile will be used. Naturally, at a far distance from the body, the considerations of the previous case will hold; but near the body, especially at the nose of the wedge, one will have essential differences of the flow. A qualitative picture of such a flow is shown in Fig. 3 with the corresponding hodograph shown in Fig. 4. The main difference of this problem in comparison to that for a profile with a rounded leading edge is seen along the upper branch of the zero stream line. The zero stream line proceeds from the stagnation point at B upstream along the contour of the wedge to the nose, where a Meyer expansion produces either zero absolute pressure in the case of cavitation or some other pressure, probably supersonic, in the case of a separation of the flow. If the angle of attack is not too excessive, the flow will again reattach, with the zero stream line returning to the wedge at some point along the side DE. A real satisfactory formulation of the boundary value problem in the nose region is probably impossible. However, it is shown in the Appendix that, if one requires simply that the boundary condition (19) is fulfilled along the entire line BDE and disregards the nose region entirely, the contribution of the flow at the nose to the total lift is negligible for sufficiently small angles of attack.

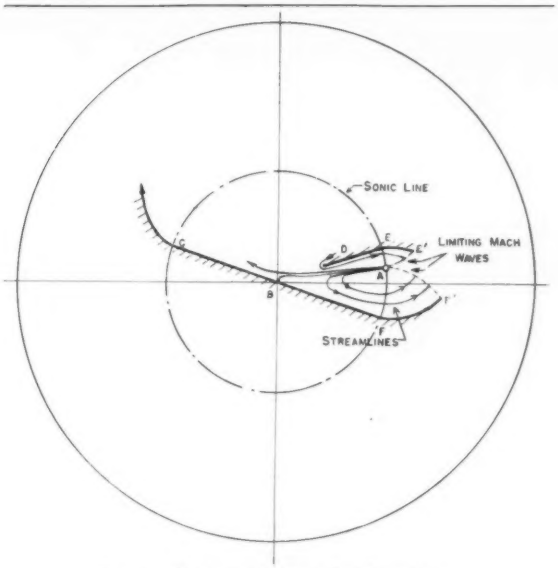

FIG. 3. Hodograph plane for the wedge.

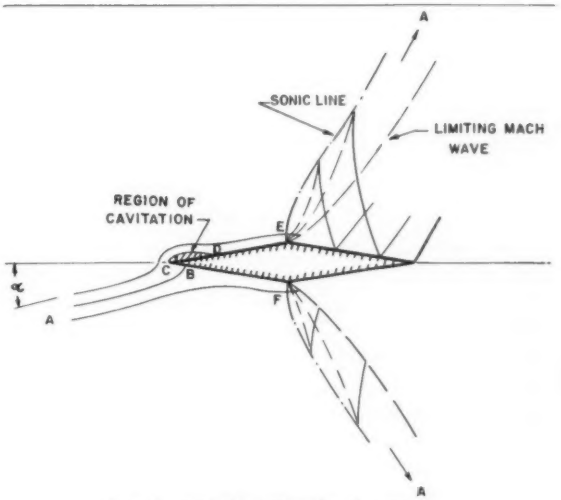

FIG. 4. Physical plane for the wedge.

Disregarding the flow over the nose we have, therefore, the problem of finding a solution of the Tricomi equation which has the required singularity at the free-stream point, as given by $\Phi_{-(5/2)}$, and which fulfills

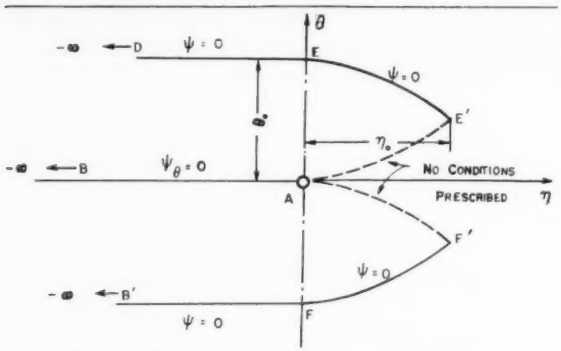

FIG. 5. Boundary conditions in the η, θ-plane.

the condition (19) along the sides of the wedge and along the characteristics representing the Meyer expansion at the shoulder of the profile.

In the present case, the boundary condition (19) can be simplified. Along the subsonic boundaries, θ is a constant, so that, here, the boundary condition becomes

$$\varphi_\theta = 0 \tag{20}$$

The supersonic boundary is formed by characteristics that are at the same time stream lines. Therefore, the image of this boundary will map to single points in the physical plane. The boundary conditions along the characteristics will thus simplify to

$$\varphi_\theta = 0, \qquad \varphi_\eta = 0 \tag{21}$$

In the case of the wedge, the boundary value problem can also be formulated in terms of the stream function. Let us denote by ψ the stream function that must be superimposed to the hodograph of the original flow in order to obtain the flow with an angle of attack. The necessary boundary condition for ψ can now be obtained by using the relation $\psi = \rho^* \varphi_\theta$ in Eqs. (20) and (21). We have, therefore, the condition $\psi = 0$ along the given boundary. Because of the symmetry of ψ, we may restrict our considerations only to the upper half of the hodograph plane. The required condition along the line of symmetry is then $\psi_\theta = 0$. These boundary conditions are illustrated in the upper half of Fig. 5.

The free-stream singularity for the complete hodograph (original flow plus the superimposed flow) was given by Eq. (14). The stream function, ψ, representing the change of the free-stream singularity due to the angle of attack, will be found in the same manner as for the Legendre potential. We have

$$\psi = -\frac{4}{9}[\Psi_{-(5/2)}(\eta, \theta) - (1 + \kappa_1(\alpha)\cdot\Psi_{-5/2}(\eta_1, \theta - \alpha)] + k_2(\alpha)\cdot\Psi_{-1}(\eta, \theta - \alpha) \tag{22}$$

Here the coefficient c_1 has been taken as $-4/9$ in order to obtain in the present paper the same scale in the physical plane as in reference 1. The functions $k_1(\alpha)$ and $k_2(\alpha)$ have been introduced, since the coefficient of the singularities at the point ($\eta = 0$, $\theta = \alpha$) are still undetermined. If in Eq. (22) we now carry out a development with respect to α and apply considerations of symmetry as was done for the Legendre potential, we obtain

$$\psi = [(14/27)\Psi_{-4}(\eta, \theta) + \beta\cdot\Psi_{-1}(\eta, \theta)]\alpha \tag{23}$$

where β is a constant independent of α.

One thus obtains a boundary value problem for ψ which contains an arbitrary parameter β. For a fixed value of β, the solution to this boundary value problem will exist and will be unique according to the proofs of Tricomi.[3] In this formulation, the statement of Eq. (21) that $\varphi_\eta = 0$ along the supersonic contour—i.e., that the superimposed solution does not change the value of x at the shoulder of the wedge—has not yet been expressed. The fulfillment of this requirement will determine the value of the parameter β.

The future computations will be based upon the formulation of the boundary value problem in terms of the stream function. Here one has the firm foundation of Tricomi's theory. Furthermore, the particular solution $\Phi_{1/2}$, which in terms of ψ appears as Ψ_{-1}, offers, in this form, less convergence difficulties, since the singularity then is treated separately and enters into the solution of the boundary value problem only in the form of the boundary values it induces. We shall, on the other hand, introduce the Legendre potential, φ, during the computations because of its convenience in performing the transformation of the results to the physical plane.

(*B*) *Fulfillment of the Boundary Conditions*

The boundary conditions will be fulfilled in two steps. We consider first the boundary condition along the horizontal lines, $\theta = 0$ and $\theta = \theta_0$ (where θ_0 is the half-angle at the nose of the wedge), disregarding the condition along the characteristic EE'. This portion of the solution will contain the required free-stream singularity. The second step will be to superimpose regular particular solutions that fulfill the remaining boundary conditions along the characteristic EE' without disturbing those that were considered in the first step.

Let us consider the conditions along the horizontal lines. These conditions can be considered as symmetry requirements that may be fulfilled by a suitable system of images of the free-stream singularity placed along the θ-axis. This portion of the solution is given by

$$\rho^{*-1}\cdot\psi = \left[\frac{14}{27}|\eta|^{-4}\sum_{m=-\infty}^{\infty}(-1)^m\cdot f(\zeta_m - 4) + \beta|\eta|^{-1}\sum_{m=-\infty}^{\infty}(-1)^m\cdot f(\zeta_m - 1)\right]\cdot\alpha \tag{24}$$

where

$$\zeta_m = 9(\theta - 2m\theta_0)^2/4\eta^3 \tag{25}$$

Here the factor $(-1)^m$ is required, since the functions $f(\zeta_m, -4)$ and $f(\zeta_m, -1)$ are symmetric with respect to the line $\theta = 2_m\theta_0$. By examining the asymptotic behavior of $f(\zeta_m, -4)$ and $f(\zeta_m, -1)$ for large values of the argument, one can show directly that the series in Eq. (24) converges uniformly in the region of the hodograph plane in which the boundary value problem is defined.

We shall next superimpose regular solutions of the Tricomi Eq. (1) which leave the boundary conditions along AB and DE undisturbed but which give the correct boundary values along EE'. The regular particular solutions to be used for this purpose correspond to Chaplygin's particular solutions, and they are given by

$$\psi^{(m)} = g(\eta, \lambda) \cdot \cos(\lambda \cdot \pi\theta/\theta_0) \tag{26}$$

where $\lambda = m + (1/2)$ and where

$$g(\eta, \lambda) = \begin{cases} \sqrt{|\eta|} \cdot i^{4/3} H_{1/3}^{(1)}(i\lambda z) & (\eta < 0) \\ \dfrac{2}{\sqrt{3}} \cdot \sqrt{\eta}\,[J_{1/3}(\lambda z) + J_{-1/3}(\lambda z)] & (\eta > 0) \\ 3^{-1/6} \dfrac{2}{(-1/3)!} \left(\dfrac{\lambda\pi}{\theta_0}\right)^{-1/3} & (\eta = 0) \end{cases}$$

with $z = (2\pi/3\theta_0)|\eta|^{3/2}$. Here $H_{1/3}^{(1)}$ is the Hanker function of the first kind of order one-third, and $J_{\pm 1/3}$ is the Bessel function or order $\pm 1/3$. This set of functions is chosen such that the nose of the wedge is not mapped to infinity in the physical plane and that the stream function is zero along the lines $\theta = \theta_0$ and ψ_θ is zero for $\theta = 0$. We shall now superimpose to the expression for the image system, Eq. (24), a linear combination of the regular functions given by Eq. (26), with suitable coefficients a_m and b_m such that the remaining boundary conditions along $F'G$ are satisfied. The stream function will therefore become

$$\rho^{*-1} \cdot \psi = \frac{14}{27} \cdot \alpha \left[|\eta|^{-4} \sum_{m=-\infty}^{\infty} (-1)^m \cdot f(\zeta_m - 4) + \sum_{m=0}^{\infty} a_m \cdot \psi^{(m)} \right] \alpha \cdot \beta \left[|\eta|^{-1} \sum_{m=-\infty}^{\infty} (-1)^m f(\zeta_m, -1) + \sum_{m=0}^{\infty} b_m \cdot \psi^{(m)} \right] \tag{27}$$

where $\psi^{(m)}$ is defined in Eq. (26).

Eq. (27) must be evaluated along the characteristic EE' and the coefficients a_m and b_m must be determined in such a manner that $\psi = 0$ along this characteristic. Since up to the present β is unknown, this condition may be fulfilled regardless of the value of β. Thus one obtains the two equations

$$|\eta|^{-4} \sum_m (-1)^m f(\zeta_m, -4) + \sum_m a_m \psi^{(m)} = 0 \tag{28}$$

$$|\eta|^{-1} \sum_m (-1)^m f(\zeta_m - 1) + \sum_m b_m \psi^{(m)} = 0 \tag{29}$$

where

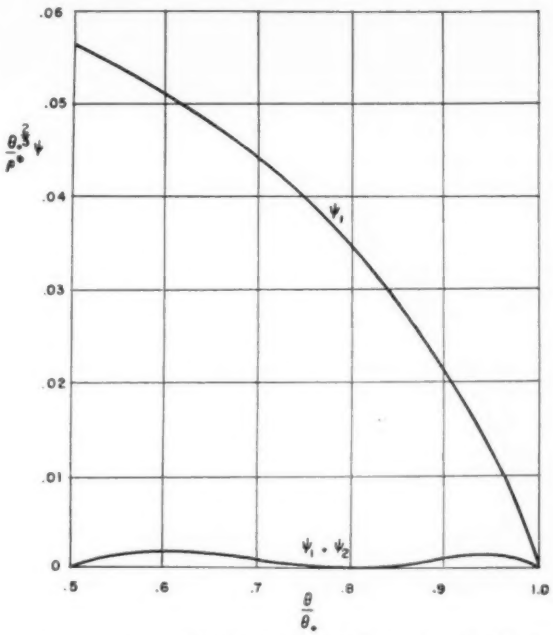

FIG. 6. Fulfillment of the boundary conditions along the Meyer expansion.

$$\eta = [(3/2)(\theta_0 - \theta)]^{2/3} \tag{30}$$

In the subsequent discussion we shall restrict ourselves to the case of the coefficients b_m.

Consider the boundary value problem for the determination of that portion of the solution which is contained in the second series within the bracket expressions of Eq. (27). According to Tricomi,[3] the solution of problem exists and is continuous. Therefore, it can be represented uniquely in the subsonic region by a series of Chaplygin solutions as given by Eq. (26). This series will converge throughout the subsonic region including the sonic line. In the supersonic region, an examination of the Bessel functions (26) in their asymptotic form will show that the stream function will converge at least to the same degree as it did along the sonic line. Therefore, the representation of the stream function in terms of the above series of Chaplygin solutions will give the desired continuation of the subsonic solution into the supersonic region. In particular, this argument shows that there will exist coefficients b_m in Eqs. (32a) and (32b) such that the given terms on the left side of the equations may be represented arbitrarily close if one takes enough terms of the series on the right-hand side.

It should be mentioned here that the continuation of the stream function into the supersonic region will represent the desired physical solution only in the region $AE'E$ in Fig. 5. It does not represent the analytic continuation of the desired solution for the flow downstream of the limiting Mach wave—that is, in the region between the limiting Mach wave AE' and the

positive η-axis. In this region, the representation gives a function that assumes, along the limiting Mach wave, the proper value of ψ and along the positive η-axis, the value zero. Along the characteristics AE', discontinuities in the second and higher derivatives are permitted and will occur. This of course explains why the solution given in terms of the Chaplygin solutions does not give the multisheeted solution that must be expected in the region between the characteristic AE' and the positive η-axis.

The coefficients b_m can be obtained in different ways; one can, for instance, minimize the integral over the square of the residues of Eq. (27), obtained with a finite number of coefficients b_m. This procedure has recently been used by Marschner[5] and proved satisfactory. We determined the coefficients b_m by a method similar to that of reference 1. Fig. 6 shows how well the condition along the characteristic is fulfilled by the coefficients utilized in the present paper. Probably the method of reference 5 would give a somewhat better agreement, but basically the solutions can be considered as satisfactory.

The coefficients a_m were then determined in the same manner. These values are now to be inserted into Eq. (27). However, this does not give us the final answer. We must still determine the constant β. For different values of β, it is found that one obtains wedge profiles in the physical plane with different lengths of the sides when the solution due to the lift, Eq. (27), is superimposed to that for the zero angle of attack. Since we are interested in the wedge with equal sides, we shall choose the constant β such that the solution due to the angle of attack does not change the location of the corner of the wedge; the nose of the wedge will map to the origin of the physical plane in any case. Since the corner of the wedge maps to the characteristic EE' of Fig. 5, this requirement is just that prescribed by the second condition, $\varphi_\eta = 0$, along this characteristic. The value of β was found to be 0.474.

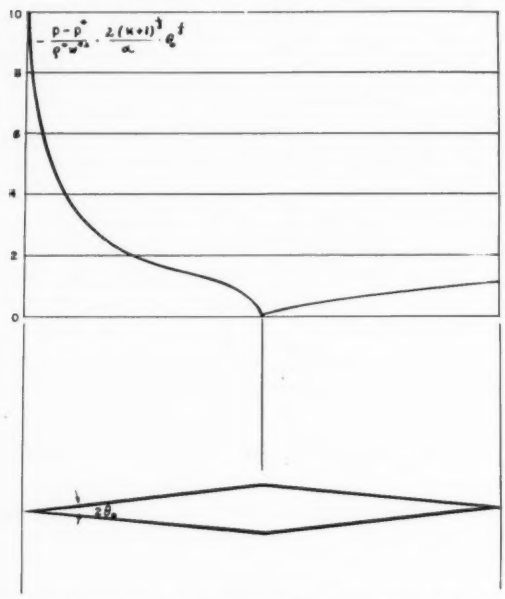

FIG. 7. Change of the pressure distribution along the wedge profile due to the angle of attack.

The continuation of the solution downstream of the limiting Mach wave is then computed by the method of characteristics. Here the result as given by Eq. (27) is first transformed to the physical plane, and the solution is then continued into the supersonic region. This result, when re-expressed in the hodograph variables, will give the value of ψ and φ_η downstream of the limiting Mach wave.

(C) Calculation of the Pressure Distribution over the Wedge

The solution of the boundary value problem given in the previous section will not give directly the change of the pressure distribution due to the angle of attack. One finds instead the amount by which a point with the conditions (η, θ) is shifted in the physical plane due to the angle of attack. Since the solution due to the angle of attack can be considered as a small perturbation of the basic flow over the wedge at zero angle of attack, the change of η may be expressed directly in terms of the hodograph solution due to the angle of attack alone. For this purpose we shall introduce the Legendre potential. The gradient of the Legendre potential in the hodograph plane gives the space vector in the physical plane,

$$\begin{aligned} w^*(\kappa+1)^{-1/2} x &= \phi_\eta \\ w^* y &= \phi_\theta \end{aligned}$$

This equation holds true in the basic flow, as well as in the flow with the potential due to the angle of attack superimposed. We now want to find the changes $\delta\eta$ and $\delta\theta$ of η and θ, which occur at a fixed point x, y by the superposition of the additional potential. Inserting the potential for zero angle of attack, $\bar{\Phi}$, and the potential with angle of attack different from zero, $\bar{\Phi} + \varphi$, into the last equations, one obtains

$$\begin{aligned} w^*(\kappa+1)^{-1/2} x &= \bar{\Phi}_\eta(\eta, \theta) \\ w^* y &= \bar{\Phi}_\theta(\eta, \theta) \end{aligned}$$

and

$$\begin{aligned} w^*(\kappa+1)^{-1/2} x &= \bar{\Phi}_\eta(\eta + \delta\eta, \theta + \delta\theta) + \varphi_\eta(\eta + \delta\eta, \theta + \delta\theta) \\ w^* y &= \bar{\Phi}_\theta(\eta + \delta\eta, \theta + \delta\theta) + \varphi_\theta(\eta + \delta\eta, \theta + \delta\theta) \end{aligned}$$

Linearizing the second pair of equations with respect to the superimposed potential φ and with respect to δ_η and $\delta\theta$, one finds

$$\begin{aligned} 0 &= \bar{\Phi}_{\eta\eta}(\eta, \theta)\delta\eta + \bar{\Phi}_{\eta\theta}(\eta, \theta)\delta\theta + \varphi_\eta(\eta, \theta) \\ 0 &= \bar{\Phi}_{\eta\theta}(\eta, \theta)\delta\eta + \bar{\Phi}_{\theta\theta}(\eta, \theta, \delta\theta) + \varphi_\theta(\eta, \theta) \end{aligned}$$

Solving for $\delta\eta$ and $\delta\theta$ in these equations, we obtain

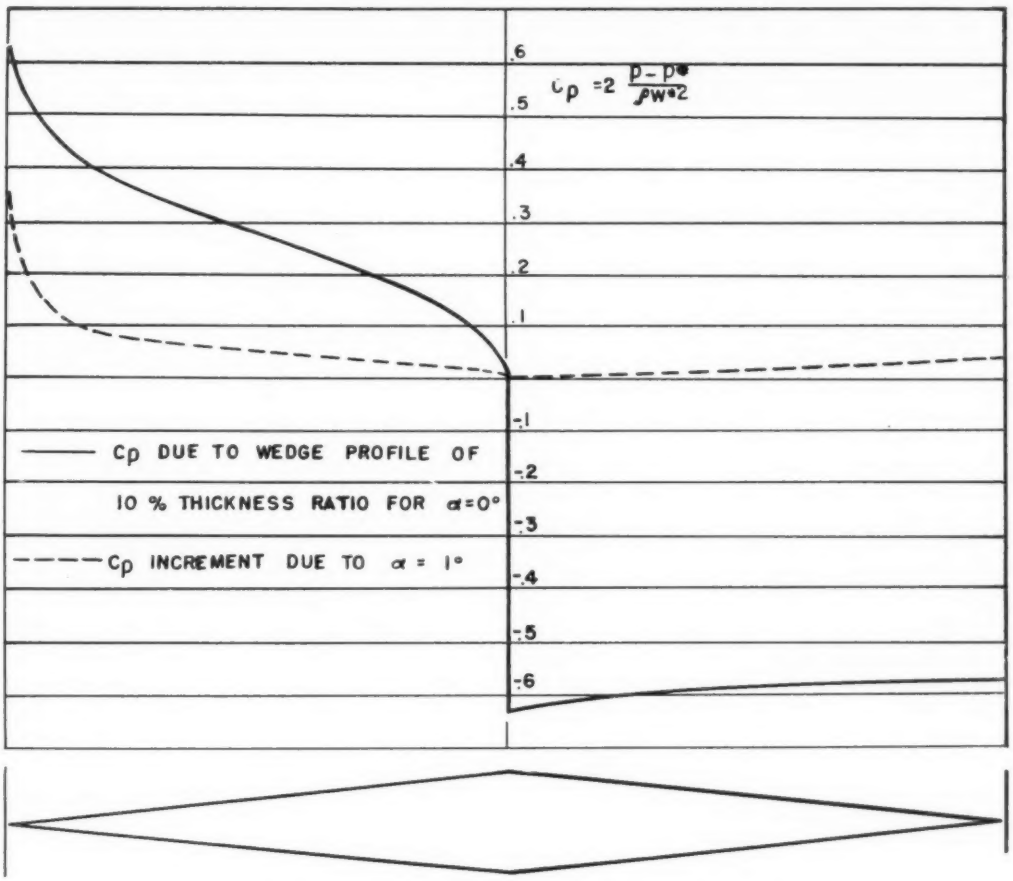

FIG. 8. Pressure distribution due to thickness and to the angle of attack.

$$\delta_\eta = -\Delta^{-1}(\bar{\phi}_{\theta\theta}\cdot\varphi_\eta + \bar{\phi}_{\eta\theta}\varphi_\theta) \qquad (31)$$
$$\delta_\theta = -\Delta^{-1}(\bar{\phi}_{\theta\theta}\varphi_\theta - \bar{\phi}_{\eta\theta}\varphi_\eta)$$

where

$$\Delta = \bar{\phi}_{\eta\eta}\cdot\bar{\phi}_{\theta\theta} - \bar{\phi}_{\eta\theta}^2$$

These expressions give the change of θ and η to be expected due to the angle of attack at a fixed point in the physical plane whose coordinates are given by the solution to the flow for zero angle of attack.

In order to find the change of the pressure distribution due to the angle of attack, we must, according to Eq. (8), compute the value of $\delta\eta$ along the profile. Along the sides of the wedge, the expression for $\delta\eta$ given by Eq. (31) may first be simplified. We have the condition $\bar{\phi}_\theta = 0$ along the sides of the wedge which are lines of constant θ; thus, we have $\bar{\phi}_{\eta\theta} = 0$. Eq. (31) for $\delta\eta$ will, therefore, simplify to

$$\delta\eta = -\varphi_\eta/\bar{\phi}_{\eta\eta}$$

and the local pressure coefficient will then be

$$c_p = 2(\kappa+1)^{-1/3}(\varphi_\eta/\bar{\phi}_{\eta\eta}) \qquad (32)$$

The total lift coefficient can be found from this equation by means of an integration.

Using the above formulas the pressure distribution and the total lift due to the angle of attack were computed. In Fig. 7 the pressure distribution due to an angle of attack is shown; this distribution is to be added to that for zero angle of attack on the upper side of the profile and subtracted from it on the lower side. Fig. 8 shows the change of the pressure distribution due to angle of attack of 1° for a wedge of 10 per cent thickness ratio as compared to the pressure distribution over the same wedge at zero angle of attack. The variation of the $dC_L/d\alpha$ at $\alpha = 0$ (α in radians) with thickness ratio is illustrated in Fig. 9. The position of the center of pressure is independent of the thickness ratio and was found to be located at the 29.4 per cent chord position from the leading edge. In Fig. 10 the results of the present paper are shown in comparison with the values of the lift curve slope for supersonic Mach Numbers for which the nose shock is attached. The latter results were computed by the shock-expansion method simplified by the transonic approximations. It appears that the values at Mach Number 1 are considerably lower than what one would expect by comparison

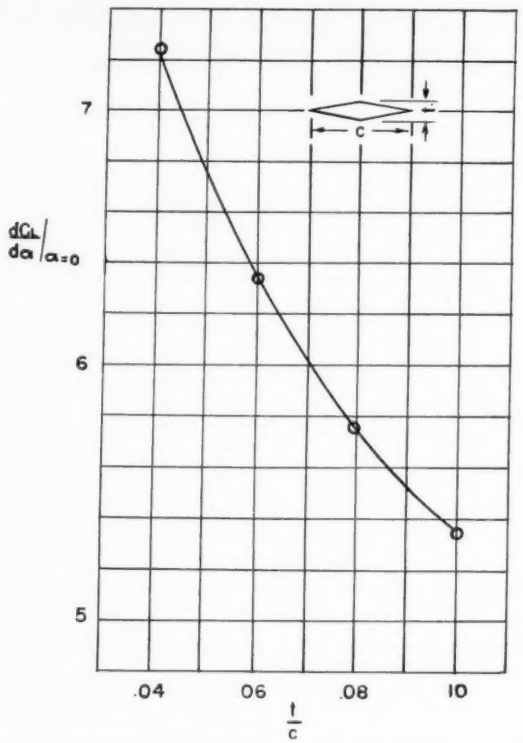

FIG. 9. Lift curve slope as a function of the thickness ratio.

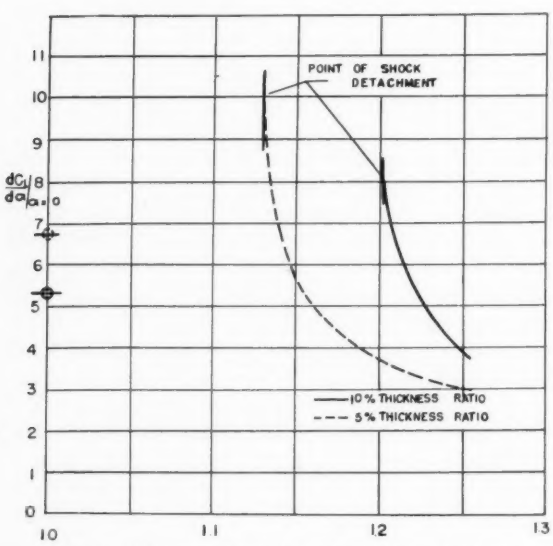

FIG. 10. Lift curve slope for various Mach Numbers.

to the supersonic results. Fig. 10 would then indicate that one must expect a considerable change of the lift curve slope through the range of Mach Numbers from 1 to that for which the shock attaches to the nose. Moreover, according to reference 4, the slope of the lift curve at Mach Number 1 must even be horizontal; this is indicated in Fig. 10 by the short horizontal lines.

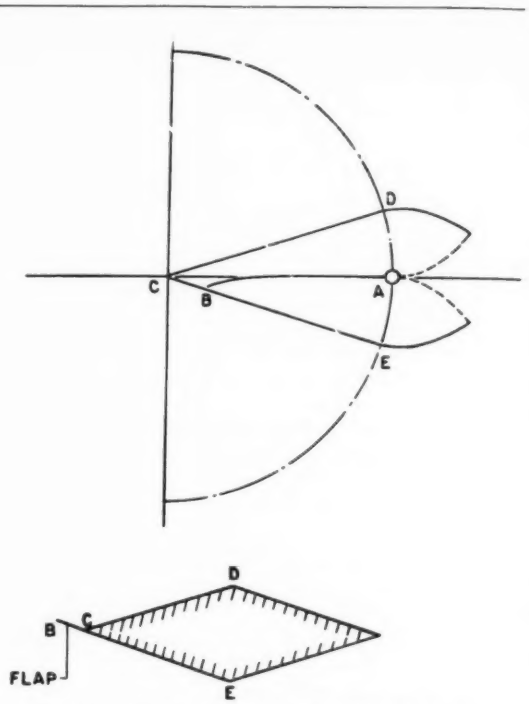

FIG. 11. Modified wedge profile and its hodograph.

This has been confirmed by recent investigations of Vincenti and Wagoner.[6]

SECTION (IV)—FINAL REMARKS

We have discussed in the present paper the flow pattern for slender profiles with a small angle of attack at Mach Number 1. It was found that the flow is uniquely determined by the boundary conditions and that no additional conditions such as the Kutta condition is required. As a specific example, the flow over a wedge profile was computed. It was assumed for this case that the angle of attack was sufficiently small so that the essential unsymmetric effects are described by the linear terms of the angle of attack and that the effect of the local supersonic region arising at the nose could be neglected.

REFERENCES

[1] Guderley, G., and Yoshihara, H., *Flow over Wedge Profile at Mach Number One*, Journal of the Aeronautical Sciences, Vol. 17, No. 11, pp. 723–735, November, 1950.

[2] Guderley, G., *Singularities at the Sonic Velocity*, Technical Report No. F-TR-1171-ND, Headquarters Air Materiel Command, Wright Field, Dayton, Ohio, June, 1948 (unclassified, English).

[3] Tricomi, F., *On Linear Partial Differential Equations of the Second Order of Mixed Type*, Brown University Translation.

[4] Guderley, G., *Two-Dimensional Flow Patterns with a Free Stream Mach Number Close to One*, USAF Technical Report No. 6343, USAF, WADC, May, 1951 (unclassified, English).

[5] Marschner, Burnhard W., *The Flow over a Body in a Choked Wind Tunnel and in a Sonic Free Jet*, Cal. Tech. Thesis, 1953.

[6] Vincenti, Walter G., and Wagoner, Cleo B., *Theoretical Study of the Transonic Lift of a Double Wedge Profile With Detached Bow Wave*, NACA TN No. 2832, December, 1952.

Appendix

Estimation of the Influence of the Supersonic Region at the Nose of the Wedge Profile

The purpose of the present appendix is to show why for small angles of attack the effect on the lift of the supersonic region at the nose of the wedge can be neglected. There are several different methods by which this can be shown. A direct procedure would be to examine the boundary value problem for the flow over the nose with respect to the angle of attack. Although the boundary value problem cannot be formulated completely, one can still show in this way that the influence of the tip region on the lift force does not appear in the terms of first order of a development with respect to the angle of attack.

We shall, however, proceed by another method that is simpler. It can be shown that the boundary value problem that was actually solved in the present paper corresponds to a flow over a wedge profile with a short flap that extends upstream from the nose (see Fig. 11). This flap becomes smaller and smaller as the angle of attack is decreased. The influence of the flow of the nose will then be estimated by examining the influence of this flap upon the overall lift.

The boundary value problem that was computed is shown in Fig. 11. Here we have $\psi = 0$ along the lines $\theta = \theta_0$ and $-\theta_0$. At the point A, which lies on the sonic line where $\theta = \alpha$, a superposition of two prescribed singularities occurs which represents the free-stream singularity. The coefficients with which these singularities are multiplied are determined by the size and shape of the wedge. This boundary value problem has a unique solution in which no parameters are left arbitrary. When $\alpha = 0$, a branch point of the stream lines will lie at the stagnation point. With an angle of attack, however, this can no longer be expected, and one will, in general, have a branch point of the stream lines that travels along the hodograph map of one of the sides of the wedge as the angle of attack changes.

Which physical significance does such a hodograph pattern have? The physical plane that belongs to this flow is also shown in Fig. 11. Here the zero stream line forms a branch point not at the stagnation point but at a finite velocity. After the branch point, the two branches still proceed in the direction of $-\theta_0$, but along one of the stream lines the flow assumes higher velocities while along the other branch the velocity decreases. The flow near the branch point, therefore, resembles the flow over a flat plate inclined at an angle θ_0. Along the upper side of the flat plate the flow decelerates and finally reaches zero velocity at some point C. Here the zero stream line assumes the direction $+\theta_0$. We see, therefore, that the flow problem given by the hodograph formulation of Fig. 11 is the flow over a wedge profile at an angle of attack with the wedge having a short flap at the nose. The branch point of the stream lines at the tip of the flap. The flap will become smaller as the angle of attack is decreased. The influence of this flap upon lift will be represented by the force that acts on the flap and furthermore by the changes of the pressure distribution over the wedge caused by the presence of the flap. If the flap is small, then it is plausible that the force caused by the change of the pressure distribution over the wedge will be of the same order of magnitude as the force that acts directly upon the flap—that is, the ratio of the force on the flap and the "interference" force will be some finite number that does not tend to infinity as the flap becomes smaller. Therefore, one obtains an estimation for the entire influence of the flap if one determines only the force that acts on the flap.

The flow velocities in the vicinity of the flap are extremely small, and they become smaller as the angle of attack is decreased. Therefore, the force on the flap can be determined by an incompressible treatment. Since we have $\psi = 0$ for $\theta = \pm\theta_0$, the solution near the stagnation point can be represented by

$$\psi = \sum_{n=1}^{\infty} a_n \cdot w^{n\pi/\theta_0} \sin \frac{n\pi\theta}{\theta_0} + \sum_{n=1}^{\infty} b_n \cdot w^{[n-(1/2)](\pi/\theta_0)} \cdot \cos \left(n - \frac{1}{2}\right)\frac{\pi\theta}{\theta_0} \quad \text{(A-1)}$$

where the constants a_n and b_n are functions of the angle of attack. If we examine the symmetry of the terms in the above equation, the form of the coefficients a_n and b_n can be given. Eq. (A-1) can be rewritten as

$$\psi = \sum_n (a_{n0} + a_{n1}\alpha^2 + \dots)\, w^{n\pi/\theta_0} \cdot \sin \frac{n\pi\theta}{\theta_0} + \alpha \sum_n (b_{n0} + b_{n1}\alpha^2 + \dots) w^{[n-(1/2)](\pi/\theta_0)} \cos \times \left(n - \frac{1}{2}\right)\frac{\pi\theta}{\theta_0} \quad \text{(A-2)}$$

where $a_{n0}, a_{n1}, \dots$, and $b_{n0}, b_{n1}, \dots$, are constants independent of α. For small values of α, only the region near the stagnation point is of interest. Under these conditions the predominating terms in Eq. (A-2) are

$$\psi = a_{10} \cdot w^{\pi/\theta_0} \cdot \sin \frac{\pi\theta}{\theta_0} + \alpha b_{10} w^{\pi/2\theta_0} \cos \frac{\pi\theta}{2\theta_0} \quad \text{(A-3)}$$

The coefficients a_{10} and b_{10} are numbers that are determined if one solves the boundary value problem.

If one now introduces the complex velocity $q = w \cdot e^{-i\theta}$, then Eq. (A-3) can be rewritten as $\psi = Im\Omega$, where

$$\Omega = -a_{10}q^{\pi/\theta_0} + i\alpha \cdot b_{10}q^{\pi/2\theta_0} \qquad \text{(A-4)}$$

The branch point of the stream lines is given by the conditions

$$\partial\psi/\partial w = 0; \qquad \partial\psi/\partial\theta = 0$$

which can also be written as

$$d\Omega/dq = 0$$

One finds that the branch point of the stream lines lies at

$$q = \alpha^{2\theta_0/\pi}\left|b_{10}/2a_{10}\right|^{2\pi/\theta_0}e^{\pm i\theta_0}$$

Here the sign to be taken in the exponent is that of the sign of the expression b_{10}/a_{10}.

In the case of incompressible theory, the physical plane is related to the hodograph plane by the equation

$$dz = dx + idy = d\Omega/q$$

Therefore, we find from Eq. (A-4) that

$$z = \frac{\pi}{\theta_0}\left(1 - \frac{\pi}{\theta_0}\right)^{-1} a_{10} \cdot q^{(\pi/\theta_0)-1} + \frac{1}{2}\,\alpha b_{10}\left(\frac{\pi}{2\theta_0} - 1\right)^{-1} q^{(\pi/2\theta_0)-1}$$

If one introduces the value of q for the branch point into this equation, then one obtains the length of the flap as measured from the stagnation point. One finds that it is proportional to $\alpha^{2-(2\theta_0/\pi)}$ if terms of higher power of α are neglected.

If one now determines the velocity at the upper or lower surface of the flap for which $z = 0$, one finds that in the lowest order approximation the absolute value of the velocity is proportional to $\alpha^{2\theta_0/\pi}$. According to Bernoulli's equation, the pressure difference between the stagnation pressure and the pressure corresponding to the velocity is proportional to w^2. In the present case, the largest pressure difference occurring along the flap is proportional to $\alpha^{4\theta_0/\pi}$. We had previously seen that the length of the flap is proportional to $\alpha^{2-(2\theta_0/\pi)}$. Therefore, the total normal force on the flap is found to be proportional to $\alpha^{2+(2\theta_0/\pi)}$. Consequently, the effect of the small flap at the nose of the wedge is of a smaller order of magnitude than the total lift of the wedge which is proportional to α.

Changes of Address

Since the Post Office Department does not as a rule forward magazines to forwarding addresses, it is important that the Institute be notified of changes in address 30 days in advance of publishing date to ensure receipt of every issue of the JOURNAL and REVIEW.

Notices should be printed legibly and sent directly to:

Institute of the Aeronautical Sciences, Inc.

2 East 64th Street, New York 21, New York

Similarity Theory of Isotropic Turbulence

J. C. ROTTA*

Max-Planck-Institut für Strömungsforschung

ABSTRACT

The basic idea of this representation is that an arbitrary homogeneous and isotropic turbulent motion tends, in the course of time, toward a universal state, in which all statistical properties are determined by only three magnitudes. From dimensional arguments a general law of similarity for isotropic turbulence can be formed. The equation for the corresponding energy spectrum is derived from the well-known equation for the change of spectrum and has a one-parametric set of solutions. But only one of these solutions is distinct, in that it satisfies the continuity condition in the range of the smallest wave numbers. This distinct solution can be considered as corresponding to the universal state.

Comparisons of the theory with measurements of turbulence produced by a uniform stream of fluid passing a mesh grid are discussed. According to this, it is at least probable that the universal state of homogeneous and isotropic turbulence is correctly described by the distinct solution of similarity.

(1) INTRODUCTION

THE TEMPORAL DEVELOPMENT OF a homogeneous isotropic field of turbulence can be followed by means of the equation for the propagation of the correlation first given by von Kármán[1] or the equation for the change of spectrum, when suitable assumptions about the triple correlations or the transfer of energy between the wave numbers can be made. The determination of the correlation function or the spectrum is a problem of continuity. That is to say, if the correlation function or the spectrum is known at any time, its further development can be determined theoretically up to infinity. Thus the difficulty lies, on one hand, in finding the correct expression for the energy transfer and, on the other, in fixing the initial distribution of energy.

The approximate similarity of the correlation functions and spectra, already observed in the early days of turbulence research, led to the conclusion that the structure of isotropic turbulence approaches a shape in course of time which does not depend on the conditions under which the turbulence is produced. This observation is again confirmed by recent measurements, reference 13. This state of turbulence could be considered as a sort of statistical equilibrium.

Under these circumstances it should be possible to determine the structure of the turbulence without having to consider its whole previous development, such that any vague assumption regarding the initial distribution could be saved. Starting with such ideas von Kármán first investigated the so-called self preserving correlation functions. Today it is realized that self preserving solutions do not exist except for the final period. The assumption of self preserving structure is too specialized. To overcome the contradictions, a portion of wave numbers had to be excluded from consideration, and to explain the behavior several authors introduced further assumptions without any of them being satisfactory.

The present paper deals with a more general treatment that does not start from the idea of self preservation of the structure. It will be shown that this treatment leads to a unique solution that is valid for the whole range of wave numbers and Reynolds Numbers.

(2) GENERAL SIMILARITY OF ISOTROPIC TURBULENCE

The basic idea is that an arbitrary homogeneous and isotropic turbulent motion tends, in course of time, toward a universal state, in which its statistical properties do not depend on the special conditions governing the turbulence at the moment of its creation. This presumes a similarity of all isotropic fields of turbulence of the universe among themselves. It does not assert a similarity of the structure during the process of decay, as is assumed in the concept of self preservation of the structure—i.e., the structure changes continuously during the decay. In this universal state, all statistical properties of isotropic turbulent motion in an incompressible Newtonian fluid are wholly determined by three independent magnitudes—viz., a characteristic velocity $V(t)$, a characteristic length $l(t)$, and the kinematic viscosity ν of the fluid. The characteristic velocity and length both are functions of the time t. From dimensional arguments we can formulate the general law of similarity for isotropic turbulence. The three-dimensional energy spectrum $F(k, t)$, which is a function of the wave number k and the time t, is given by

$$F(k, t) = V^2(t)l(t)f(\chi, R) \tag{2.1}$$

where χ is a nondimensional wave number

$$\chi = kl(t) \tag{2.2}$$

R is a Reynolds Number

$$R = V(t)l(t)/\nu \tag{2.3}$$

and $f(\chi, R)$ is a universal function of χ and R. This similarity includes as special cases all the similarity

Received October 21, 1952. Revised and received March 23, 1953.

* Wissenschl. Mitarbeiter.

hypotheses known up to the present time. In fact, only when such a universal state of turbulence exists does it seem to be reasonable to study the entire structure without taking into account the initial conditions of the turbulence. The progress consists in that the universal function $f(\chi, R)$ in Eq. (2.1) depends on two variables. The elimination of the second variable R reduces the consideration to the less general conception of self preserving structure.

Eq. (2.1) holds generally; however, V and l may be chosen. It is convenient to put V proportional to the mean square root fluctuation $u' = \sqrt{\overline{u^2}}$ of any velocity component. The characteristic length l can, for example, be put equal to the integral scale L or Taylor's microscale λ. It is also possible to introduce the energy dissipation ϵ per unit mass of fluid instead of one of these magnitudes.

At this point we remember that locally isotropic turbulence is determined by two magnitudes only—viz., the dissipation ϵ and the viscosity ν. From this the well-known law of similarity

$$F(k) = \epsilon^{1/4}\nu^{5/4}\varphi(\eta) \tag{2.4}$$

follows, where $\varphi(\eta)$ is a universal function of its argument

$$\eta = k\nu^{3/4}\epsilon^{-1/4} \tag{2.5}$$

This particular case can also be deduced from Eqs. (2.1) and (2.2), putting $V = \epsilon^{1/4}\nu^{1/4}$ and $l = \epsilon^{-1/4}\nu^{3/4}$. From Eq. (2.3) then results $R = 1$. Eq. (2.4), of course, holds only for a limited range of large wave numbers. The validity can be extended over the whole wave number range, when a third magnitude (say, u') is introduced. The function φ then depends again on two variables—viz., η and $u'\epsilon^{-1/4}\nu^{-1/4}$. Goldstein[14] also came to similar conclusions. Eq. (2.4), generalized in this manner, expresses the same idea as Eq. (2.1). This consideration shows that there are different ways to formulate the similarity, a nondimensional function of *two* independent variables is, however, necessary in each case to describe exactly the whole structure and to deduce the law of decay.

(3) The Equation of General Similarity

In order to derive an equation for the corresponding similarity spectrum, it is necessary to transform the well-known equation for the change of the spectrum,

$$\frac{\partial}{\partial t}\int_0^k F(k', t)\,dk' + \int_0^k W(k', t)\,dk' + \nu\int_0^k 2k'^2F(k', t)\,dk' = 0 \tag{3.1}$$

into an equation between the variables $f(\chi, R)$, χ, and R. Here the term $W(k, t)$ of the energy transfer between the wave numbers can be written as

$$W(k, t) = V^3(t)w(\chi, R) \tag{3.2}$$

where $w(\chi, R)$ is also a universal function of χ and R. Since V and l are both functions of the time, the Reynolds Number R is also a function of time. However, we find, as a consequence of the supposed similarity, that the expression

$$d\ln l(t)/d\ln V^2(t) = -\zeta(R) \tag{3.3}$$

is a universal function of R only. This can be deduced from any two different integral moments of the equation for the change of spectrum.

Introducing the relations (2.1), (2.2), (2.3), (3.2), and (3.3) we obtain, from Eq. (3.1),

$$\frac{1}{R}\int_0^\infty 2\chi^2 f\,d\chi\left\{\int_0^\chi f\,d\chi' - \zeta(R)\chi f + \left[\frac{1}{2} - \zeta(R)\right]R\int_0^\chi \frac{\partial f}{\partial R}\,d\chi'\right\} - \left\{\int_0^\infty f\,d\chi + \left[\frac{1}{2} - \zeta(R)\right]R\frac{d}{dR}\int_0^\infty f\,d\chi\right\}\left(\int_0^\chi w\,d\chi' + \frac{1}{R}\int_0^\chi 2\chi'^2 f\,d\chi'\right) = 0 \tag{3.4}$$

Besides this equation, the nondimensional spectrum f must satisfy some additional conditions that depend on how V and l are defined. Although all the above-given statements and relationships are not influenced by the choice of V and l, it is convenient for purposes of the following analysis to define V and l so that simple forms result for these additional conditions. If we put

$$V^2 = \frac{3}{2}u'^2 = \int_0^\infty F(k, t)\,dk \tag{3.5}$$

$$l = L = \frac{\pi}{4u'^2}\int_0^\infty F(k, t)\frac{dk}{k} \tag{3.6}$$

the additional conditions to be satisfied are

$$\int_0^\infty f(\chi, R)\,d\chi = 1; \quad \int_0^\infty f(\chi, R)\frac{d\chi}{\chi} = \frac{8}{3\pi} \tag{3.7}$$

In this case L is the transverse scale

$$L = \int_0^\infty g(r)\,dr \tag{3.8}$$

where $g(r)$ is the transverse correlation function. The magnitude of $\zeta(R)$ of Eq. (3.3) then becomes

$$\zeta(R) = 1 - \frac{3\pi}{8}\frac{\int_0^\infty 2f\chi\, d\chi + R\int_0^\infty w\, d\chi/\chi}{\int_0^\infty 2f\chi^2\, d\chi} \tag{3.9}$$

which can be derived from Eq. (3.1).

(4) Similarity Solutions for the Spectrum

From the great variety of solutions given by Eq. (3.4), those have to be selected which have no properties depending on the arbitrary initial distribution.

When R is extremely small, the energy transfer becomes negligible, and Eq. (3.4) reduces to

$$\int_0^\infty 2\chi^2 f\, d\chi\left[\int_0^\chi f\, d\chi' - \zeta(0)\chi f\right] = \int_0^\infty f\, d\chi\int_0^\chi 2\chi'^2 f\, d\chi' \tag{4.1}$$

In this equation R no longer appears. Hence, $\zeta(0)$ becomes a constant, and a solution is found which is independent of R,

$$f(\chi, 0) = b\chi^{(1/\zeta_0)-1}e^{-a\chi^2} \tag{4.2}$$

The constants a and b depend on the definition of V and l. This special solution is identical with the self preserving solutions first suggested by von Kármán and Howarth.[1] The magnitude of $\zeta(0)$ is determined by the preceding history of turbulence.

At extremely high Reynolds Numbers, the influence of viscosity is restricted to large wave numbers. Consequently, a value χ_1 can be defined such that the energy containing portions of the spectrum falls mainly within the range $0 \leq \chi \leq \chi_1$ and the viscous dissipation is due essentially to that portion of the spectrum lying beyond χ_1. If V and l are defined by Eqs. (3.5) and (3.6), respectively, Eq. (3.4) for the range of $0 \leq \chi \leq \chi_1$ and Eq. (3.9) can now be transformed to

$$\int_0^{\chi_1} w\, d\chi\left[\int_0^\chi f\, d\chi' - \zeta\chi f + \left(\frac{1}{2} - \zeta\right)R\frac{d}{dR}\int_0^\chi f\, d\chi'\right] = \int_0^\chi w\, d\chi' \tag{4.3}$$

$$\zeta(R \to \infty) = 1 - \frac{3\pi}{8}\left(\int_0^{\chi_1} w\, d\chi/\chi \Big/ \int_0^{\chi_1} w\, d\chi\right) \tag{4.4}$$

With the supposition that w represents an energy transfer from small to large wave numbers, these equations have a set of special solutions that are also independent of the Reynolds Number and which are called by von Kármán solutions of nonviscous similarity. For the portion of spectrum of $\chi \geq \chi_1$, the equilibrium spectrum of locally isotropic turbulence holds. The details of the solutions of nonviscous similarity depend, of course, on the relation between the energy transfer term $W(k, t)$ and the spectrum $F(k, t)$. Batchelor[3] has shown that $W(k, t)$ commences with a higher power of k than $F(k, t)$. Accordingly, the solutions of nonviscous similarity have, for small values of χ, the form

$$f(\chi, \infty) = \text{const. } \chi^m \tag{4.5}$$

where

$$m = (1/\zeta_\infty) - 1 \tag{4.6}$$

As already mentioned, from a spectral distribution, given at $t = t_0$, the temporal development of the spectrum can be deduced by means of Eq. (3.1). Thus we will find, in the case of decreasing Reynolds Number, all the appropriate solutions by a step-by-step integration over the whole range of R if we start at a sufficiently high Reynolds Number with a solution of nonviscous similarity, which is completed, for large wave numbers, by the equilibrium spectrum of locally isotropic turbulence. Since the first approximation to $F(k, t)$ for small k—namely, $F \propto k^m$—is constant throughout the decay, from a comparison of Eqs. (4.5) and (4.2) it results that

$$\zeta(0) = \zeta(\infty) \tag{4.7}$$

This simple relation associates the solution for extremely small R with the corresponding solution of nonviscous similarity.

The procedure described for obtaining the similarity solutions is somewhat laborious. A simplification of the equations is thus desirable. When V and l are defined by Eqs. (3.5) and (3.6), respectively, the nondimensional spectrum function $f(\chi, R)$ changes fairly slowly with R. Further, the magnitude of $\zeta(R)$, for any value of R, does not greatly differ from the values corresponding to infinite and zero Reynolds Number. This follows from calculations of reference 2. Accordingly, the term $\partial f/\partial R$ may be neglected and $\zeta(R)$ may be made constant,

$$\zeta(R) = 1/\xi \tag{4.8}$$

Reintroducing the original functions $F(k, t)$, $W(k, t)$,

and k in place of $f(\chi, R)$ and χ, we derive, from Eq. (3.4),

$$\frac{2\epsilon(t)}{3u'^2(t)}\left[\int_0^k F(k', t)\,dk' - \frac{1}{\xi}kF(k, t)\right] - \int_0^k W(k', t)\,dk' - \nu\int_0^k 2k'^2F(k', t)\,dk' = 0 \quad (4.9)$$

which seems to be a rather good approximation for the similarity solutions. The energy dissipation is

$$\epsilon(t) = \nu\int_0^\infty 2k^2F(k, t)\,dk \quad (4.10)$$

The author first used Eq. (4.9) for an estimation of the spectrum of isotropic turbulence in 1948.[4] Using the energy transfer relation,

$$\int_0^k W\,dk = \kappa\int_k^\infty \sqrt{F/k''^3}\,dk''\int_0^k 2k'^2F\,dk' \quad (4.11)$$

suggested by Heisenberg,[5] solutions for different ξ have been investigated in reference 2. If desired, the solution of Eq. (4.9) can be iteratively improved by substituting in the exact Eq. (3.4). Eq. (4.9) satisfies exactly, for large R, the condition of nonviscous similarity in the low and medium wave number range and the equilibrium condition of locally isotropic turbulence in the high wave number range and, for small R, the similarity condition of the final period when viscous dissipation prevails in the whole range of wave numbers.

TABLE 1

Variation of Characteristic Magnitudes with Time

	Large Reynolds Number, $R \to \infty$	Small Reynolds Number, $R \to 0$
Energy per unit mass, $(3/2)u'^2$	$\propto t^{-2\xi/(2+\xi)}$	$\propto t^{-\xi/2}$
Integral scale, L	$\propto t^{2/(2+\xi)}$	$\propto t^{1/2}$
Microscale, λ	$= \left(5\frac{2+\xi}{\xi}\nu t\right)^{1/2}$	$= \left(\frac{20}{\xi}\nu t\right)^{1/2}$
Reynolds Number, $R = \sqrt{3/2}(u'L/\nu)$	$\propto t^{(2-\xi)/(2+\xi)}$	$\propto t^{(2-\xi)/4}$

In Table 1 the variation of some characteristic magnitudes with time in the large and small Reynolds Number region are given.

It may be explicitly pointed out that Eqs. (3.4) and (4.9) have not a unique similarity solution but a one-parametric set of solutions. The parameter $\xi = (1 + m)$ must be >1, otherwise the integral of the second condition Eq. (3.7) does not exist. In the next section it will be seen which of these solutions is physically significant.

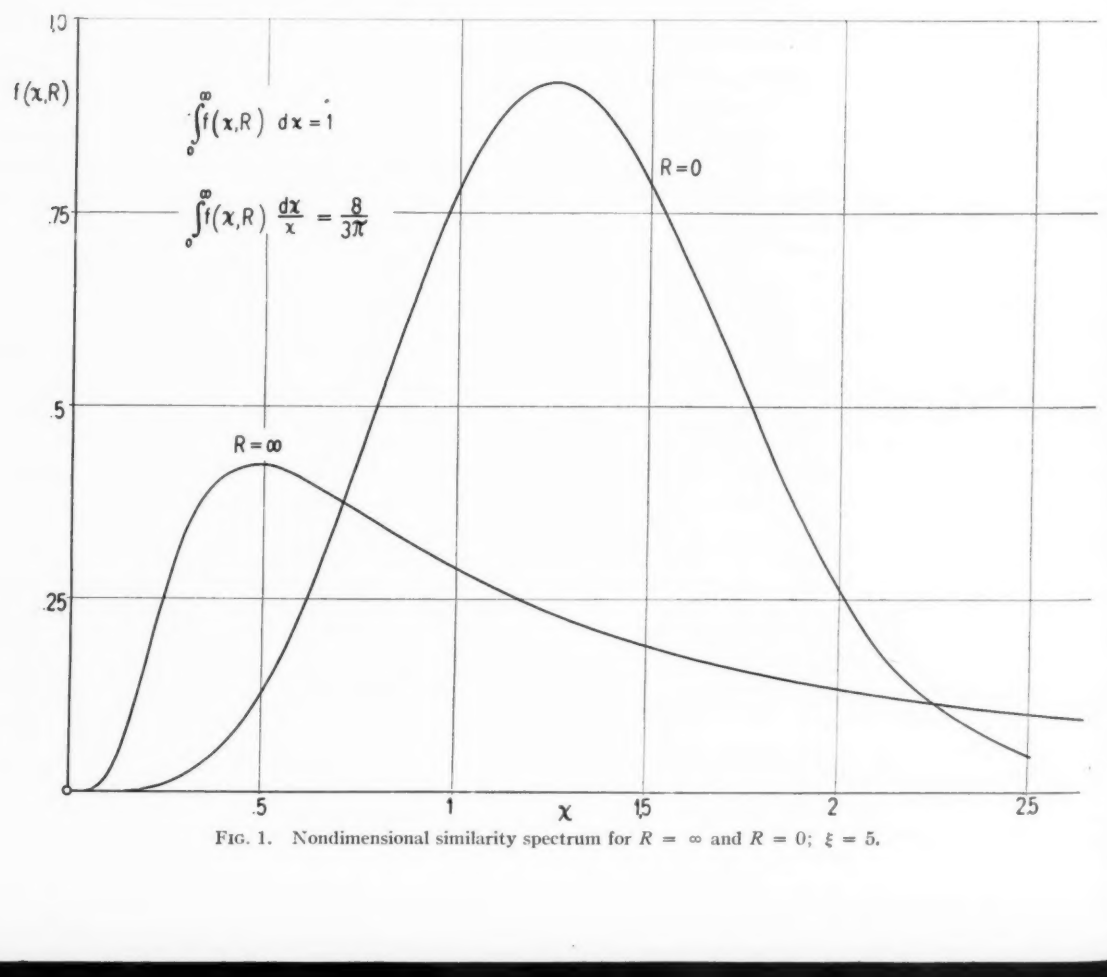

FIG. 1. Nondimensional similarity spectrum for $R = \infty$ and $R = 0$; $\xi = 5$.

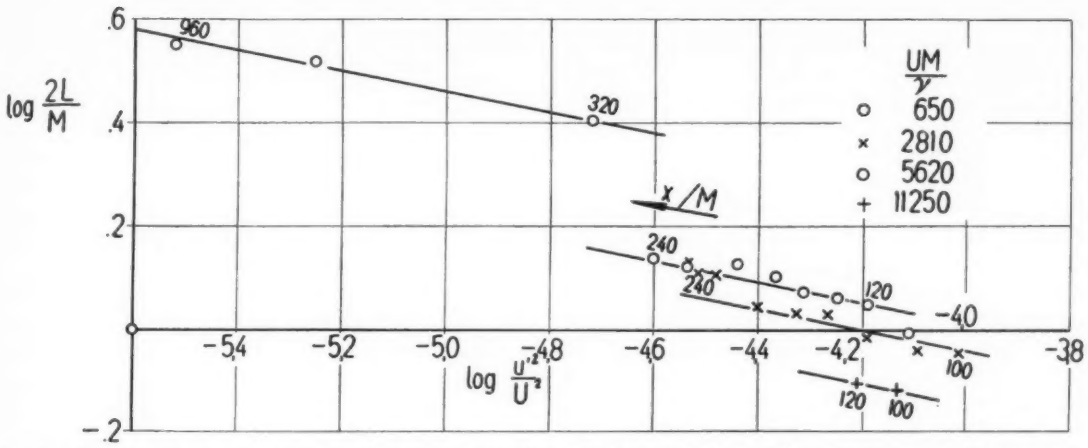

FIG. 2. Variation of integral scale with mean square fluctuation of turbulence behind a grid. Measurements are from references 7 and 9. Theoretical slope, $d \ln L/d \ln u'^2 = -(1/5)$.

(5) THE PHYSICALLY DISTINCT SOLUTION OF SIMILARITY

The similarity solutions discussed represent that shape of spectrum toward which any initially given distribution $F(k, t_0)$ tends after a sufficiently long time of decay, when the initial distribution begins at small wave numbers with

$$F(k, t) \propto k^{\xi-1} \tag{5.1}$$

If we commence with any given distribution of $F(k, t_0)$, for which the integrals

$$\int_0^\infty F\,dk \quad \text{and} \quad \int_0^\infty k^2 F\,dk$$

exist, a step-by-step integration of Eq. (3.1), using the transfer relation Eq. (4.11), we can see how the similarity solution develops. The energy of large wave numbers decays much faster than that of small wave numbers and approaches rapidly to a local similarity according to the theory of locally isotropic turbulence. As a result, the wave number range, which contributes essentially to the kinetic energy, decreases continuously with time, and, finally, the remaining energy is distributed mainly over a wave number range that initially contributed only a small fraction to the total energy. When the range of wave numbers in which the energy is contained has diminished nearly to a range within which the spectrum did not initially deviate essentially from Eq. (5.1), the spectrum has attained one of the above similarity solutions. The corresponding Reynolds Number depends on the value of the Reynolds Number in the initial stage. If the latter is not high, the procedure yields only similarity solutions having low R. If the initial value of R is, however, extremely high and the starting spectrum does not deviate too much from the similarity spectrum, the case of nonviscous similarity may be realized. A more detailed discussion on the physical background is presented in the Appendix.

The preceding history of turbulence enters into the similarity solutions still in the form of spectrum at lowest wave numbers. Now we know from the continuity condition at low wave numbers,[3] as well as from Loitsianskij's invariant relation, that the spectrum of homogeneous turbulence begins with the universal power law

$$F \propto k^4 \tag{5.2}$$

Thus only the similarity solution with the parameter $\xi = 5$ is completely independent of any arbitrary condition of the initial state and can really be established for the whole wave number range. We conclude that this physically distinct solution corresponds to the universal state of isotropic turbulence.

For extremely low Reynolds Numbers this solution is identical with that of the final period given by Batchelor and Townsend.[7] The decay is $u'^2 \propto t^{-5/2}$. At extremely high Reynolds Numbers, the intensity decays according to the law $u'^2 \propto t^{-10/7}$, which was first suggested by Kolmogoroff.[8]

Fig. 1 represents the nondimensional spectrum for both cases, $R = 0$ and $R = \infty$, the latter being computed by the method given in reference 2. A more exact computation for the whole Reynolds Number range is being carried out and will be published later.

(6) DECAY OF TURBULENCE BEHIND A GRID

To support theoretical deductions of isotropic turbulence, a great number of experimental investigations have been made in wind tunnels. Unfortunately, the case of turbulence produced by a flow through a mesh grid is not exactly homogeneous, though the deviations are, except for small distances x from the grating, not serious. Nevertheless, it is possible that some of the observations made are not causally concerned with the idealized case of a homogeneous isotropic field of turbulence.

This seems to come true for the decay of energy. It is seen that existing experimental results, in the initial period, show a law of decay, $u'^2 \propto x^{-1}$, which does not agree with the similarity solution with $\xi = 5$. The experimental law of decay corresponds rather to a solution of Eq. (4.9) with $\xi = 2$. This solution has been suggested by Heisenberg[6] and is mathematically distinguished by a constancy of the Reynolds Number throughout the decay. At small wave numbers this theory predicts a linear relation between $F(k, t)$ and k, which is, however, at variance with the continuity condition. Any experimental evidence for the linear part of the spectrum has not been found. Since the similarity solutions represent the remainders of any initial distributions that have, at small wave numbers, the form of Eq. (5.1), a plausible explanation for setting-in of the solution with $\xi = 2$ can hardly be given. If this consideration is correct, it is not probable that the actual behavior of isotropic turbulence is exactly described by this solution.

On the other hand, the measurements point to the fact that, in the early stage of turbulence behind a grid, the experimentally observed decay $u'^2 \propto x^{-1}$ generally holds. It is not too much to suppose that a characteristic phenomenon of turbulence behind a grid is here in question. This supposition is supported by the fact that the turbulent energy in the wake of a single rod decays also approximately by the same law. Behind a grid, each rod forms a wake in a similar way. Possibly the mechanism that governs the law $u'^2 \propto x^{-1}$ is already set in motion before the mixing of the wakes begins. Undoubtedly the phenomena in this stage of turbulence are not yet quite understood. But it is probable that they cannot be explained with the conceptions of homogenity and isotropy only.

(7) Comparisons with Experiments

Comparing experimental observations, we must bear in mind that the turbulence needs a certain time until similarity according to Eq. (2.1) is achieved. Hence, only such observations that have been made at not too small distances from the grid can properly be considered. It is for this reason that the discrepancy with the decay in the initial period does not matter greatly. On the contrary, for extremely low Reynolds Numbers and extremely large distances, the theory is the same as that suggested by Batchelor and Townsend,[7] which was found to be in full accordance with experimental observations. Therefore, what we need are comparisons at higher Reynolds Numbers and sufficiently large distances.

From published experiments,[9] it results that the decay law shows, at certain distances x ($x/M \sim 100$ to 200), deviations from the initial decay $u'^2 \propto x^{-1}$ which seem to correspond to the law predicted by our theory. This is only a qualitative comparison. An extended region with the law $u'^2 \propto x^{-10/7}$, which corresponds to the case with $\xi = 5$ at high Reynolds Numbers, cannot be observed because the Reynolds numbers of measurements are too small. But we are able to check quantitatively the relation (3.3) between L and u'^2. It was pointed out that, for extremely high Reynolds Numbers, as well as for extremely low ones, the value of $\zeta(R)$ equals $1/\xi = 1/5$. Further, it was mentioned that, for moderate Reynolds Numbers also, no great deviations of $\zeta(R)$ from $1/5$ are expected. On Fig. 2, the longitudinal scale $2L$ divided by the periodic spacing M of the turbulence-producing grid is plotted, to a logarithmic scale, against the intensity u'^2 divided by the square of the uniform stream velocity U relative to the grid. Only such measurements of references 7 and 9 have been used, which were carried out at distances $x > 100M$. The straight lines drawn in have a slope of $-1/5$. It is seen that

$$d \ln (L/d) \ln u'^2 \sim -(1/5)$$

when x/M is not too small. This comparison completely confirms the prediction of the theory and covers a range of Reynolds Numbers up to

$$u'\lambda/\nu \sim 30(\sqrt{3/2}u'L/\nu \sim 45)$$

whereas the final period sets in, according to Batchelor and Townsend,[7] at $u'\lambda/\nu < 5$.

A direct examination of the energy decay has been carried out over a wide range of distances and various grid shapes by Baines and Peterson.[10] The compared measurements were made at high Reynolds Numbers of the order $u'L/\nu = 1{,}000$ to $1{,}600$. These authors state that their data, for large values of x, fit the decay law $u'^2 \propto x^{-10/7}$ much better than the law $u'^2 \propto x^{-1}$. Also, Frenkiel[11] found the decay $u'^2 \propto x^{-10/7}$ to be in accordance with measurements of several authors.

The most critical check of the decay is a comparison of measured values of the microscale λ. Values of λ^2 from reference 13, which have been determined by different methods—viz., Townsend's differentiation method, Liepmann's method of zero countings, and calculation from measured spectrums—are presented in Figs. 3 and 4. For distances $x > 100$ cm. ($x/M > 60$), the results of each method follow closely the slope $d\lambda^2/dx = 7\nu/U$. This is the slope predicted by the present theory with $\xi = 5$ at high Reynolds Numbers. These experiments agree with the initial decay $u'^2 \propto x^{-1}$ for a much less extended region than those of reference 9. The authors of reference 13 also found that the quantity

$$C = (u'^2/u_0'^2)^{1/5} F_n(0)\ U$$

does not show a definite trend. This is identical with

$$d \ln L/d \ln u'^2 = -(1/5)$$

since the frequency spectrum $F_n(0)U$ at zero frequency is proportional to L.

To check the theoretical spectrum functions, measurements made at sufficiently large distances from the

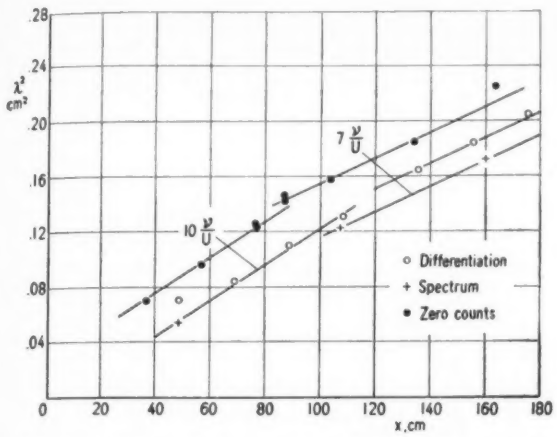

FIG. 3. Variation of microscale with distance from the grid. Measurements from reference 13. $M = 1.68$ cm.; $U = 1{,}130$ cm. per sec.

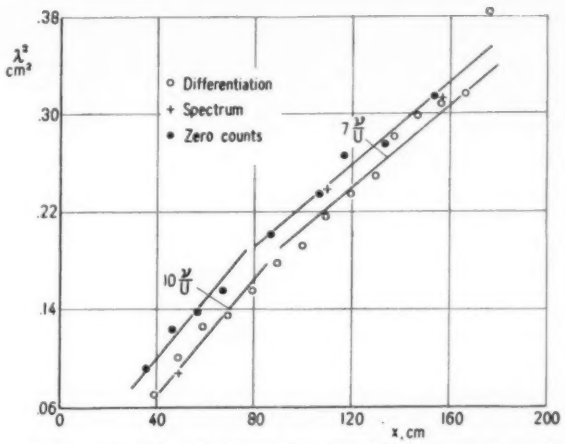

FIG. 4. Variation of microscale with distance from the grid. Measurements from reference 13. $M = 1.68$ cm.; $U = 630$ cm. per sec.

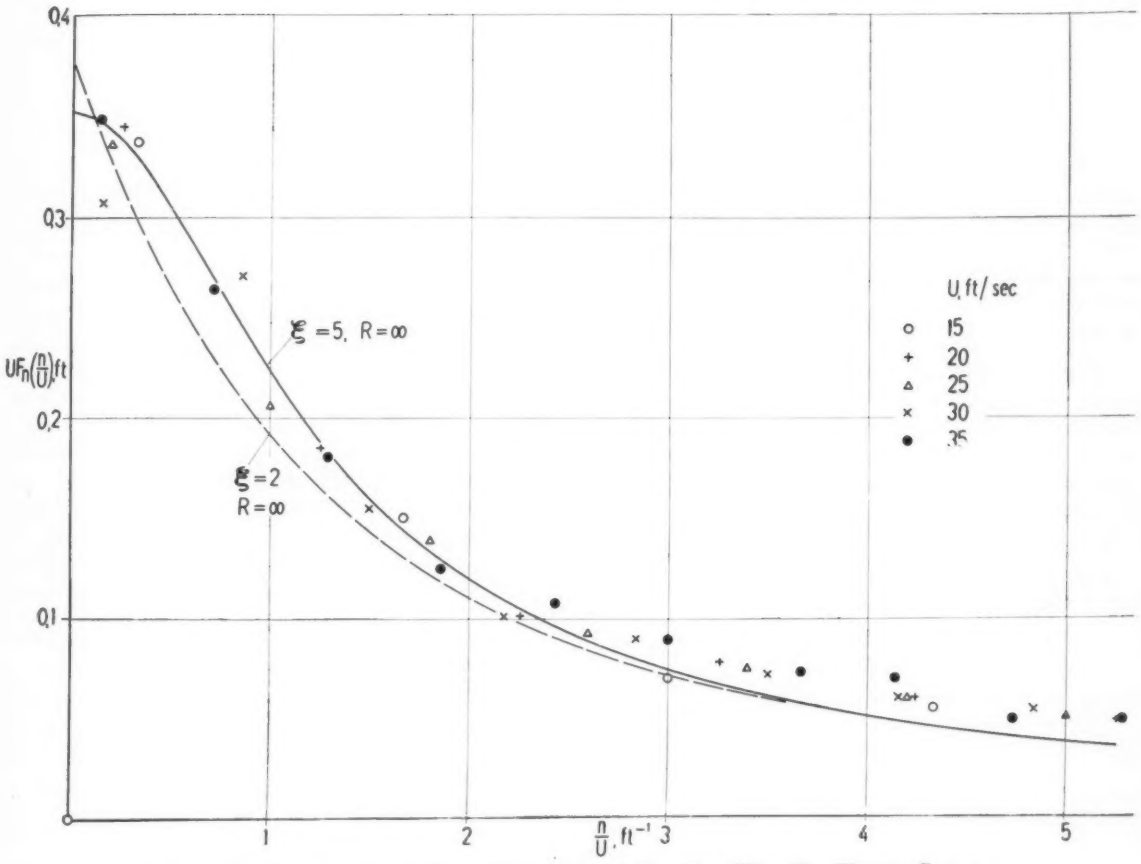

FIG. 5. Frequency spectrum. Measurements from reference 12: $x/M = 27$. Theory: $R = \infty$.

grid are scarcely available, except for those at extremely low Reynolds Numbers. However, the decay, especially the slope of the curve $(\lambda^2, xv/u)$, which corresponds to the second derivative of u'^2 with respect to x, will be perceptibly influenced already by such local deviations of the spectrum from the universal state which lie within the scatter of measurements. Thus, a comparison with measurements of spectrum made at smaller distances, where the decay law of the universal state has not yet been completely established, seems to be justified.

The exact shapes of the theoretical spectrum and correlation functions are, of course, influenced by the particular assumptions regarding the energy transfer term. If we decide to use Heisenberg's relation (4.11), the similarity solutions are still affected by the choice of the constant κ. For that reason Figs. 5 to 9 compare the solution of Eq. (4.9) for $\xi = 5$ and $R = \infty$ with measurements, the comparison then being independent of the arbitrary choice of a constant. As an alternative, the solution of Heisenberg's similarity hypothesis ($\xi = 2$, $R = \infty$) is also plotted.

The theoretical frequency spectrum* for $\xi = 5$ fits well the measurements of Simmons and Salter[12] in the low-frequency range, Fig. 5. The theoretical curve plotted in a normalized form on Fig. 6 also agrees well with the measurements of reference 13 made at extremely high Reynolds Numbers. The deviation of the theoretical transverse correlation function,† Figs. 7 to 9, from measurements by Batchelor and Townsend[9] are mainly caused by the final Reynolds Number. To illustrate this, the solution for $R = 0$ is also represented on Fig. 7. The measurements join the theoretical curve with $\xi = 5$, $R = \infty$ more closely when the mesh grid Reynolds number UM/ν is high. The agreement of the solution with $\xi = 2$ and of the function $\sigma = (1 + \zeta^2)^{-1}$ on Fig. 6, with the measurements is worse.

From these comparisons of the theory with measurements of different origins, it can be concluded that the turbulence behind a grid obeys, with increasing distance, more and more the laws that correspond to the discussed similarity solution with $\xi = 5$. Therefore, it is probable that this solution correctly represents the universal state of isotropic turbulence.

* The frequency spectrum is obtained from the three-dimensional wave number spectrum by

$$UF_n\left(\frac{n}{U}\right) = \frac{2\pi}{u'^2}\int_{2\pi n/U}^{\infty} \frac{k^2 - (2\pi n/U)^2}{k^3} F(k)\, dk$$

where n is the number of cycles per second.

† The transverse correlation function is related with the non-dimensional spectrum function by the equation

$$g\left(\frac{r}{L}, R\right) = \frac{3L^3}{2r^2}\int_0^{\infty} \frac{f(\chi, R)}{2}\left(\chi\frac{r}{L}\sin\frac{\chi r}{L} + \cos\frac{\chi r}{L} - \frac{L}{\chi r}\sin\frac{\chi r}{L}\right) d\chi$$

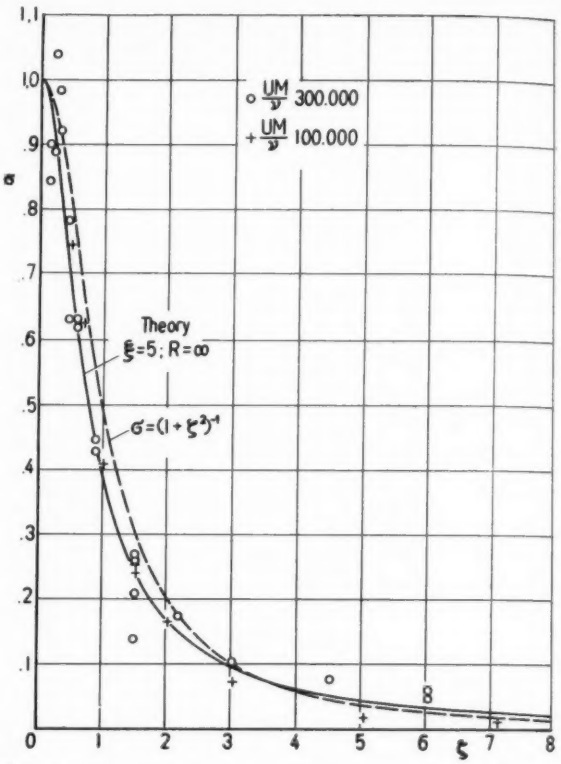

FIG. 6. Frequency spectrum. Measurements from reference 13. Theory: $R = \infty$. $\sigma = F_n(n)/F_n(0)$; $\zeta = (\pi/2)F_n(0)n$.

Appendix

On the Establishment of the Universal State

Batchelor and Townsend[7] have clearly shown that isotropic turbulence approaches to a universal state in course of time. This consideration neglects, however, the nonlinear terms in the Navier-Stokes equations and thus proves only that the universal state is established at extremely low Reynolds Numbers—i.e., in the final period of decay. We must examine the question whether there is a physical basis for the assumption that a universal state may be accomplished also in the case of any arbitrary Reynolds Number.

Some study referring to the establishment of similarity has already been presented in reference 2. It could be shown that the large wave number part of spectrum decays considerably faster than the small wave number part. The direct consequence—viz., the continuous diminution of the wave number range containing the major part of kinetic energy and viscous dissipation—has been experimentally verified (compare Figs. 17, 18, 20, 21, 23, and 24 of reference 13). Further, using Heisenberg's transfer relation, Eq. (4.11), it has been pointed out that local disturbances of the spectrum decrease more rapidly than the undisturbed spectrum. Disturbances at large wave numbers decay much faster than those at small ones.

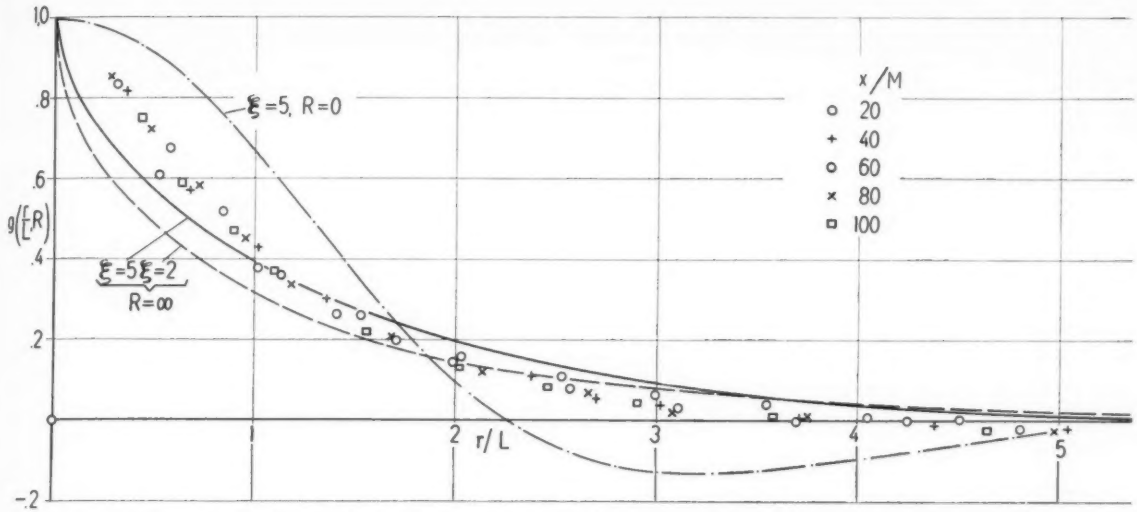

FIG. 7. Transverse correlation function. Measurements from reference 9: $UM/\nu = 5{,}600$. Theory: $R = \infty$ and $R = 0$.

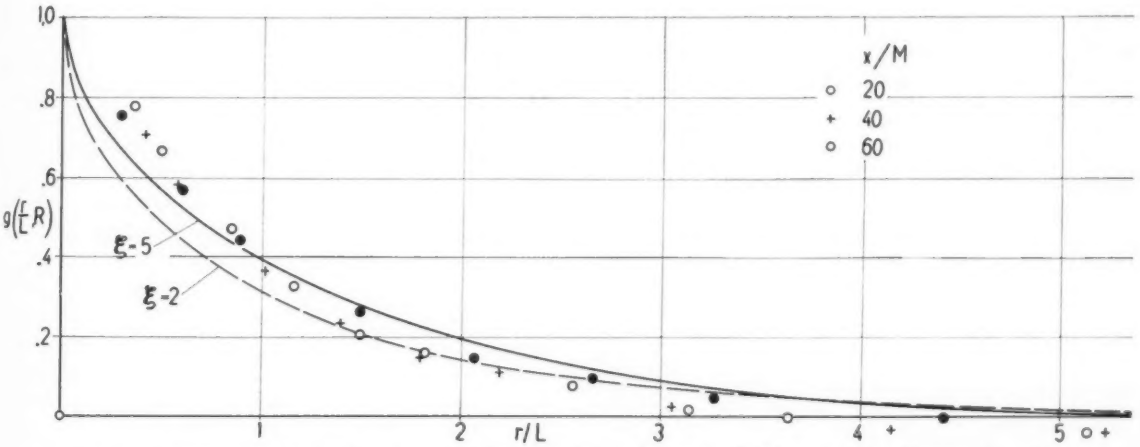

FIG. 8. Transverse correlation function. Measurements from reference 9: $UM/\nu = 11{,}000$. Theory: $R = \infty$.

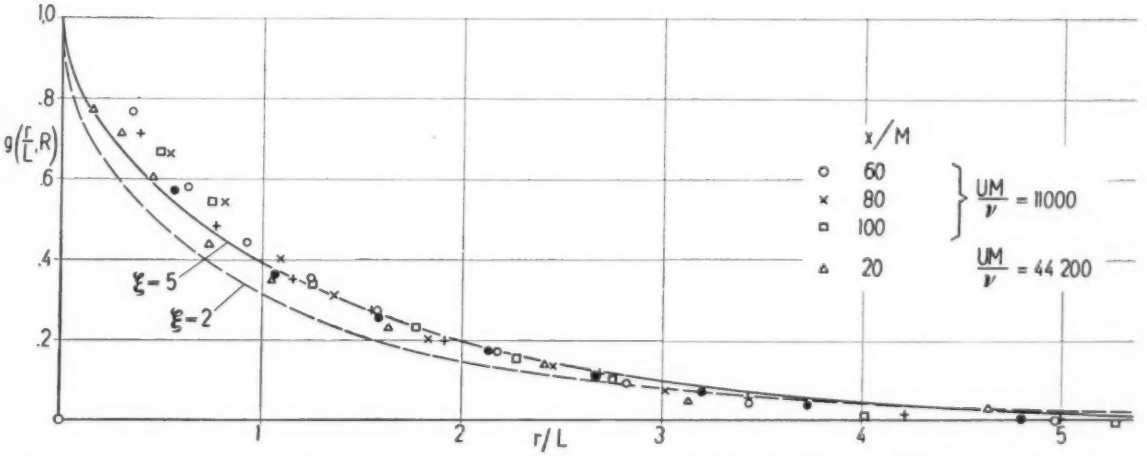

FIG. 9. Transverse correlation function. Measurements from reference 9: $UM/\nu = 11{,}000$ and 44,200. Theory: $R = \infty$.

This means that there is a strong tendency of the spectrum to compensate every irregularity and discontinuity.

Now we are going to consider two spectra that coincide initially within the range $0 < k \leq k_c$ and differ from each other for $k > k_c$. For simplicity we assume firstly, as has been suggested by Kovasznay,[15] that the contribution to the energy transfer

$$\int_0^k W(k')\, dk'$$

comes from a narrow wave number band in the immediate vicinity of k—i.e., that $W(k)$ depends only on $F(k)$ and k in the vicinity of k. In this case we see, from the equation for the change of spectrum,

$$(\partial F/\partial t) + W + \nu 2k^2 F = 0 \qquad (1)$$

that the differences of F for $k > k_c$ do not influence the change of F in the range $0 < k \leq k_c$. Consequently, the two curves of spectrum will still coincide in the range $0 < k \leq k_c$ after an arbitrary period of time.

The assumption that only an extremely small wave number band in the vicinity of k contributes to

$$\int_0^k W(k')\, dk'$$

is not exactly true. But one may say more generally that the essential contribution to

$$\int_0^k W(k')\, dk'$$

comes, in fact, from a wave number band of restricted finite width in the neighborhood of k. This is in accordance with Heisenberg's transfer relation Eq. (4.11) and is the physical hypothesis underlying the theory of locally isotropic turbulence. Thus the change of $F(k)$ within the range $0 < k \leq k_c$ is indeed not completely unaffected by the range $k > k_c$, it will certainly not be affected, however, by the spectrum of wave numbers much larger than k_c.

Next we add a consideration that applies to the initial stage. The energy contained in the region $0 < k \leq k_c$ in which the spectra coincide may be a small fraction of the total energy only. In this case, according to Batchelor,[3] it is possible to express the transfer term approximately in the form

$$W(k) = \eta 2k^2 F(k) \qquad (2)$$

where η is the turbulent friction coefficient that is considered to be nearly independent of k within the range $0 < k \leq k_c$. η is, of course, a function of the time and changes according to the decay of the part $k > k_c$. Substitution of Eq. (2) into Eq. (1) and integration gives

$$F(k, t) = F(k, t_0) \exp\left[-2k^2 \int_{t_0}^{t} (\eta + \nu)\, dt' \right] \qquad (3)$$

which holds for the region $0 < k \leq k_c$. Consider again the two spectra F_1, F_2 having different η (because of different shapes at higher wave numbers $k > k_c$). From Eq. (3) it follows that the curve $F(k)$ has the same shape for $0 < k \leq k_c$ in both cases, if different time intervals of decay are compared, such that

$$\int_{t_0}^{t_1} (\eta_1 + \nu)\, dt' = \int_{t_0}^{t_2} (\eta_2 + \nu)\, dt' \qquad (4)$$

We can now discuss more thoroughly the behavior of the two spectra having properties defined above. During the first period, according to Eq. (3), no differences occur between the shape of the two spectra in the range $0 < k \leq k_c$, despite initially significant differences in the upper range $k > k_c$. With proceeding time, the energy of the part $k > k_c$ decays and the range of k for which Eq. (2) is valid decreases. As an important fact, however, the initial difference between the two spectra decreases rapidly at the same time and a large part of spectrum with higher wave numbers quickly approaches a state of local similarity. Consequently, although the two spectra will no more exactly coincide for the entire range $0 < k \leq k_c$ after a certain time of decay, the initially existing difference will not be able to influence the shape within a less extended finite region $0 < k \leq k_i < k_c$. When the energy initially contained in the range $k > k_i$ has died away, the remaining energy is entirely contained within $0 < k \leq k_i$, the shape of the spectra then being wholly determined by the initial conditions for $0 < k \leq k_c$.

From this consideration result several different spectra having, initially, the same form in the wave number range $0 < k \leq k_c$; for instance, $F \propto k^{\xi - 1}$ achieves with certainty equal forms over the entire energy and dissipation bearing wave number range after corresponding lengths of time. This is the same conclusion that was obtained above in Section (5). In case the initial shape, within $0 < k \leq k_c$, is of universal type—i.e., $F \propto k^4$—the spectra take a universal form. This is the physical picture underlying the idea that any homogeneous isotropic field of turbulence approaches a universal state with time.

Any statement regarding the extension of the region $0 < k \leq k_i$ and the energy contained at the moment when the universal state is accomplished cannot be made. They depend on the initial conditions. However, there is no limitation to the Reynolds Number. There is some indication that the given criterion is too strong. Because of the tendency of the spectrum to compensate irregularities and to approach to a quasi-equilibrium in the upper wave number range, the universal state actually is expected to be established at least when the maximum of the spectrum curve approaches the limit within which the initial deviations from the form $F \propto k^4$ are small.

(*Concluded on page 800*)

LUDWIG PRANDTL
1875–1953

The long-time director of the Kaiser Wilhelm and Max Planck Institute for Flow Research, Prof. Dr. phil., Dr.-Ing. e.h., Dr. rer. techn. h.c., D.Sc. h.c. Ludwig Prandtl, died in Göttingen on August 15 in his 79th year. In deep sorrow we mourn the passing of this prominent scientist, this gracious and beloved person. As founder of flow research he has labored for this science all his life and has created the reputation and tradition of the Göttingen Institute.

Max Planck Society for Scientific Research
Otto Hahn, *President*

As the first half-century of human flight nears its close, this official announcement informs the scientific world of the death of the architect and builder of modern fluid mechanics. His creative mind discerned the essential key physical phenomena in complex fluid motions, established new concepts that are the daily tools of thought of aeronautical scientists and designers and formulated the analytical and quantitative procedures for mathematical study and optimization of proposed designs of aircraft. His influence on aeronautical progress within the last 30 years has been greater than that of any other individual except the Wright brothers themselves.

Before Prandtl, aerodynamic theories were essentially mathematical exercises completely sterile so far as any application to practical problems was concerned. Experimental aerodynamics was purely empirical. When Prandtl, after a short but successful service as mechanical engineer, with Maschinenfabrik Augsburg-Nürnberg and 3 years as professor of mechanics at Hanover, accepted appointment to the chair of applied mechanics at Göttingen, he found a long-established tradition in process of further development by the great mathematician, Felix Klein. Klein believed that there should be a close connection between the general abstract mathematical theories and the experimental facts and practical applications. Prandtl proceeded to select suitable basic problems, to create new experimental apparatus, and to refine experimental methods, all looking toward a method of analysis embodying the essential physical aspects of the problem and in agreement with the data resulting from experiments. He drew around him a group of collaborators who were stimulated by his leadership to productive and creative extensions and applications of his own basic concepts.

Prandtl's most important contribution to aeronautics was his wing theory—i.e., the discovery and computation of induced drag by means of which rational design procedures were established to compute the influence of wing span, to compare monoplanes and biplanes, to estimate influence of stagger and gap in biplanes, and to compute load distribution, down-wash, and so on. The development of the high aspect ratio monoplane wing of great efficiency was directly stimulated by Prandtl's work. This theory was developed during the first World War and not known to others outside Germany until 1921.

Another concept regarded by many as equally important is that of the boundary layer, historically antedating the wing theory. More correctly, Prandtl's contribution was a theory of the motion of fluids with small friction, dealing with the whole flow field. Approximate methods of solution of the differential equations were given, and the large effect of a small friction in producing separation of flow in adverse pressure gradients was explained.

In these days of supersonic interest, we must rank highly Prandtl's contributions to compressible flow—first, his studies of the efflux of gases and vapors under high pressure. Some doubted that supersonic efflux speeds were possible, but Prandtl applied the Riemann theory of shock waves and the experimental schlieren method of Mach to give a full description and explanation. These contributions were made in the 1904–1907 period. Later, as propeller tips approached supersonic speed, he developed a linearized theory of compressible flow. Such terms as Prandtl-Meyer expansion and Prandtl-Glauert approximation remind us of his work in this field.

(*Concluded on page 800*)

Readers' Forum

BRIEF REPORTS of investigations in the aeronautical sciences and discussions of papers published in the JOURNAL are presented in this special department. Publication will be completed as soon as possible after receipt of the material. The Editorial Committee does not hold itself responsible for the opinions expressed by the correspondents. Contributions should not exceed 800 words in length.

On Laminar Boundary Layer over a Rotating Blade*

H. S. Tan
Graduate of Aeronautical Engineering, Cornell University, Ithaca, N.Y.
July 20, 1953

CONSIDER A CYLINDRICAL BLADE extending infinitely in y-direction and rotating about z-axis with angular speed Ω. The boundary-layer flow about the blade is given by differential equations,

$$\left.\begin{aligned} uu_x + vu_y + wu_z - 2v\Omega - x\Omega^2 &= -(1/\rho)p_x + \nu u_{zz} \\ uv_x + vv_y + wv_z + 2u\Omega - y\Omega^2 &= -(1/\rho)p_y + \nu v_{zz} \\ u_x + v_y + w_z &= 0 \end{aligned}\right\} \quad (1)$$

together with boundary conditions

$$\left.\begin{aligned} u = v = w &= 0, \qquad z = 0 \\ u \to \bar{U},\quad v \to \bar{V},\quad w \to \bar{W},&\quad z \to \infty \end{aligned}\right\} \quad (2)$$

where $\bar{U}$, $\bar{V}$, $\bar{W}$ are velocity components of outside potential flow, readily obtainable as

$$\left.\begin{aligned} \bar{U} &= y\Omega\,\phi_{1x}(x, z) \\ \bar{V} &= \Omega[\phi_1(x, z) - 2x] \\ \bar{W} &= y\Omega\phi_{1z}(x, z) \end{aligned}\right\} \quad (3)$$

in which ϕ_1 denotes the potential for plane flow past the cylinder in uniform stream along x-direction.[1] From Eqs. (3), the pressure gradients p_x, p_y follow at once by using Bernoulli's equation,

$$\left.\begin{aligned} (1/\rho)p_x &= x\Omega^2 - \bar{U}\bar{U}_x - \bar{V}\bar{V}_x \\ (1/\rho)p_y &= y\Omega^2 - \bar{U}\bar{U}_y \end{aligned}\right\} \quad (4)$$

Now, because of the nonlinearity of equations and coupling of dependent variables, a general solution of Eqs. (1) cannot be expected. However, if one restricts oneself to regions in the neighborhood of leading edge, where $x/y \ll 1$, it will be shown that a perturbation procedure can be set up so that all the successive approximations are linearized. Indeed, both u and v velocities are then expressible in terms of a single parameter $\eta = (z/2)\sqrt{y\Omega/x\nu}$ as follows:

$$\left.\begin{aligned} u &= \frac{y\Omega}{2}\sum_0\left(\frac{x}{y}\right)^n F_n'(\eta) \\ v &= \frac{y\Omega}{2}\sum_0\left(\frac{x}{y}\right)^n G_n'(\eta) \end{aligned}\right\} \quad (5)$$

To proceed, let us first observe that since Eqs. (3) give $\bar{U}$, $\bar{W} \sim y$, $\bar{V} \sim x$, we are justified in writing

$$\left.\begin{aligned} u &= u^0 + u^{(1)} + u^{(2)} + \dots \\ v &= v^{(1)} + v^{(2)} + \dots \\ w &= w^0 + w^{(1)} + w^{(2)} + \dots \\ p &= p^0 + p^{(1)} + p^{(2)} + \dots \end{aligned}\right\} \quad (6)$$

where $(\ )^n \sim O(x/y)^n$.

On substituting Eqs. (6) into Eqs. (1), collecting terms according to different orders in (x/y), and equating to zero respectively, it is seen that the nth approximation are given by differential equations,

$$\left.\begin{aligned} \sum_0^n[u^{(s)}u_x^{(n-s)} + w^{(s)}u_z^{(n-s)}] + \sum_1^{n-1} v^{(s)}u_y^{(n-1-s)} - \\ 2v^{(n-1)}\,\Omega - x\Omega^2\delta_2{}^n = -(1/\rho)p_x{}^{(n)} + \nu u_{zz}{}^{(n)} \\ \sum_0^n[u^{(s)}v_x^{(n-s)} + w^{(s)}v_z^{(n-s)}] + \sum_1^{n-1} v^{(s)}v_y^{(n-1-s)} + \\ 2u^{(n-1)}\,\Omega - y\Omega^2\delta_1{}^n = -(1/\rho)p_y{}^{(n-1)} + \nu v_{zz}{}^{(n)} \\ u_x{}^{(n)} + w_z{}^{(n)} + v_y{}^{(n-1)} = 0 \end{aligned}\right\} \quad (7)$$

together with boundary conditions

$$\left.\begin{aligned} u^{(n)} = v^{(n)} = w^{(n)} &= 0, \qquad z = 0 \\ u^{(n)} \to \bar{U}^{(n)},\quad v^{(n)} \to \bar{V}^{(n)},&\quad w^{(n)} \to \bar{W}^{(n)},\quad z \to \infty \end{aligned}\right\} \quad (8)$$

SOLUTION FOR ROTATING FLAT PLATE

In case of a rotating flat plate, Eqs. (3) and (4) give

$$\left.\begin{aligned} \bar{U} = y\Omega, \qquad \bar{V} = -x\Omega, \qquad \bar{W} = 0 \\ p_x = p_y = 0 \end{aligned}\right\} \quad (9)$$

so that Eq. (7) leads readily to the following results:

(i) Zero-Order Solution:

$$\left.\begin{aligned} u^0u^0x + w^0u_z{}^0 &= \nu u_{zz}{}^0 \\ u_x{}^0 + w_z{}^0 &= 0 \end{aligned}\right\} \quad (10)$$

with $u^0 = w^0 = 0$ at $z = 0$, and $u^0 \to y\Omega$, $w^0 \to 0$ as $z \to \infty$.

Now Eqs. (10) are exactly the well-known Blasius problem. On introducing

$$\left.\begin{aligned} \eta &= \frac{z}{2}\sqrt{\frac{y\Omega}{x\nu}}, \qquad u^0 = \frac{y\Omega}{2}F' \\ w^0 &= \frac{1}{2}\sqrt{\frac{y\Omega\nu}{x}}\,(\eta F' - F) \end{aligned}\right\} \quad (11)$$

where F is a function of η alone, we arrive at equation

$$F''' + FF'' = 0 \quad (12)$$

with $F(0) = F'(0) = 0$ and $F'(\infty) = 2$. The solution of Eq. (12) was obtained by numerical integration.[2, 3]

(ii) First-Order Solution:

$$\left.\begin{aligned} u^0u_x{}^{(1)} + u^{(1)}u_x{}^0 + w^0u_z{}^{(1)} + w^{(1)}u_z{}^0 &= \nu u_{zz}{}^{(1)} \\ u^0v_x{}^{(1)} + w^0v_z{}^{(1)} + 2u^0\Omega - y\Omega^2 &= \nu v_{zz}{}^{(1)} \\ u_x{}^{(1)} + w_z{}^{(1)} &= 0 \end{aligned}\right\} \quad (13)$$

* This research was supported by the USAF under Contract No. AF 33-(038)-21406, monitored by the Office of Scientific Research, Air Research and Development Command.

with $u^{(1)} = v^{(1)} = w^{(1)} = 0$ at $z = 0$, and $u^{(1)} = w^{(1)} = 0$, $v^{(1)} = -x\Omega$ as $z \to \infty$.

By comparing Eqs. (13.1), (13.3) with Eqs. (10), it is easily verified that $u^{(1)} = w^{(1)} \equiv 0$ are solutions for Eqs. (13).

Now as Eq. (13.2) contains only $v^{(1)}$, it can be solved separately. Indeed, putting

$$v^{(1)} = (x\Omega/2)G'(\eta) \tag{14}$$

Eq. (13.2) reduces directly to following differential equation for G

$$G''' + FG'' - 2F'G' = 8(F' - 1) \tag{15}$$

with $G(0) = G'(0) = 0$, and $G'(\infty) = -2$. Eq. 15 has been integrated numerically for G' in references 4 and 5.

(iii) Second-Order Solution:

$$\left.\begin{aligned} &u^0u_x^{(2)} + u^{(2)}u_x^0 + v^{(1)}u_y^0 + w^0u_z^{(2)} + \\ &\qquad w^{(2)}u_z^0 - 2v^{(1)}\Omega - x\Omega^2 = \nu u_{zz}^{(2)} \\ &u^0v_x^{(2)} + w^0v_z^{(2)} = \nu v_{zz}^{(2)} \\ &u_x^{(2)} + w_z^{(2)} + v_y^{(1)} = 0 \end{aligned}\right\} \tag{16}$$

with $u^{(2)} = v^{(2)} = w^{(2)} = 0$ at $z = 0$ and as $z \to \infty$.

By comparing Eq. (16.2) with Eq. (13.2), it is easily verified that $v^{(2)} \equiv 0$ is a solution of Eq. (16.2). Now,

$$\left.\begin{aligned} u^{(2)} &= (x^2\Omega/2y)f'(\eta) \\ w^{(2)} &= \frac{x\Omega}{y}\,2\sqrt{\frac{\nu x}{y\Omega}}\left[\frac{1}{4}(\eta f' - f) - 1/4(\eta G' - G) - f\right] \end{aligned}\right\} \tag{17}$$

satisfies Eqs. (16.3). Introducing Eqs. (11), (14), and (17) into Eqs. (16), we arrive at the differential equation for f as follows:

$$f''' + Ff'' - 4F'f' + 5F''f = 2(F' - 4)G' + F''G - 8 \tag{18}$$

with $f(0) = f'(0) = 0$ and $f'(\infty) = 0$.

(iv) Third-Order Solution:

$$\left.\begin{aligned} &u^0u_x^{(3)} + u^{(3)}u_x^0 + w^0u_z^{(3)} + w^{(3)}u_z^0 = \nu u_{zz}^{(3)} \\ &u^0v_x^{(3)} + u^{(2)}v_x^{(1)} + v^{(1)}v_y^{(1)} + w^0v_z^{(3)} + \\ &\qquad w^{(2)}v_z^{(1)} + 2u^{(2)}\Omega = \nu v_{zz}^{(3)} \\ &u^{(3)} + w_z^{(3)} = 0 \end{aligned}\right\} \tag{19}$$

with $u^{(3)} = v^{(3)} = w^{(3)} = 0$ at $z = 0$ and as $z \to \infty$.

Comparing Eqs. (19.1) and (19.3) with Eqs. (13), it is easily verified that $u^{(3)} = w^{(3)} \equiv 0$ are solutions.

Now Eq. (19.2) can be solved for $v^{(3)}$ separately. Indeed, putting

$$v^{(3)} = \frac{x^3\Omega}{2y^2}g'(\eta) \tag{20}$$

Eq. (19.2) reduces directly to the following differential equation for g:

$$g''' + Fg'' - 6F'g' = 2(G' + 4)f' - 5G''f + GG'' \tag{21}$$

with $g(0) = g'(0) = 0$ and $g'(\infty) = 0$.

If we denote functions F, G, f, g, etc., by f_0, f_1, f_2, f_3, etc., respectively, then Eqs. (12), (15), (18), (21), etc., take on the following form:

$$\left.\begin{aligned} &f_0''' + f_0f_0'' = 0 \\ &f_1''' + f_0f_1'' - 2f_0'f_1' = 8(f_0' - 1) \\ &f_2''' + f_0f_2'' - 4f_0'f_2' + 5f_0''f_2 = 2(f_0' - 4)f_1' + f_0''f_1 - 8 \\ &f_3''' + f_0f_3'' - 6f_0'f_3' = 2(f_1' + 4)f_2' - 5f_1''f_2 + f_1''f_1 \\ &\cdots\quad\cdots\quad\cdots \end{aligned}\right\} \tag{22}$$

with $f_n(0) = f_n'(0) = 0$ for all n and with $f_0'(\infty) = 2$, $f_1'(\infty) = -2$, and $f_n'(\infty) = 0$ for $n \geq 2$. We are thus able to write

$$\left.\begin{aligned} u &= \frac{y\Omega}{2}\sum_0\left(\frac{x}{y}\right)^{2n} f_{2n}'(\eta) \\ v &= \frac{y\Omega}{2}\sum_0\left(\frac{x}{y}\right)^{2n+1} f_{2n+1}'(\eta) \end{aligned}\right\} \tag{23}$$

It might be of interest to compare Eqs. (22) with corresponding set of differential equations for two-dimensional boundary-layer flow expanded in powers of x, having a linear outside velocity distribution $U = U_0 + cx$.[6] Indeed this noted resemblance makes it possible to carry out our numerical calculation entirely after the manner of reference 7.

References

[1] Sears, W. R., *Potential Flow Around a Rotating Cylindrical Blade*, Journal of the Aeronautical Sciences, Vol. 17, No. 3, p. 183, March, 1950.

[2] Blasius, H., *Grenzschichten in Flüssigkeiten mit kleiner Reibung*, Zs. Math. u. Phys., Bd. 56, p. 1, 1908.

[3] Goldstein, S., *Modern Developments in Fluid Dynamics*, Vol. 1; Oxford, 1938.

[4] Fogarty, L. E., *The Laminar Boundary Layer on a Rotating Blade*, Journal of the Aeronautical Sciences, Vol. 18, No. 4, pp. 247–252, April, 1951.

[5] Fogarty, L. E., *The Laminar Boundary Layer on a Rotating Blade*, Thesis for Ph.D., Cornell University, September, 1950.

[6] Tani, I., *On the Solution of the Laminar Boundary Layer Equations*, Journal of Phys. Soc. of Japan, Vol. 4, No. 3, pp. 149–154, May, 1949.

[7] Howarth, L., Reports and Memoranda No. 1632, 1934.

On the Evaluation of the Function $f_\lambda(M, \tilde{\omega})$

G. Zartarian and H. M. Voss

Aeroelastic and Structures Research Laboratory, Massachusetts Institute of Technology, Cambridge, Mass.

July 27, 1953

THROUGHOUT THE FIELD of unsteady supersonic aerodynamics, it becomes necessary to evaluate a function of the form

$$f_\lambda(M, \tilde{\omega}) = \int_0^1 \exp.(-i\tilde{\omega}u)J_0\left(\frac{\tilde{\omega}}{M}u\right)u^\lambda\,du \tag{1}$$

wherein M is the Mach Number, $\tilde{\omega}$ is a frequency parameter defined by

$$\tilde{\omega} = 2kM^2/(M^2 - 1) \tag{2}$$

and k is the familiar reduced frequency parameter in unsteady flow. For example, the forces and moments for the two-dimensional oscillating airfoil in supersonic flow are given by Garrick and Rubinow[1] in terms of functions that can be reduced to combinations of f_λ with $\lambda = 0, 1, 2$, and 3. The work by Miles[2] on the forces and moments on a rigid oscillating wide delta in supersonic flow requires, in addition, the function f_4.

Further work with the wide delta plan form shows that the elastic motions will require the values of f_λ for λ of even higher order. For example, the moment due to parabolic camber will involve f_6, and the generalized force in the camber mode due to the camber mode itself requires evaluation of f_8. Similarly, spanwise modes (normal to the stream) lead to integrals of the form of Eq. (1) but with Bessel functions of higher order. Such integrals can be reduced by partial integration to the exact form of Eq. (1) but result in higher order λ. The generalized force in a parabolic bending mode due to the mode includes f_λ up to and including f_6.

Previous methods of evaluation of the functions f_λ have relied on precise determination of f_0 and continued use of the recursion formula developed by Borbely,[3]

$$\frac{M^2 - 1}{M^2}\,\tilde{\omega}\,f_\lambda(M, \tilde{\omega}) = \left\{i + (1 - \lambda)\frac{1}{\tilde{\omega}}\right\}e^{-i\tilde{\omega}}J_0\left(\frac{\tilde{\omega}}{M}\right) - \frac{1}{M}e^{-i\tilde{\omega}}J_1\left(\frac{\tilde{\omega}}{M}\right) + i(1 - 2\lambda)f_{\lambda-1}(M, \tilde{\omega}) + (1 - \lambda)^2\frac{1}{\tilde{\omega}}f_{\lambda-2}(M, \tilde{\omega}) \tag{3}$$

The function f_0 was evaluated by Borbely to five decimal places from the infinite Bessel function series.

$$f_0(M, \bar{\omega}) = e^{-i\bar{\omega}} \sum_{n=0}^{\infty} \left(\frac{M^2 - 1}{M^2}\,\bar{\omega}\right)^n \times \frac{1}{2^n n!\,(2n+1)} [J_n(\bar{\omega}) + iJ_{n+1}(\bar{\omega})] \quad (4)$$

Also included in reference 3 are f_1, f_2, and f_3 as calculated from the recursion Eq. (3) above, and these results are reproduced by Miles.[2] Schwarz has determined f_0 to eight significant figures by expansion of the function as an infinite integral series that leads to a doubly infinite power series expansion. The results of Schwarz are continued in reference 1.

A difficulty involved in use of the above is that the arguments M and $\bar{\omega}$ for which the functions are tabulated are not convenient to the problem at hand, particularly for the case of a control surface wherein modified f_λ functions are required.

$$g_\lambda(M, \bar{\omega}) = f_\lambda(M, \bar{\omega}x_1)$$
$$h_\lambda(M, \bar{\omega}) = f_\lambda(M, \bar{\omega}\{1 - x_1\})$$

where x_1 is the location of the aileron hinge line.[1] Furthermore, it is found that, because of the inherent nature of the recursion formula, evaluation of f_λ for higher order λ by Eq. (2) results in continued loss in accuracy.

For these reasons it is desirable to have available a method of evaluation of f_λ which is accurate in itself to any degree and which permits simple variation of the frequency parameter, $\bar{\omega}$. Such a form can be obtained by expansion of both the exponential and the zero-order Bessel function of the integrand as infinite power series, followed by term-by-term integration. There results,

$$f_\lambda(M, \bar{\omega}) = \sum_{s=0}^{\infty} \sum_{r=0}^{\infty} \frac{(-1)^s(-i)^r}{r + 2s + \lambda + 1} \left(\frac{1}{2M}\right)^{2s} \times \frac{1}{(s!)^2}\,\frac{1}{r!}\,(\bar{\omega})^{r+2s} \quad (5)$$

This can be more simply expressed in terms of the real and imaginary parts of the function,

$$f_\lambda(M, \bar{\omega}) = \sum_{n=0}^{\infty} \frac{(-1)^n}{\lambda + 2n + 1}\, a_{2n}(M)\,(\bar{\omega})^{2n} - i\bar{\omega} \sum_{n=0}^{\infty} \frac{(-1)^n}{\lambda + 2n + 2}\, b_{2n}(M)\,(\bar{\omega})^{2n} \quad (6)$$

where the coefficients are themselves finite series,

$$\left.\begin{aligned} a_{2n}(M) &= \sum_{j=0}^{n} \frac{1}{(j!)^2}\,\frac{1}{[2(n-j)]!} \left(\frac{1}{2M}\right)^{2j} \\ b_{2n}(M) &= \sum_{j=0}^{n} \frac{1}{(j!)^2}\,\frac{1}{[2(n-j)+1]!} \left(\frac{1}{2M}\right)^{2j} \end{aligned}\right\} \quad (7)$$

Since both the exponential and the Bessel functions are analytic in the entire finite complex plane, their power series expansions, and hence the integrand of Eq. (1), is uniformly convergent throughout the finite complex $\bar{\omega}z$ plane, and in particular along the real axis. Then, by change of variable to $\bar{\omega}u$, the integral is everywhere regular, including the origin, and convergence of the term-by-term integration to the value of $f_\lambda(M, \bar{\omega})$ is assured for all values of $\bar{\omega} < \infty$ and M from the theory of functions (cf. reference 5).

The advantage of the series representation above is that the dependence of f_λ on λ, M, and $\bar{\omega}$ is completely separated, so that the coefficients a_{2n} and b_{2n} can be tabulated for a given Mach Number. The function can then be determined for any λ and $\bar{\omega}$ to an accuracy limited only by the tabulated coefficients. It will also be noted that, for a given accuracy, the number of terms required decreases with increasing λ and M.

Table 1 presents values of the coefficients a_{2n} and b_{2n} for the range $n = 0$ to 6 and for most of the customarily used Mach Numbers. This table has been used to calculate f_0 to nine places, and the results were compared with the values obtained from Eq. (4). In all cases the results agree to within one in the ninth place. Since the accuracy improves with increasing λ, the accuracy for higher λ is assured.

In conclusion it is worth noting that one set of coefficients can be written in terms of the other—i.e.,

$$b_{2n} = \sum_{j=0}^{n} a_{2n}(-1)^{n-j}\,\frac{2^{(n-j+1)}\,(2^{(n-j+1)} - 1)}{|2(n-j+1)|!} B_{2n2j+1} \quad (8)$$

where the B_n's are Bernoulli's Numbers, $B_1 = 1/6$, $B_3 = 1/30$, $B_5 = 1/42$, $B_7 = 1/30$, $B_9 = 5/66$, $B_{11} = 691/2{,}730$, $B_{13} = 7/6$, ... This form is often more convenient for calculation of the second set of coefficients when the first set has been evaluated.

References

[1] Garrick, I. E., and Rubinow, S. I., *Flutter and Oscillating Air-Force Calculations for an Airfoil in Two-Dimensional Supersonic Flow*, NACA TR No. 846, 1946.

[2] Miles, J. W., *On Harmonic Motion of Wide Delta Airfoils at Supersonic Speeds*, Navord Report 1234, June 13, 1950.

[3] von Borbely, S., *Aerodynamic Forces on a Harmonically Oscillating Wing at Supersonic Velocity (Two-Dimensional Case)*, R.T.P. Translation No. 2019, British Ministry of Aircraft Production. (From Z.F.a.M.M., Bd. 22, Heft 4, pp. 190–205, August, 1942.

[4] Schwarz, L., *Untersuchung einiger mit den Zylinderfunktionen Nullter Ordnung Verwandter Functionen*, Luftfahrtforschung, Bd. 20, Lfg. 12, pp. 341–372, February 8, 1944.

[5] Knopf, K., *Theory of Functions, Elements of the General Theory of Analytic Functions*, Translated by Bagemihl, F.; Dover Publications, New York. 1945.

TABLE 1
Table of Functions a_{2n}, b_{2n}

M	5/4	10/7	3/2	5/3	2	5/2
$\bar{\omega} = \rightarrow$	$(50/9)k$	$(200/51)k$	$(18/5)k$	$(25/8)k$	$(8/3)k$	$(50/21)k$
a_0	1	1	1	1	1	1
a_2	0.660,000,000	0.622,500,000	0.611,111,111	0.590,000,000	0.562,500,000	0.540,000,000
a_4	0.128,066,667	0.106,668,230	0.100,308,642	0.088,691,667	0.073,893,229	0.062,066,667
a_6	0.011,369,333	0.008,419,900	0.007,599,832	0.006,171,639	0.004,488,119	0.003,257,333
a_8	0.000,571,718	0.000,377,178	0.000,327,040	0.000,244,416	0.000,155,716	0.000,097,918
a_{10}	0.000,018,450	0.000,010,850	0.000,009,040	0.000,006,222	0.000,003,478	0.000,001,900
a_{12}	0.000,000,414	0.000,000,217	0.000,000,174	0.000,000,110	0.000,000,053	0.000,000,026
b_0	1	1	1	1	1	1
b_2	0.326,666,667	0.289,166,667	0.277,777,778	0.256,666,667	0.229,166,667	0.206,666,667
b_4	0.041,400,000	0.032,501,563	0.029,938,272	0.025,358,333	0.019,726,563	0.015,400,000
b_6	0.002,712,190	0.001,895,569	0.001,676,845	0.001,306,163	0.000,888,788	0.000,600,191
b_8	0.000,107,937	0.000,067,226	0.000,057,138	0.000,040,977	0.000,024,451	0.000,014,326
b_{10}	0.000,002,881	0.000,001,600	0.000,001,307	0.000,000,863	0.000,000,452	0.000,000,230
b_{12}	0.000,000,055	0.000,000,027	0.000,000,021	0.000,000,012	0.000,000,005	0.000,000,003

Spanwise and Chordwise Loadings for Rectangular Wings of Aspect Ratio near Unity

William R. Laidlaw
Department of Aeronautical Engineering, Aeroelastic and Structures Research Laboratory, Massachusetts Institute of Technology, Cambridge, Mass.
July 6, 1953

THE LIFTING SURFACE INTEGRAL EQUATION has been formulated by Reissner[1] and for the rectangular wing may be stated as follows:

$$w(x, y) = -\frac{1}{4\pi b}\oint_{-s}^{s}\frac{d\Gamma}{d\eta}\frac{d\eta}{(y-\eta)} - \frac{1}{4\pi}\oint_{-s}^{s}\int_{-1}^{1}\frac{\partial\gamma}{\partial\eta}\frac{\sqrt{(x-\xi)^2+(y-\eta)^2}}{(x-\xi)(y-\eta)}\,d\xi\,d\eta \quad (1)$$

In the present notation, the wing has a span of $2sb$ and a chord of $2b$. The local vorticity γ is related to the total pressure difference at a point by

$$\gamma = \Delta p/\rho U \quad (2)$$

The circulation Γ is the chordwise integral of the local vorticity at any spanwise station; hence,

$$\Gamma(y) = \frac{L(y)}{\rho U} = b\int_{-1}^{1}\gamma(\xi, y)\,d\xi \quad (3)$$

In considering a wing of aspect ratio (s) near unity we may simplify the radical of Eq. (1) by the following considerations.

$$R = \sqrt{(x-\xi)^2+(y-\eta)^2} = \sqrt{u^2+v^2}$$

where $u = |x-\xi|$ and $v = |y-\eta|$.
Therefore,

$$R = (u+v)\left\{1 - \frac{uv}{(u+v)^2} - \frac{1}{8}\left[\frac{uv}{(u+v)^2}\right]^2 \cdots\right\}$$

Neglecting second-order and higher order terms

$$R \cong (u+v) - [uv/(u+v)] \quad (4)$$

Now

$$\frac{uv}{u+v} \equiv \frac{1}{4}\left\{(u+v) - \frac{(u-v)^2}{(u+v)}\right\} \quad (5)$$

Over the range of integration u and v are of the same order of magnitude, and, consequently, the second term of Eq. (5) may be dropped so that we have, finally,

$$R \cong \frac{3}{4}(u+v) = \frac{3}{4}(|x-\xi| + |y-\eta|) = R_a \quad (6)$$

It may be noted by a comparison of R_a with R that for a fixed point (x, y) the maximum error (i.e., 25 per cent) occurs when $\xi \to x$, or $\eta \to y$. The integral involving R is, however, singular at $\xi = x$ and $\eta = y$, and, consequently, when taking the principal value, we find that near these singularities errors in R have a negligible effect upon the final result.

Substituting Eq. (6) into Eq. (1) and simplifying, we have

$$w(x, y) = -\frac{1}{16\pi b}\oint_{-s}^{s}\frac{d\Gamma}{d\eta}\frac{d\eta}{(y-\eta)} - \frac{3}{8\pi}\times \oint_{-s}^{s}\frac{\partial\varphi}{\partial\eta}\cdot\frac{d\eta}{(y-\eta)} - \frac{3}{8\pi}\oint_{-1}^{1}\frac{\gamma(\xi, y)}{(x-\xi)}\,d\xi \quad (7)$$

where

$$\varphi = \varphi(x, \eta) = \int_{-1}^{x}\gamma(\xi, \eta)\,d\xi$$

We may next proceed to a solution of this equation by specifying a pressure distribution of the form,

$$\frac{\Delta p}{\rho U^2} = X(\Phi)\cdot Y(\Psi) \quad (8)$$

where the angular variables are defined as follows:

$$x = -\cos\Phi, \quad y = s\cos\Psi$$

This assumed form of solution is restrictive in the sense that it makes no provision for the spanwise variation of section center of pressure, but from the standpoint of obtaining total lift and pitching moment, spanwise and chordwise lift distributions, and approximate chordwise pressure distributions it should provide reasonable results.

TABLE 1
Fourier Coefficients for Flat Plate Wing in Symmetrical Flight

S	K_1	K_3	K_5	$\frac{C_0}{\alpha}$	$\frac{C_1}{\alpha}$	$\frac{C_2}{\alpha}$	$\frac{C_3}{\alpha}$	$\frac{C_4}{\alpha}$	$\frac{C_5}{\alpha}$	$\frac{dC_L}{d\alpha}$	$\frac{C.P.}{c}$
0.50	1.0000	0.0562	0.0117	0.7244	−0.7848	−0.8899	−0.7643	−0.6083	−0.4969	0.8192	0.1220
0.75	1.0000	0.0718	0.0156	0.8873	−0.8225	−0.8527	−0.6732	−0.5223	−0.4148	1.1747	0.1460
1.00	1.0000	0.0864	0.0195	1.0225	−0.8312	−0.8100	−0.6024	−0.4768	−0.3612	1.4974	0.16222
1.25	1.0000	0.0998	0.0234	1.1388	−0.8261	−0.7677	−0.5469	−0.4164	−0.3228	1.7910	0.1738
1.50	1.0000	0.1112	0.0269	1.2419	−0.8141	−0.7298	−0.5022	−0.3812	−0.2938	2.0600	0.1827
1.75	1.0000	0.1248	0.0312	1.3334	−0.7987	−0.6958	−0.4706	−0.3531	−0.2712	2.3046	0.1897
2.00	1.0000	0.1365	0.0351	1.4162	−0.7812	−0.6649	−0.4348	−0.3297	−0.2522	2.5306	0.1953

Let

$$Y(\Psi) = \sum_{m=1}^{M} K_m \frac{\sin m\Psi}{m} \qquad (K_1 = 1) \tag{9}$$

$$X(\Phi) = c_0 \cot \frac{\Phi}{2} + \sum_{n=1}^{N} c_n \frac{\sin n\Phi}{n} \tag{10}$$

Substituting Eqs. (8), (9), and (10) in Eq. (7) and performing the necessary integrations, we have

$$\frac{z(\Psi)}{8s}\left(3\Phi + \frac{\pi}{2}\right)\left(c_0 + \frac{c_1}{2}\right) + \frac{3c_0}{8s} z(\Psi) \sin \Phi + \frac{3}{16s} z(\Psi) \sum_{n=1}^{N}{}' \frac{c_n}{n}\left[\frac{\sin (n-1)\Phi}{n-1} - \frac{\sin (n+1)\Phi}{n+1}\right] + \frac{3}{8} Y(\Psi)\left[c_0 - \sum_{n=1}^{N} c_n \frac{\cos n\Phi}{n}\right] \equiv -\frac{w(\Phi, \Psi)}{U} \tag{11}$$

where

$$z(\Psi) = \sum_{m=1}^{M} K_m \frac{\sin m\Psi}{\sin \Psi}$$

$$\sum_{n=1}^{N}{}' \text{ — omit } \frac{\sin (n-1)}{n-1}\Phi \text{ for } n = 1$$

When the downwash function $w(\Phi, \Psi)$ has been prescribed, the unknown constants $K_2, K_3, \ldots, K_m$, and $c_0, c_1, \ldots, c_n$ may be determined by causing the above identity to be satisfied at a number of points on the plan form equal to the number of unknowns (collocation scheme).

Another and somewhat more desirable process is to use Eq. (11) in combination with a weighted integral procedure to generate the required number of equations.

For instance, if the integral operator

$$\int_0^{\pi}\int_0^{\pi}\{\quad\}\cos k\Phi \sin \Psi \, d\Phi \, d\Psi$$

$$(k = 0, 1, 2, \ldots, N)$$

is used on both sides of Eq. (11), a number of equations equal to the number of unknowns in the chordwise series may be developed. These equations will involve the unknown c_n's and the quantity $\sum_{m=1}^{M} K_m/m$. We may designate this set of equations as "Group I." Similarly, "Group II" may be generated by using the operator

$$\int_0^{\pi}\int^{\pi}\{\quad\} \sin p\Psi \, d\Phi \, d\Psi$$

$$(p = 2, 3, \ldots, M)$$

In this set there are m equations equal to the number of unknown coefficients in the spanwise series, and once again the equations contain the unknowns c_n and K_m.

The coefficients are obtained by a method of successive approximations. As a first approximation it is assumed that $K_m = 0$ for $m \geqq 2$. (This is equivalent to assuming an elliptical spanwise lift distribution.) Group I is then solved to obtain a first approximation to the chordwise coefficients. These results are substituted into Group II to obtain the second approximation to the spanwise coefficients. The procedure is repeated until convergence is obtained.

The following aerodynamic properties of the wing may be derived readily by making use of Eqs. (8), (9), and (10).

Spanwise lift distribution:

$$l = \rho U^2 b\pi[c_0 + (c_1/2)]Y(\Psi) \tag{12}$$

Total lift:

$$L = \rho U^2 sb^2(\pi^2/2)[c_0 + (c_1/2)] \tag{13}$$

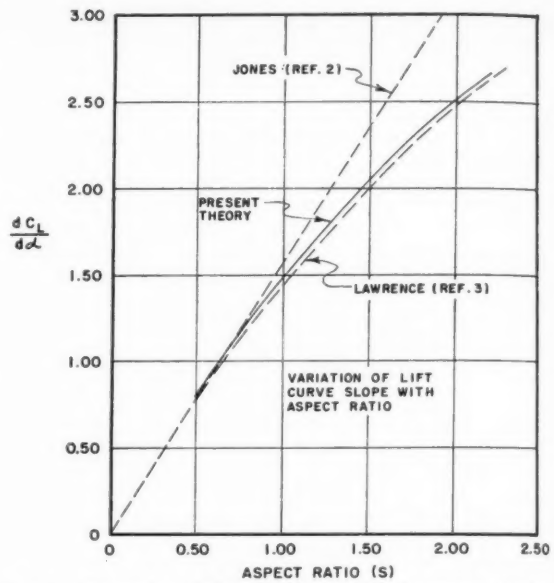

FIG. 1. Comparison of lift curve slope with the results of other theories.

Section pitching moment about leading edge:

$$m = -\rho U^2 b^2 \frac{\pi}{2}\left(c_0 + c_1 - \frac{c_2}{4}\right) Y(\Psi) \tag{14}$$

Total pitching moment about leading edge:

$$M = -\rho U^2 sb^2 \frac{\pi^2}{4}\left(c_0 + c_1 - \frac{c_2}{4}\right) \tag{15}$$

Chordwise lift distribution:

$$l_c = \rho U^2 sb(\pi/2)X(\Phi) \tag{16}$$

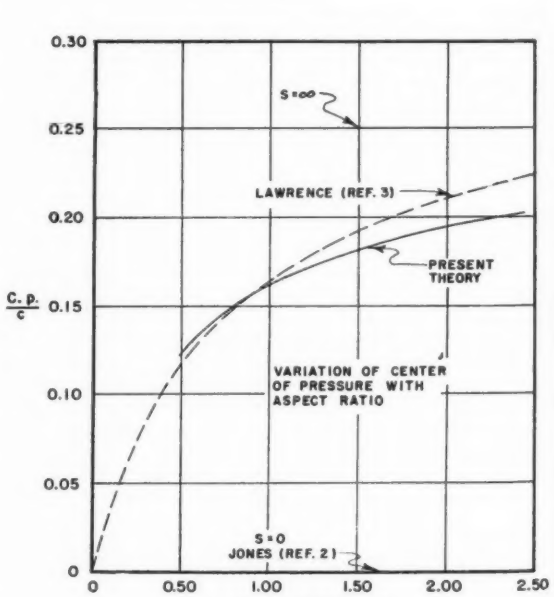

FIG. 2. Comparison of the center of pressure location with the results of other theories.

Rolling moment:

$$\bar{L} = -\rho U^2 s^2 b^2 \frac{\pi^2}{8}\left(c_0 + \frac{c_1}{2}\right) K_2 \qquad (17)$$

Calculations have been performed for a family of flat plate rectangular wings at an angle of attack α, with aspect ratios ranging from $^1/_2$ to 2. In this case, it is necessary to consider only the odd harmonics in the spanwise series; hence,

$$K_2, K_4, K_6, \ldots, K_{2m+1} = 0$$

For a spanwise series of three terms and a chordwise series of six terms the results are presented in Table 1. Fig. 1 illustrates the variation of the lift curve slope $dC_L/d\alpha$ as a function of aspect ratio. Fig. 2 presents the effect of aspect ratio on the center of pressure location. In both figures comparisons with the results of Jones[2] and Lawrence[3] are given.

References

Reissner, Eric, *On the General Theory of Thin Airfoils for Non-uniform Motion*, NACA TN No. 946, 1944.

[2] Jones, R. T., *Properties of Low-Aspect-Ratio pointed Wings at Speeds Below and Above the Speed of Sound*, NACA Report No. 835, 1946.

[3] Lawrence, H. R., *The Lift Distribution on Low Aspect Ratio Wings at Subsonic Speeds*, Journal of the Aeronautical Sciences, Vol. 18, No. 10, p. 683, October, 1951.

A Note on Poisson's Ratio*

Morris Feigen

Department of Engineering, University of California at Los Angeles; Now Hughes Research and Development Laboratories, Culver City, Calif.

July 14, 1953

Poisson's ratio defines the ratio of lateral contraction to axial extension under an axial load and is constant as long as the action is wholly elastic. In the inelastic range Poisson's ratio is no longer a constant as long as the axial load is increasing.

In inelastic buckling of plates and columns it is assumed that the buckled state is a deflected state of equilibrium which is arbitrarily close to the uniform state of compression which preceded it. In passing from the uniform state of compression to the buckled state, incremental axial extensions and lateral contractions (negative) occur. In this case the strains of interest must be the incremental changes that occur. In reference 1 it is these incremental changes that are used in the analysis of buckling of plates.

This note proposes a new terminology in order that ratio of incremental contraction to extension be differentiated from the overall ratio of total contraction to extension. It also shows how the two above ratios may be expressed in terms of the variables of the uniaxial stress-strain diagram.

If ϵ_x is the total axial extension under an axial stress σ_x and if ϵ_y is the corresponding total lateral contraction, then the usual definition of Poisson's ratio is

$$\nu = \epsilon_y/\epsilon_x \qquad (1)$$

This is defined as *Poisson's secant ratio*, ν_S.

If at any point on the stress-strain diagram an incremental stress $\Delta\sigma_x$ is added, there results an incremental axial extension $\Delta\epsilon_x$ and an incremental lateral contraction $\Delta\epsilon_y$. The ratio of these incremental strains will be defined as *Poisson's tangent ratio*, ν_T, where

$$\nu_T = \Delta\epsilon_y/\Delta\epsilon_x \qquad (2)$$

Shanley[2] shows that *Poisson's secant ratio* can be expressed as

$$\nu_S = (\nu'\epsilon_x' + \nu''\epsilon_x'')/\epsilon \qquad (3)$$

where ϵ_x' is the elastic component of the total strain, ϵ_x'' is the plastic component of the total strain, ν' is Poisson's ratio in the elastic range, and ν'' is Poisson's ratio defining only the plastic extensions. The usual assumptions made are that $\epsilon_x' + \epsilon_x'' = \epsilon$ and $\nu'' = 1/2$.

In order to express Eqs. (1) and (2) in other terms, the following values are used:

$$\epsilon_x = \frac{\sigma_x}{E_S}; \quad \epsilon_x' = \frac{\sigma_x}{E}; \quad \epsilon_x'' = \sigma_x\left(\frac{1}{E_S} - \frac{1}{E}\right)$$

where E is Young's modulus and E_S is the secant modulus. Substituting the above into Eq. (3), *Poisson's secant ratio* becomes

$$\nu_S = \nu'\frac{E_S}{E} + \nu''\left(1 - \frac{E_S}{E}\right) \qquad (4)$$

Similarly, if

$$\Delta\epsilon_x = \Delta\sigma_x/E_T; \qquad \Delta\epsilon_x' = \Delta\sigma_x/E$$
$$\Delta\epsilon_x'' = \Delta\sigma_x[(1/E_T) - (1/E)]$$
$$\Delta\epsilon_y' = \nu'\,\Delta\epsilon_x'; \qquad \Delta\epsilon_y'' = \nu''\,\Delta\epsilon_x''$$

where E_T is the tangent modulus, is substituted into Eq. (2), *Poisson's tangent ratio* becomes

$$\nu_T = \nu'(E_T/E) + \nu''[1 - (E_T/E)] \qquad (5)$$

ν_S and ν_T as expressed by Eqs. (4) and (5) are plotted on Fig. 1 for a non-dimensional Ramberg-Osgood[3] stress-strain relation for $\nu' = 0.33$ and $\nu'' = 0.50$. The Ramberg-Osgood stress-strain relation is

$$E\epsilon/\sigma_{0.7} = (\sigma/\sigma_{0.7}) + (3/7)(\sigma/\sigma_{0.7})^{10} \qquad (6)$$

where $\sigma_{0.7}$ is the stress at which the secant modulus is equal to 0.7 the elastic modulus.

It should be observed in Fig. 1 that the tangent ratio approaches $^1/_2$ more rapidly than does the secant ratio.

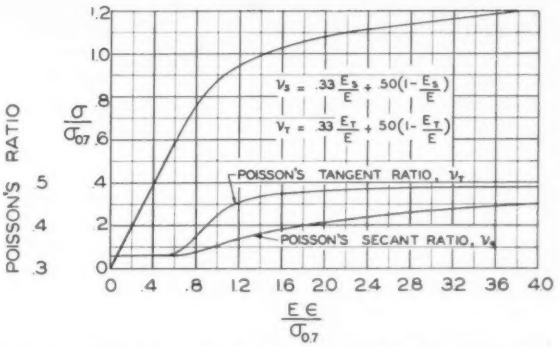

FIG. 1. Poisson's ratio for a Ramberg-Osgood stress-strain relation, $E\epsilon/\sigma_{0.7} = (\sigma/\sigma_{0.7}) + (3/7)(\sigma/\sigma_{0.7})^{10}$.

References

[1] Handleman, G. H., and Prager, W., *Plastic Buckling of a Rectangular Plate Under Combined Edge Thrusts*, NACA TN No. 1530, 1948.

[2] Shanley, F. R., *Weight-Strength Analysis of Aircraft Structures;* McGraw-Hill Book Company, Inc., New York, 1952.

[3] Ramberg, Walter, and Osgood, Wm. R., *Description of Stress-Strain Curves by Three Parameters*, NACA TN No. 902, 1943

* This paper is an excerpt from a thesis submitted in partial fulfillment of the requirements for the degree of Doctor of Philosophy in Engineering, University of California at Los Angeles.

Two-Dimensional Correction of the Outlet Angle in Cascade Flow

N. Scholz
Institute of Fluid Mechanics, Technical University, Braunschweig, Germany
July 14, 1953

IT IS WELL KNOWN that there are considerable difficulties in obtaining two-dimensional flow in cascade experiments, because of the boundary layers on the side walls of the cascade tunnel. These boundary layers generally have two different influences on the flow in the middle section of the cascade: (1) From the decay of lift at the side walls there arises a free vortex sheet that induces a secondary flow in the whole field. (2) Because of the displacement of the boundary layers at the side walls, there is a contraction of the flow in the middle section of the cascade, so that the two-dimensional equation of continuity is no longer fulfilled there. Both influences may be dealt with separately as long as they are small.

In this note we want to deal only with the influence of the contraction in the middle section on the outlet angle of the cascade flow. The disturbances due to the vortex sheet have already been investigated by several authors.[2–4]

In the normal cascade tunnel, the inlet flow comes through a closed channel, Fig. 1, so that the direction of this flow is given by the axis of the channel. Behind the cascade there are usually no tunnel walls so that there is a free jet. In a plane normal to the side walls there is a contracting flow due to the displacement effect of the boundary layers on these walls (see Fig. 1b). The rate of mass flow per unit of width and for one spacing of the cascade

$$Q = \int_{y}^{y+t} w(y) \sin \beta(y)\, dy \tag{1}$$

increases downstream for the middle section, Fig. 1c, whereas the flow is deflected when going through the cascade. For a simple calculation we replace each of the blades by its load concentrated at its aerodynamic center. The flow in plane 1 in front of the cascade and in plane 2 behind the cascade is assumed to be known from experiment. For reasons of simplification we assume that from plane 1 to plane c there is no deflection but only a contraction from Q_1 to Q_c. Furthermore, we assume that in plane c the flow obtains an impulse in the y-direction, which is necessary for the deflection of the flow. Further downstream between planes c and 2 there is some more contraction from Q_c to Q_2. But this second part of the contraction also gives an alteration of the outlet angle due to the momentum theorem.

We apply the momentum theorem for the y-direction for a control surface in the middle section of the flow, Figs. 1a and 1b, which consists of two identical stream line planes having the distance of the blades and two planes parallel to the side walls with the small distance Δz. For the application of the momentum theorem it is not necessary to know the velocity distribution in plane c. It is sufficient that in plane c the incoming momentum in the y-direction is known. By definition, the incoming y-momentum is determined by the condition that the flow would attain the outlet angle $\beta_{2\,cor}$ behind the cascade if there were no contraction downstream from plane c. Therefore,

$$I_c = \rho \cdot Q_c \cdot w_{2\cos} \cdot \cos \beta_{2\,cor} \tag{2}$$

Furthermore, the outgoing y-momentum in plane 2 is

$$I_2 = \rho \cdot Q_2 \cdot w_2 \cdot \cos \beta_2 \tag{3}$$

Because of the contraction of the flow between planes c and 2, there is an additional incoming momentum through the planes parallel to the side walls. The incoming rate of flow is from the equation of continuity $\Delta Q = Q_2 - Q_c$. The velocity component in the y-direction is not known, but it may be assumed to be between those in planes c and 2. As an approximation we take the arithmetic mean value of these velocity components, and therefore the incoming additional flow of momentum in the y-direction is

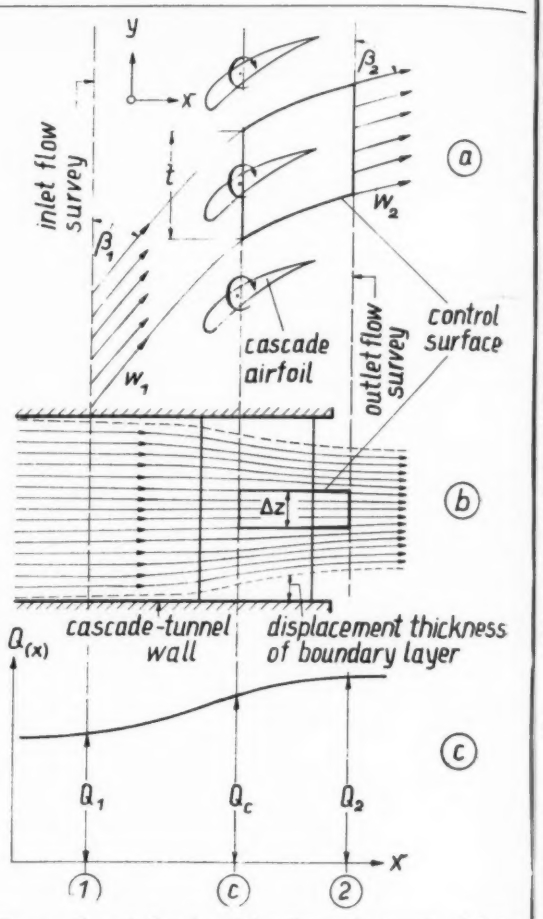

FIG. 1. Cascade flow for solid wall cascade tunnels. (a) Flow in the middle plane. (b) Flow between the tunnel side walls. (c) Mass flow in the middle plane.

$$\Delta I = \rho(Q_2 - Q_c)\,(1/2)\,(w_{2\,cor} \cdot \cos \beta_{2\,cor} + w_2 \cdot \cos \beta_2) \tag{4}$$

Since there are no external forces on the control surface in the y-direction, the incoming flow of momentum is equal to the outgoing flow; therefore, $I_c + \Delta I = I_2$. Considering that

$$Q_c = t \cdot w_{2\cos} \cdot \sin \beta_{2\,cor}$$
$$Q_2 = t \cdot w_2 \cdot \sin \beta_2$$

one obtains for the corrected outlet angle, after some calculation,

$$\operatorname{ctg} \beta_{2\,cor} = (Q_2/Q_c) \operatorname{ctg} \beta_2 \tag{5}$$

Because $\operatorname{ctg} \beta = t \cdot w \cdot \cos \beta / Q$, this means that the velocity component in the y-direction is not influenced by the contraction but only by the x-component according to the increased rate of mass flow. For the evaluation of Eq. (5), not only a measurement of the wake in plane 2 would be necessary for obtaining Q_2 but also a detailed measurement for the flow in plane c between the blades at the position of the aerodynamic center, which is laborious. As has been shown by unpublished measurements of the author, it is possible to relate Q_c to Q_1 in plane 1. One obtains

$$\frac{Q_c - Q_1}{Q_2 - Q_1} = \text{const.} = K(c); \quad 0 < K(c) < 1 \tag{6}$$

For fixed positions of planes 1 and 2, the constant $K(c)$ depends only on the position of the plane c between the entrance and exit plane. This means, that the contraction $Q(x) - Q_1$, as indicated in Fig. 1, is always approximately the same for a certain cascade tunnel if it is related to the total contraction $Q_2 - Q_1$. The curve of the acceleration on the mean stream line is assumed to be independent of the local cross section as given by the displacement due to the boundary layers on the side walls. This is evident if the distance of the side walls is not too small.

The constant K, therefore, is of universal character and must be determined from experiments once and for all. The influence of the position of the aerodynamic center of the blade on K is also small for small total contraction. Therefore it is not necessary to know this position exactly; a rough estimate is sufficient.

In some concluding remarks something may be said about how other proposals for correcting the outlet angle are related to our results. Mortarino[5] assumes that the outlet angle is independent of the contraction. This would mean that there is no contraction between planes c and 2; therefore, $Q_c = Q_2$ and $K = 1$. The other limit, $K = 0$, has been proposed by Katzoff, Bogdonoff, and Boyet,[6] who take the x-component of the velocity of the exit cross section to be equal to that of the entrance cross section, $Q_c = Q_1$. Another proposal[1] gives corrections for the entrance angle, as well as for the exit angle. This cannot be related to our result. Hawthorne[7] from the free vortices obtains an x-component of the velocity at the position of the blade, which is the arithmetic mean value of the x-components in front of and behind the cascade. This means

$$Q_c = (1/2)(Q_1 + Q_2)$$

and therefore $K = 1/2$.

References

[1] Erwin, J. R., and Emery, J. C., *Effect of Tunnel Configuration and Testing Technique on Cascade Performance*, NACA Report No. 1016, 1951.

[2] Hausmann, F., *The Theoretical Induced Deflection Angle in Cascades Having Wall Boundary Layers*, Journal of the Aeronautical Sciences, Vol. 15, No. 11, p. 686, November, 1948.

[3] Carter, A. D. S., and Cohen, M. E., *Preliminary Investigation into the Three-Dimensional Flow Through a Cascade of Airfoils*, R. & M. No. 2339, British ARC, 1946.

[4] Squire, H. B., and Winter, K. G., *The Secondary Flow in a Cascade of Airfoils in a Nonuniform Stream*, Journal of the Aeronautical Sciences, Vol. 18, No. 4, p. 271, April, 1951.

[5] Mortarino, C., *Esperimenti su una chiera di pelettaggi per compressore*, Aerotechnica, Vol. 30, p. 59, 1950.

[6] Katzoff, S., Bogdonoff, E. H., and Boyet, H., *Comparison of Theoretical and Experimental Lift and Pressure Distributions on Airfoils in Cascade*, NACA TN No. 1388, 1947.

[7] Hawthorne, W. R., *Induced Deflection Angle in Cascades*, Readers' Forum, Journal of the Aeronautical Sciences, Vol. 16, No. 4, p. 252, April, 1949.

Mean Skin-Friction Coefficients for Biconvex Airfoils in Supersonic Flow

J. Christopher Boison
North American Aviation, Inc., Downey, Calif.

July 13, 1953

THE PURPOSE OF THE PRESENT NOTE is to show the effect of a chordwise pressure gradient (function of thickness ratio, t/c) on the mean skin-friction coefficient of biconvex airfoils in supersonic flight with a compressible laminar boundary layer.

Weil's procedure[1] was used in determining the variation of the local chordwise skin-friction coefficient on the airfoils, except that a linear chordwise velocity distribution was assumed. The present results are shown in Fig. 1 as solid lines. Also indicated in the figure are results of an analysis that separately assumes the boundary layer to be incompressible, the local free-stream flow, however, still remaining supersonic. The increase in coefficient owing to compressibility in the boundary layer is quite evident.

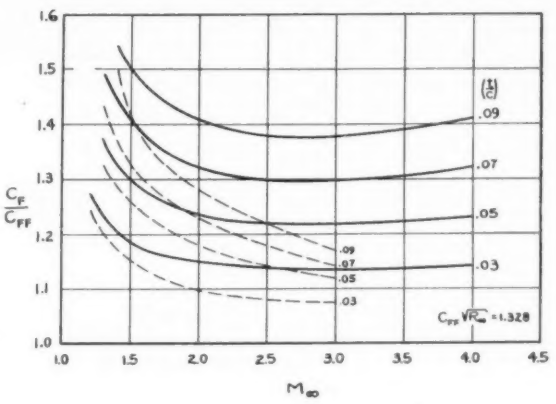

FIG. 1

The ordinary nonlinear differential equation (Eq. (21), reference 1) was solved numerically with the aid of a Magnetic Drum Digital Differential Analyzer (MADDIDA), where the accuracy of the solution was maintained at one part in a thousand.

An approximation was used in the determination of mean skin-friction coefficients. The biconvex airfoil was assumed to be made up of two sections; the first 5 per cent of chord was a flat plate with incompressible boundary-layer flow, and the remaining 95 per cent was a biconvex airfoil with a compressible boundary layer. Mean skin-friction coefficients were obtained separately for each section by integration of the local coefficients. These mean coefficients were then weighted over a dimensionless chord, therefore giving an overall mean skin friction ($C_F \sqrt{R_\infty}$). The effect of R_∞, undisturbed free-stream Reynolds Number, was eliminated by ratioing the biconvex mean skin friction to the mean skin friction for a flat plate ($C_{FF} \sqrt{R_\infty}$) with an incompressible boundary layer.

Reference

[1] Weil, H., *Effects of Pressure Gradient on Stability and Skin Friction in Laminar Boundary Layers in Compressible Fluids*, Journal of the Aeronautical Sciences, Vol. 18, No. 5, pp. 311–318, May, 1951.

On Theories of Plasticity and the Plastic Stability of Cruciform Sections

P. P. Bijlaard and H. A. B. Wiseman
Cornell University and The Pennsylvania State College, Respectively

July 8, 1953

AN INTERESTING PAPER IN THIS JOURNAL,[1] which deals with the plastic torsional buckling of cruciform sections, is based on the contention that theoretical, as well as all direct experimental, evidence has shown that a simple flow theory would be valid rather than a deformation theory. Using simple flow theory and assuming initial distortions, the authors show that the resulting buckling stress for a special case is in good agreement with that from deformation theory and, therefore, with experiments.

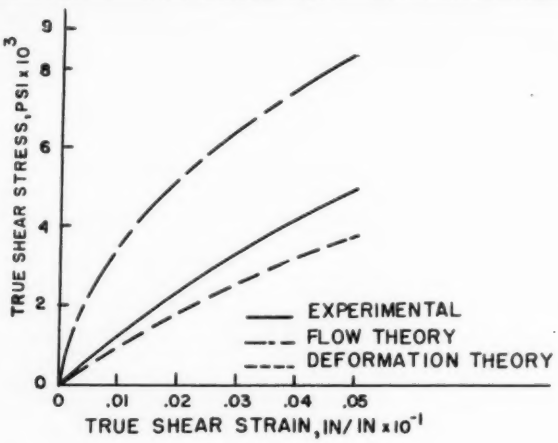

FIG. 1

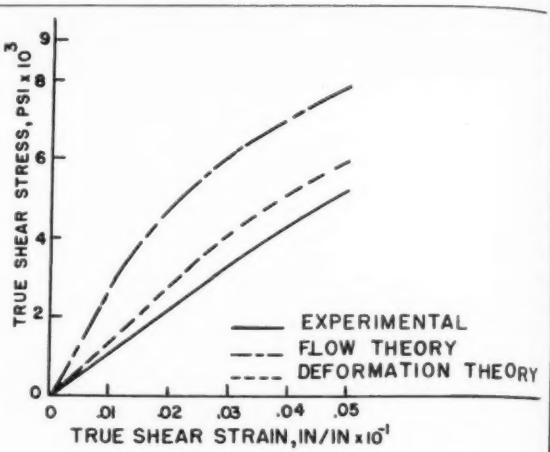

FIG. 2

FIGS. 1 AND 2. Stress-strain curves of aluminum alloys for shear superimposed on tension. Fig. 1 refers to 14S-T4; Fig. 2 refers to 14S-T6.

In the first place we should like to point out that until now it has not been possible to predict, by pure mathematics or otherwise, how a highly complex polycrystalline material, with its flaws, dislocations, etc., will behave under the action of states of stress with varying ratios between the stress components. At most it may be concluded that for a quasi-isotropic material the actual behavior generally will be between that according to simple flow and deformation theories. The first writer calculated the plastic buckling stress from both these theories and showed that deformation theory leads to the smallest and thus to safe critical stresses.[2] Later experiments appeared to be in good agreement with his results based on deformation theory, as was shown in reference 3. In certain cases deformation theory leads to impossible results, such as negative work done by positive stress, as shown on page 734 of reference 2. However, in the special case of plastic buckling, where, in connection with the Shanley principle and small eccentricities, the shear stresses in all planes will increase during buckling, there is *theoretically* no reason why the final deformation should not be about the same as in a case where the ratio of the stress components remains constant—that is, in agreement with the deformation theory, as was stated on pages 532 and 533 of reference 3. Batdorf and Budiansky's theory of slip,[4, 5] which is theoretically sound, is based on the same principle and leads also to the conclusion that for plastic plate buckling the deformation theory leads to correct results.

Although this theory was not confirmed by the special direct tests on compressed and then twisted tubes set up for that purpose,[6] these tests reveal that for finite superimposed shear stresses, as occur in the case of buckling, due to unavoidable eccentricities, the simple flow theory is also not correct. Moreover, recent tests conducted at The Pennsylvania State College[7] with aluminum alloy 14S-T4, show that over the entire range its behavior is in much better agreement with deformation than with simple flow theory. This is illustrated by Fig. 1, which is identical with part of Fig. 13, Set A, test 4, of reference 7, referring to shear stresses superimposed on pure tension. From more recent tests on 14S-T6, the experimental curve (partly shown in Fig. 2) usually falls to the right of both flow and deformation theories, so that in all cases the flow theory is much worse than the deformation theory.

It should be kept in mind that, in connection with unavoidable eccentricities, for the behavior in cases of buckling of cruciform sections it is not so important, as often implied, how the material behaves under superimposed infinitely small shear strains or stresses, as how it behaves under superimposed finite shear strains of the order of 0.001. For such shear strains, even from Fig. 12 of reference 6, the behavior becomes closer to deformation than to flow theory. This is in agreement with Dr. Budiansky's feeling (from letter to first writer) that it would be unwise to pay too

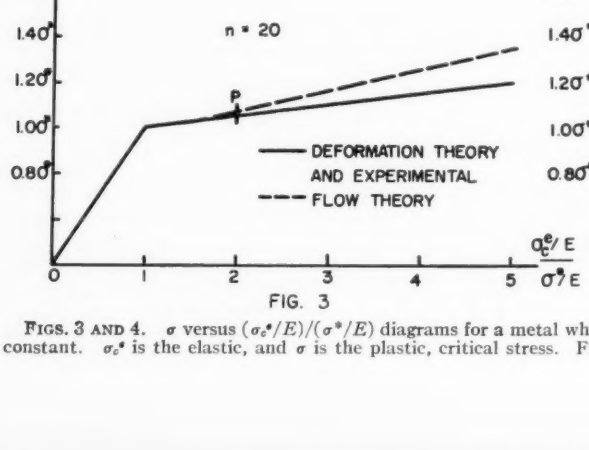

FIG. 3

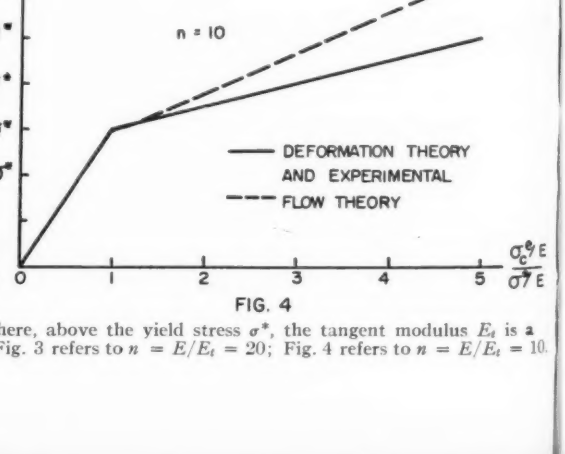

FIG. 4

FIGS. 3 AND 4. σ versus $(\sigma_c^e/E)/(\sigma^*/E)$ diagrams for a metal where, above the yield stress σ^*, the tangent modulus E_t is a constant. σ_c^e is the elastic, and σ is the plastic, critical stress. Fig. 3 refers to $n = E/E_t = 20$; Fig. 4 refers to $n = E/E_t = 10$.

much attention to the *initial* shear modulus as found from his tests.

It would, of course, be nice if, as suggested in reference 1, flow theory would lead to the same results as deformation theory, but this is true only for the special case considered in reference 1. From Fig. 9 of that reference, where $n = E/E_t = 20$ and where $\sigma_c^f/\sigma^* = 2$, with $\psi_0 = 10^{-3}$, the buckling load from flow theory coincides with that from deformation theory. This means that, in a σ versus σ_c^e/E diagram, with $n = 20$ and for $\sigma_c^e/E = 2\sigma^*/E$, the critical stresses from both theories are indicated by the same point P, as shown here in Fig. 3. However, from Eq. (20) of reference 1, for $n = 20$ and $\psi_0 = 10^{-3}$, the buckling stress for other values of σ_c^e/E is given by the dash line in Fig. 3, as calculated conservatively for $\psi = 0.05$. Hence, for all other points than that considered in reference 1 (point P) there is no agreement. The disagreement becomes more pronounced if $n = E/E_t$ is smaller, as shown in Fig. 4 for $n = 10$. Actually, the tests for cruciform sections, as given in reference 8, refer to a stress-strain diagram, which is practically identical to one for $n = 10$. Moreover, for equal initial angle rotations, ψ_0 is less for larger ratios σ_c^f/σ^* than for smaller ratios, so that the disagreement with flow theory is still worse than is shown in Fig. 4.

The obvious reason why (even by assuming initial distortions $\psi_0 = 10^{-3}$, or $2b\theta_0 = 38'$, which is ten times those that the authors of reference 1 assume as existent) the results from flow theory do not agree with the test results is, as explained above, that the material does not behave according to the simple flow theory but behaves in sufficiently accurate agreement with the deformation theory. Nevertheless, reference 1 is a welcome contribution to indicate that small deviations in the direction of the simple flow theory are canceled by unavoidable eccentricities.

References

[1] Onat, E. T., and Drucker, D. C., *Inelastic Instability and Incremental Theories of Plasticity*, Journal of the Aeronautical Sciences, Vol. 20, No. 3, pp. 181–186, March, 1953.

[2] Bijlaard, P. P., *A Theory of Plastic Stability and its Application to Thin Plates of Structural Steel*, Proc. Royal Netherlands Acad. of Sciences, Amsterdam, Vol. 41, No. 7, pp. 731–743, September, 1938.

[3] Bijlaard, P. P., *Theory and Tests on the Plastic Stability of Plates and Shells*, Journal of the Aeronautical Sciences, Vol. 16, No. 9, pp. 529–541, September, 1949.

[4] Batdorf, S. B., *Theories of Plastic Buckling*, Journal of the Aeronautical Sciences, Vol. 16, No. 7, pp. 405–408, July, 1949.

[5] Batdorf, S. B., and Budiansky, B., *A Mathematical Theory of Plasticity Based on the Concept of Slip*, NACA TN No. 1871, April, 1949.

[6] Budiansky, B., Dow, N. T., Peters, R. W., and Shephard, R. P., *Experimental Studies of Polyaxial Stress-Strain Laws of Plasticity*, Proceedings, First U.S. National Congress of Applied Mechanics, pp. 503–512, 1951.

[7] Marin, J., and Wiseman, H. A. B., *Plastic Stress-Strain Relations for Combined Tension and Compression*, NACA TN No. 2737, July, 1952.

[8] Stowell, E. Z., *Compressive Strength of Flanges*, NACA TN No. 2020, January 1950.

Note on the Prandtl Number for Dissociated Air

C. Frederick Hansen

Aeronautical Research Scientist, Ames Aeronautical Laboratory, NACA, Moffett Field, Calif.

July 27, 1953

IN A RECENT ARTICLE, Moore[1] calculates a Prandtl Number for high-temperature air which varies from the usual 0.7 to values as high as 6, due to dissociation. Moore's calculation depends on the assumption that the ratio of the coefficients of thermal conductivity and viscosity, K/μ, is not affected by dissociation. Crown[2] reports a different result—namely, that Prandtl Number for dissociated air is given by the same formula that Eucken deduced for normal gases,[3–5]

$$Pr = 4\gamma/(9\gamma - 5) \tag{1}$$

In this expression the Prandtl Number, Pr, depends only on the ratio of specific heats, γ, and cannot exceed unity. Crown's argument is based on the assumption that the difference between the heat capacities at constant pressure and at constant volume, $C_p - C_v$, is the gas constant R.

According to kinetic theory of gases, the ratio K/μ varies approximately in proportion to C_v,[4, 5] which is greatly increased by dissociation.[6, 7] Thus, it is apparent from the definition of Prandtl Number,

$$Pr = C_p\mu/K \tag{2}$$

that the values given by Moore are much too large. Crown's result is also in doubt, since the difference, $C_p - C_v$, for partly dissociated air becomes many times the gas constant R.[6, 7] Moreover, both Moore and Crown treat dissociated air, in effect, as a homogeneous gas rather than a mixture of atomic and molecular gases. Since mixing dissimilar gases can strongly influence transport properties, such as viscosity and thermal conductivity,[8] it seems appropriate to investigate the atom-molecule mixing effect and to re-estimate the Prandtl Number for dissociated air.

A rather rigorous analysis of gas mixtures has been developed by Chapman,[4] Enskog, and others. However, this analysis requires knowledge of the properties of the mixture components, and for the atomic components of dissociated air such knowledge is uncertain. Therefore, the following discussion will be limited to a simple analysis, based on elementary kinetic theory, leading to a first approximation of the mixing effect. In view of the order of the approximation, air will be treated as a mixture of two pure components: molecular gas with mol fraction n_1 and atomic gas with mol fraction n_2. The coefficient of viscosity for the mixture may be expressed[5] as

$$\mu = \frac{5\pi}{32}\left(\rho_1\,\bar{u}_1 L_1 + \rho_2 \bar{u}_2 L_2\right) \tag{3}$$

where ρ_i, $\bar{u}_i$, and L_i are, respectively, the density, mean random velocity, and mean free path of the ith component. If we invoke Eucken's assumption that internal energy is distributed among the gas particles independently of their velocity distribution,[3] the expression for coefficient of thermal conductivity becomes[4, 5]

$$K = \frac{5\pi}{32}\left[\left(\frac{5}{2}\,C_1^t + C_1^i\right)\rho_1\bar{u}_1 L_1 + \left(\frac{5}{2}\,C_2^t + C_2^i\right)\rho_2\bar{u}_2 L_2\right] \tag{4}$$

where C_1^t and C_2^t are the translational heat capacities of the molecular and atomic components of the gas, C_1^i is the internal heat capacity of the molecular component due to rotational and vibrational energy, and C_2^i is the heat capacity associated with dissociational energy of the atomic component. With the assumption that the mean free paths are the same for momentum and energy transport,[5] it follows that

$$\frac{K}{\mu} = \frac{\left(\frac{5}{2}\,C_1^t + C_1^i\right) + r\left(\frac{5}{2}\,C_2^t + C_2^i\right)}{1 + r} \tag{5}$$

where

$$r = \rho_2\bar{u}_2 L_2/\rho_1\bar{u}_1 L_1$$

In terms of the molecular weight ratio, M_1/M_2,

$$\rho_2/\rho_1 = (M_2/M_1)\,(n_2/n_1)$$
$$\bar{u}_2/\bar{u}_1 = (M_1/M_2)^{1/2}$$

$$L_2/L_1 = \frac{n_1 S_{11}\sqrt{2} + n_2 S_{12}\sqrt{1 + (M_1/M_2)}}{n_2 S_{22}\sqrt{2} + n_1 S_{12}\sqrt{1 + (M_2/M_1)}}$$

where

$$S_{ij} = \pi[(\sigma_i + \sigma_j)/2]^2$$

is the effective collision cross section for particles with diameters σ_i and σ_j.

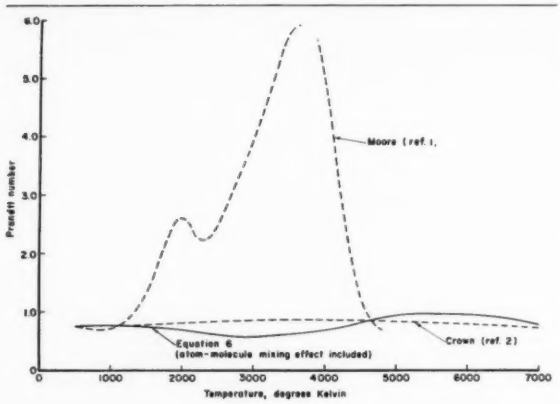

Figure 1.– Prandtl number for air as a function of temperature (pressure = 0.1 atmosphere).

Combining Eqs. (5) and (2) defines the Prandtl Number as a function of the heat capacities, component mol fractions, molecular weight ratio, and the collision diameters,

$$Pr = \frac{\gamma\,(1 + r)\,C_v}{\left(\frac{5}{2}\,C_1' + C_1^{i}\right) + r\left(\frac{5}{2}\,C_2' + C_2^{i}\right)} \tag{6}$$

The heat capacities and component mol fractions may be deduced from the equilibrium properties of dissociated air given in references 6 or 7, and M_1/M_2 is taken as 2, of course, for the dissociation of diatomic gases. The collision diameter ratio, σ_2/σ_1, is uncertain but probably lies in the interval from M_2/M_1 to 1. This uncertainty does not influence the order of approximation, since the value of r is largely determined by the component mol fraction ratio, n_2/n_1, and is only weakly dependent on the collision diameter ratio or the molecular weight ratio as long as these ratios are near unity.

The Prandtl Numbers calculated from Eq. (6), using properties of air taken from Krieger and White[7] and a collision diameter ratio of 0.5, are shown in Fig. 1 as a function of temperature for a pressure of 10^{-1} atmospheres. Similar results were obtained for pressures from 10^{-5} to 10 atmospheres, and only small differences occurred when collision diameter ratios of unity were used. For comparison, the Prandtl Numbers given by Moore[1] and by Crown[2] are also shown in Fig. 1. Moore's values are too large by a factor that is approximately the factor change in C_v due to dissociation. On the other hand, the Eucken formula used by Crown [Eq. (1)] gives values of the same magnitude as those calculated from Eq. (6), since neglecting the effect of dissociation on the difference $C_p - C_v$ partly compensates for the neglect of the mixing effect. Admittedly, the atom-molecule mixing effect has been accounted for only to the first order of approximation in the present analysis, and a more rigorous treatment of the problem is in order. Nevertheless, it seems fair to conclude from this analysis that Prandtl Numbers for dissociated air remain in the region from about 0.5 to 1.

References

[1] Moore, L. L., *A Solution of the Laminar Boundary-Layer Equations for a Compressible Fluid with Variable Properties, Including Dissociation*, Journal of the Aeronautical Sciences, Vol. 19, No. 8, pp. 505–518, August, 1952.

[2] Crown, J. C., *The Laminar Boundary Layer at Hypersonic Speeds*, NAVORD Report 2299, 1952.

[3] Eucken, Arnold, *On the Heat Conductivity, the Specific Heat, and the Internal Friction of Gases*, Physikalische Zeitschrift, Vol. 14, No. 8, pp. 324–332, 1913.

[4] Chapman, S., and Cowling, T. G., *The Mathematical Theory of Non-Uniform Gases;* Cambridge University Press, New York, 1939.

[5] Kennard, E. H., *Kinetic Theory of Gases*, McGraw-Hill Book Company, Inc., New York, 1938.

[6] Hirschfelder, J. O., and Curtiss, C. F., *Thermodynamic Properties of Air II*, Univ. of Wisconsin CM-518, 1948.

[7] Krieger, F. J., and White, W. B., *The Composition and Thermodynamic Properties of Air at Temperatures from 500 to 8000° K and Pressures from 0.00001 to 100 Atmospheres*, RAND Report R-149, 1949.

[8] Brunot, A. W., *Properties of Hydrogen Mixtures*, A.S.M.E. Trans., Vol. 62, No. 7, pp. 613–619, 1940.

A Double-Diaphragm Shock Tube to Produce Transient High Mach Number Flows

Harry Bernstein
Lewis Flight Propulsion Laboratory, NACA, Cleveland

August 3, 1953

THE EQUATIONS GOVERNING THE OPERATION of the simple shock tube have been treated by several authors (e.g., reference 1). In the present note, the transient flow phenomena resulting from the combination of two shock tubes are considered. This double-diaphragm shock tube consists of a long, constant-area tube divided into three chambers (R, S and T) by two thin diaphragms. Rupture of the first diaphragm is manual, while the second is shattered when subjected to the pressure behind the strong shock caused by the disintegration of the first diaphragm. The unsteady flow phenomena, for the required initial pressures $p_R > p_S > p_T$, are depicted in the x-t diagram of Fig. 1.

The gas originally in the middle chamber (region S of the x-t plane) is first compressed by the passage of a shock and then expanded isentropically by a rarefaction wave. Upon entering region s' (the test region), the gas is at a high Mach Number and static temperature. The magnitudes of these quantities are, as in the case of the simple shock tube, wholly dependent upon the pressures, temperatures, and gases in the chambers prior to rupture.

Sample calculations have been performed for such a device employing a helium → air → helium gas combination, the results of which are presented in Figs. 2 through 4.

Figs. 2 and 3 indicate that high Mach Number flows, free of gas condensation, may be produced. For example, the use of diaphragm pressure ratios of 0.01 and 0.01 yields a transient flow of Mach Number 7.51 at a static temperature of 0.943 times the gas temperature prior to rupture. The time duration of the transient flow is plotted in Fig. 4 as a function of the diaphragm pressure ratios. For the previously mentioned case, the duration of the flow is 1.01×10^{-4} sec. per ft. of middle chamber length. Hence, for a 50-ft. middle chamber length, a time duration of 5.05 millisec. will be obtained. Time durations of this order of magnitude are sufficient for some types of model tests utilizing high-speed pressure or force-measuring instruments.

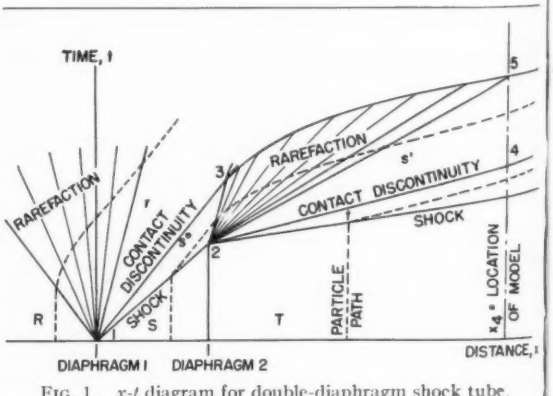

FIG. 1. x-t diagram for double-diaphragm shock tube.

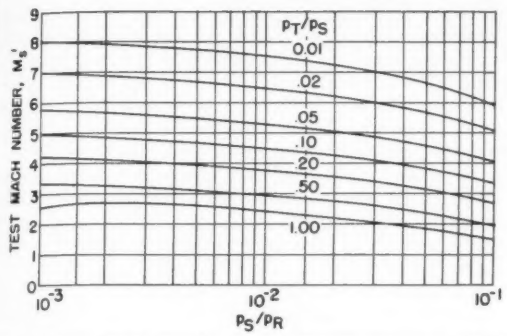

FIG. 2. Test Mach Number vs. diaphragm pressure ratios for helium → air → helium. Initial temperatures = 560°R.

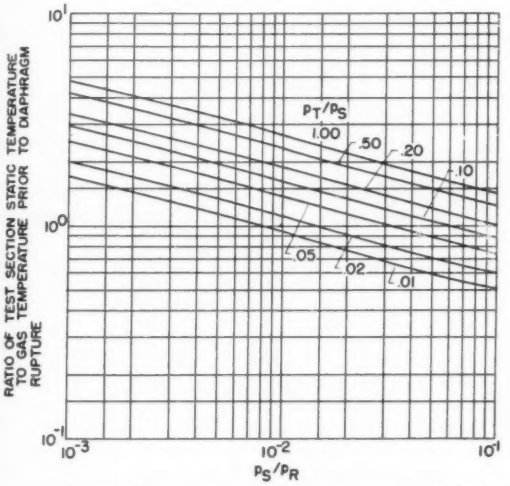

FIG. 3. Ratio of test-section static temperature to initial gas temperature vs. diaphragm pressure ratios for helium → air → helium. Initial temperatures = 560°R.

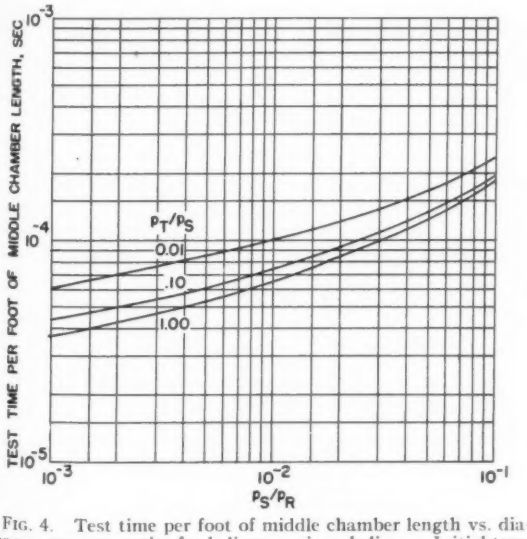

FIG. 4. Test time per foot of middle chamber length vs. diaphragm pressure ratios for helium → air → helium. Initial temperatures = 560°R.

The requirement of a middle section of such a large length, however, introduces a disadvantage in the form of large overall tube lengths. For the 0.01, 0.01 pressure ratio combination, the distance x_4 (see Fig. 1) was calculated to be 324 ft. for a 50-ft. middle chamber length. This is not the total tube length, for additional length must be provided to prevent wave reflections from the tube ends into the test region. Though no computations were performed, the indications are that the total tube length will be roughly twice x_4.

The required tube lengths may be reduced, by a factor of approximately 3, if argon, a gas of higher molecular weight, is used instead of helium in the R and T chambers. Such a substitution would, however, require slightly larger pressure ratios (p_R/p_S and p_S/p_T) across the diaphragms to produce the same Mach Number.

REFERENCE

[1] Patterson, G. N., *Theory of the Shock Tube*, Naval Ordnance Laboratory Memorandum 9903, September 21, 1948.

A Note on the Contribution of Higher Mode Resonance to Bending in the Teetering Rotor Blade

R. M. Carlson and D. R. Jacoby
Structures and Aerodynamics Group Leaders, Respectively, Hiller Helicopters, Palo Alto, Calif.

July 13, 1953

IN A RECENT ARTICLE presented in the JOURNAL, Hirsch[1] discussed the resonance diagram for flapwise bending in a helicopter blade. He pointed out that this diagram was invaluable as a means of predicting resonance in the preliminary stages of design, and so it is. It is the purpose of this note to discuss an interesting variation or expansion of the resonance diagram as it applies to the teetering rotor blade.

The teetering rotor, as contrasted to the articulated rotor, is capable of performing the fixed-end modes of vibration, as well as the pinned-end modes. In general, this situation applies when specifically considering a single blade. However, when considering the entire rotor, with a rigid attachment between blades, it is evident that there is a restriction that dictates how the rotor performs in the pinned and fixed-end modes. Of necessity, the rotor must behave in a symmetrical fashion when performing fixed-end modes and in an asymmetric fashion when performing pinned-end modes. Considering the fact that the teetering rotor behaves in this manner, it is convenient to utilize two resonance diagrams. One diagram plots the first, second, and third mode pinned-end rotating natural frequencies and a spectrum of the odd harmonic air loadings versus rotor angular velocity; another diagram plots the first, second, and third fixed-end rotating natural frequencies and a spectrum of the even harmonic air loading versus rotor angular velocity.

For purposes of illustration, C.A.L. fiberglass blade No. 2 was considered as a teetering rotor, and the two resonance diagrams were constructed (see Figs. 1 and 2). Fig. 1 is simply a portion of the diagram presented by Hirsch.[1] For this illustration the effect of the eccentric flapping hinge on the rotational constant was not extracted. Fig. 2 utilizes the static natural frequencies employed in Fig. 1, modified to the fixed-end modes and the rotational constants for the fixed-end modes.[2]

It is of interest to note that, for this particular blade, by arbitrarily considering it as a teetering rotor, its resonance characteristics are considerably altered. The blade, as an articulated rotor, exhibited considerable second- and fourth-order harmonic

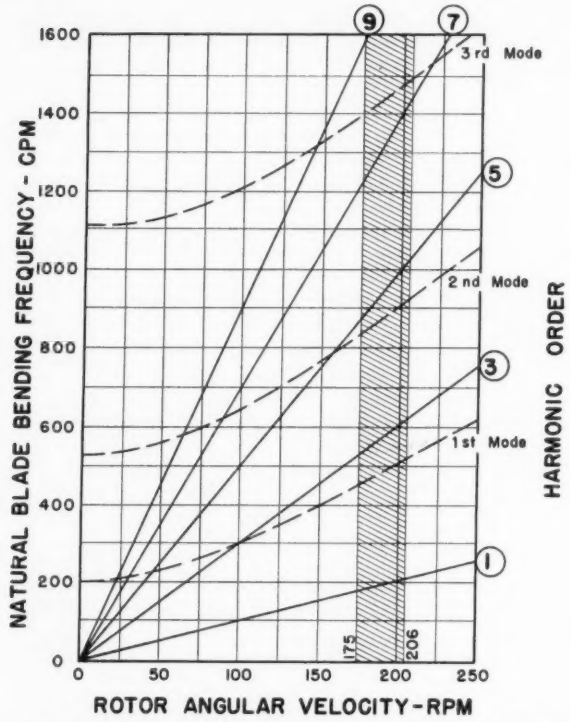

FIG. 1. Resonance diagram for asymmetric flapwise bending of C.A.L. fiberglass blade No. 2, represented as a teetering blade (pinned-end modes).

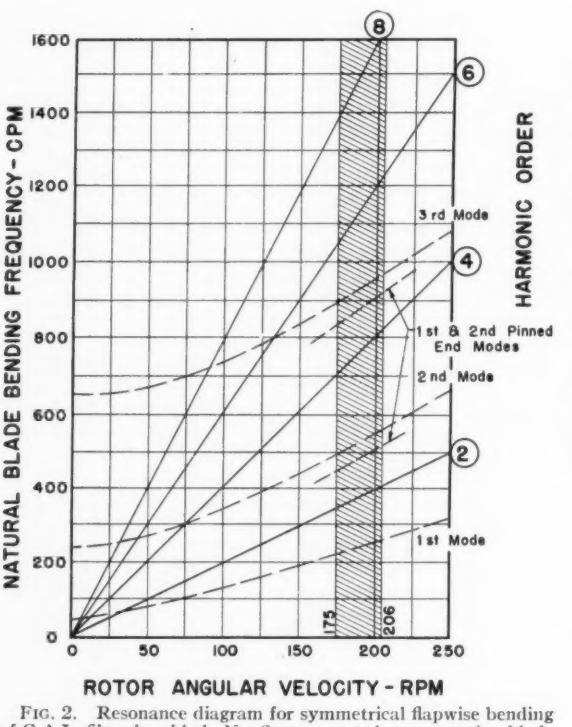

FIG. 2. Resonance diagram for symmetrical flapwise bending of C.A.L. fiberglass blade No. 2, represented as a teetering blade (fixed-end modes).

content throughout the operating r.p.m. range. Inspection of Fig. 2 indicates that as a teetering rotor this content would be appreciably reduced. It is also indicated that the eighth-order, third-mode resonance that was present on the Hirsch diagram[1] is no longer present; however, it appears probable that the eighth-order resonance will manifest itself in the fourth fixed-end mode. It is evident from the above inspection of the resonance diagrams that it becomes increasingly more difficult to avoid resonance in the operating r.p.m. range as the harmonic order increases.

From the vibration point of view, the teetering rotor presents no more or no less problems than the articulated rotor. This note serves only to point out a situation that is not present in the articulated blade but is of fundamental importance when appraising the teetering blade.

REFERENCES

[1] Hirsch, Harold, *The Contribution of Higher Mode Resonance to Helicopter Rotor-Blade Resonance*, Journal of the Aeronautical Sciences, Vol. 20, No. 6, p. 407, June, 1953.

[2] Den Hartog, J. P., *Mechanical Vibrations*, 3rd Ed., p. 331; McGraw-Hill Book Company, Inc., New York, 1947.

Differentiation of Experimental Data by Means of Higher Order Finite-Difference Formulas

Chi-Teh Wang and Daniel F. DeSanto
Daniel Guggenheim School of Aeronautics, New York University, New York
June 13, 1953

IN A NOTE IN THE READERS' FORUM of the June, 1953, JOURNAL Kauffman and Shinbrot[1] presented a method for calculating the derivatives of experimentally obtained functions. The method consists of calculating two forward and two backward first-order finite differences at the given point with different intervals and then obtaining the "derivatives" by a graphical interpolation. The authors have demonstrated the accuracy of this method by working out a test problem.

It appears to the present authors that good accuracy can also be obtained if the higher order finite-difference formulas are used in the "differentiation" of experimental data. This method has the additional advantage of being purely mechanical—viz., no intermediate graphical interpolation is necessary—and therefore, it is faster.

To demonstrate this point, let us take the same example analyzed by Kauffman and Shinbrot—namely,

$$x = 6 \sin t + 0.5 \sin 3t \qquad (0 \leq t \leq \pi) \tag{1}$$

The values of x at t-intervals of 0.2 were computed as in the Kauffman and Shinbrot case. Using the values of x at two stations ahead of and behind and at the station itself, the "derivatives" at $t = T$ in terms of the higher order central differences are written as follows:

$$\left(\frac{dx}{dt}\right)_T = \frac{1}{h}\left[\Delta x(T) - \frac{1}{6}\,\Delta^3 x(T)\right] \tag{2}$$

$$\left(\frac{d^2x}{dt^2}\right)_T = \frac{1}{h^2}\left[\Delta^2 x(T) - \frac{1}{12}\,\Delta^4 x(T)\right] \tag{3}$$

where

$$\Delta x(T) = (1/2)\,[x(T + h) - x(T - h)] \tag{4}$$

$$\Delta^2 x(T) = x(T + h) - 2x(T) + x(T - h) \tag{5}$$

$$\Delta^3 x(T) = (1/2)\,[x(T + 2h) - 2x(T + h) + 2x(T - h) - x(T - 2h)] \tag{6}$$

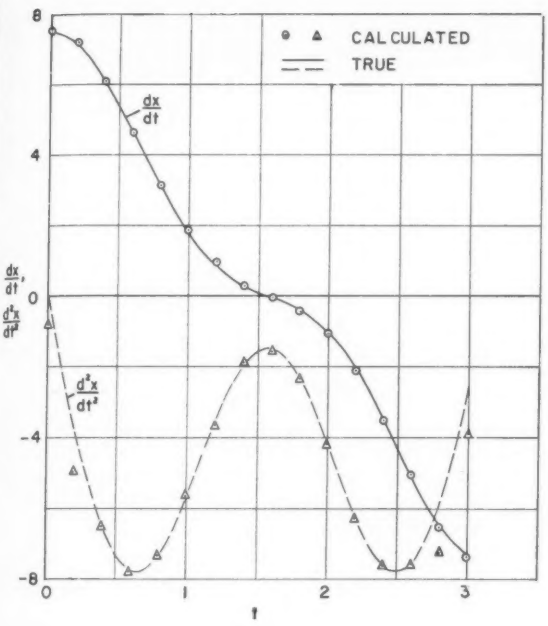

FIG. 1.

$$\Delta^4x(T) = x(T + 2h) - 4x(T + h) + 6x(T) - 4x(T - h) + x(T - 2h) \quad (7)$$

and where h is the t-interval between successive values of x; Δ, Δ^2, Δ^3, and Δ^4 denote the first, second, third, and fourth central differences, respectively. If the values of x at more stations are allowed to be used, Eqs. (2) and (3) can be extended still further. The derivatives given by Eqs. (2) and (3), utilizing x-values at five neighboring points, are plotted with their exact values given by (1) in Fig. 1. The agreement is excellent. The derivation of Eqs. (2) and (3) can be found, for example, in reference 2.

It is to be noted that it becomes impossible to use the preceding equations for points in the vicinity of the end points on the curve; this failing, however, also occurs in the case of the method proposed in reference 1. If it is necessary to evaluate derivatives at such points, then the derivatives must be expressed as series involving either backward or forward differences, depending on which end of the curve the evaluation is to be carried out. At the initial end of the curve,

$$\left(\frac{dx}{dt}\right)_T = \frac{1}{h}\left[\bar{\Delta}\,x(T) - \frac{\bar{\Delta}^2x(T)}{2} + \frac{\bar{\Delta}^3x(T)}{3} - \frac{\bar{\Delta}^4x(T)}{4}\right] \quad (8)$$

$$\left(\frac{d^2x}{dt^2}\right)_T = \frac{1}{h^2}\left[\bar{\Delta}^2x(T) - \bar{\Delta}^3x(T) + \frac{11}{12}\bar{\Delta}^4x(T)\right] \quad (9)$$

where $\bar{\Delta}$, $\bar{\Delta}^2$, $\bar{\Delta}^3$, and $\bar{\Delta}^4$ denote first, second, third, and fourth forward differences, respectively, and are

$$\bar{\Delta}x(T) = x(T + h) - x(T) \quad (10)$$

$$\bar{\Delta}^2x(T) = x(T + 2h) - 2x(T + h) + x(T) \quad (11)$$

$$\bar{\Delta}^3x(T) = x(T + 3h) - 3x(T + 2h) + 3x(T + h) - x(T) \quad (12)$$

$$\bar{\Delta}^4x(T) = x(T + 4h) - 4x(T + 3h) + 6x(T + 2h) - 4x(T + h) + x(T) \quad (13)$$

In the case of the terminal end, the backward-difference formulas are

$$\left(\frac{dx}{dt}\right)_T = \frac{1}{h}\left[\underline{\Delta}x(T) + \frac{\underline{\Delta}^2x(T)}{2} + \frac{\underline{\Delta}^3x(T)}{3} + \frac{\underline{\Delta}^4x(T)}{4}\right] \quad (14)$$

$$\left(\frac{d^2x}{dt^2}\right)_T = \frac{1}{h^2}\left[\underline{\Delta}^2x(T) + \underline{\Delta}^3x(T) + \frac{11}{12}\underline{\Delta}^4x(T)\right] \quad (15)$$

where $\underline{\Delta}$, $\underline{\Delta}^2$, $\underline{\Delta}^3$, and $\underline{\Delta}^4$ denote first, second, third, and fourth backward differences, respectively, and are

$$\underline{\Delta}x(T) = x(T) - x(T - h) \quad (16)$$

$$\underline{\Delta}^2x(T) = x(T) - 2x(T - h) + x(T - 2h) \quad (17)$$

$$\underline{\Delta}^3x(T) = x(T) - 3x(T - h) + 3x(T - 2h) - x(T - 3h) \quad (18)$$

$$\underline{\Delta}^4x(T) = x(T) - 4x(T - h) + 6x(T - 2h) - 4x(T - 3h) + x(T - 4h) \quad (19)$$

The derivation of the higher order forward- and backward-difference formulas can also be found in reference 2. The derivatives given by Eqs. (8), (9), (14), and (15) are plotted in Fig. 1, together with their exact values at $t = 0.0$, 0.2, 2.8, and 3.0, again using five neighboring points as in the case of the central-difference formulas; the agreement appears satisfactory but not so good as that when the central difference formulas can be used.

The authors found that in employing this method for the case in which x-values at the various values of t were furnished correct to three decimal places, the root mean square errors in dx/dt and d^2x/dt^2 were 0.058 and 0.593, respectively, for the condition where forward and backward differences were used to calculate derivatives at points near the ends of the curve. In instances where inner points only were investigated, the accuracy was considerably improved; the root mean square errors in dx/dt and d^2x/dt^2 were found to be 0.055 and 0.037, respectively, for the condition where forward and backward differences were used to calculate derivatives at points near the ends of the curve. In instances where inner points only were investigated, the accuracy was considerably improved; the root mean square errors in dx/dt and d^2x/dt^2 were found to be 0.055 and 0.037, respectively.

REFERENCES

[1] Kauffman, W. M., and Shinbrot, M., *A Method for Differentiation of Experimental Data*, Journal of the Aeronautical Sciences, Vol. 20, No. 6 pp. 428–430, June, 1953.

[2] Wang, Chi-Teh, *Applied Elasticity*, pp. 124–125; McGraw-Hill Book Company, Inc., New York, 1953.

Note on Model Effective Span for Wind-Tunnel Wall Corrections

Alan Pope
Supervisor, Experimental Aerodynamics Division, Sandia Corporation, Albuquerque, N.M.

July 6, 1953

AN IMPORTANT PARAMETER in the determination of the wind-tunnel wall correction factor δ is the ratio of the model span to tunnel width. Accordingly, agreement on the proper span to use can result in correction uniformity and better correlation in the results of tests on a given wing model in several tunnels.

Difficulty arises in selecting the model span. It is well known that the trailing vortex sheet shed by a lifting wing rolls up into two trailing vortices whose span is somewhat less than the geometric span of the wing. The question is, hence, whether to use the geometric span, the vortex span, or some value in between when setting up the image system, which in turn determines δ.

Since the wing is to be replaced by a simple horseshoe vortex that simulates uniform loading, there appears little reason to assume the vortex span to be equal to the geometric wing span. Silverstein in reference 1 suggested reducing the geometric span

TABLE 1
Comparison of Wall Corrections, Eq. (1) and Other Sources

Source	Aspect Ratio	Taper Ratio	Plan Form	Tunnel	$\Delta\alpha$	$\Delta\alpha$, Eq. (1)
RM A52L04	2	0	Delta	6 × 6	$0.55C_L$	$0.554C_L$
RM A52L02	2	1	Rect.	6 × 6	$0.55C_L$	$0.55C_L$
	2	0.333	Swept	6 × 6	$0.55C_L$	$0.55C_L$
	2	0	Delta	6 × 6	$0.93C_L$	$0.92C_L$
RM A52L15a	3.1	0.388	Rect.	6 × 6	$0.57C_L$	$0.555C_L$
	3.0	0	Delta	6 × 6	$0.55C_L$	$0.55C_L$
	3.0	0.40	Swept	6 × 6	$0.55C_L$	$0.555C_L$
L-603	5.87	0.66	Rect.	7 × 10	$1.02C_L$	$1.04C_L$
					b_e/b_g	b_e/b_g [Eq. (1)]
TR 770	...	1.0	...	7 × 20	0.93	0.94
	...	0.5	...	7 × 20	0.88	0.89
	...	0.25	...	7 × 20	0.83	0.86

by a factor of 0.85 for rectangular wings and 0.8 for tapered wings. This essentially suggests using the vortex span instead of the geometric span. However, Swanson and Toll in reference 2 suggest values somewhat larger than those of reference 1. In order to provide a simple but rational approach to the problem, the writer suggests assuming that, inasmuch as the complete roll-up occurs somewhat downstream of the model station, a reasonable compromise would be to select a value midway between the geometric and vortex span—that is, the span that should be used for computing the model span-tunnel width ratio should be calculated from

$$b_e = (b_g + b_v)/2 \qquad (1)$$

where

b_e = effective span
b_g = geometric span
b_v = vortex span

Eq. (1) at least has the advantage of making an allowance for the widely different vortex spans experienced for a wide range of aspect and taper ratios. Still further, numerical checks of the wall corrections actually used in many tests reported by the NACA and others indicates that Eq. (1) is closely in line with constants used. (See Table 1.)

Fig. 1 has been provided both to yield vortex spans for a wide range of plan forms and to illustrate the wide variation possible for the useful range of aspect and taper ratios. Use of Fig. 1 (which was calculated by the method of reference 3 and is reproduced from reference 4) and Eq. (1) for all wing tests will result in corrections that are both uniform and reasonable. Since this effective span is used for all the horseshoe vortices in the image system, it is equally applicable to corrections for wall effect aft of the wing. It also appears satisfactory for swept models.

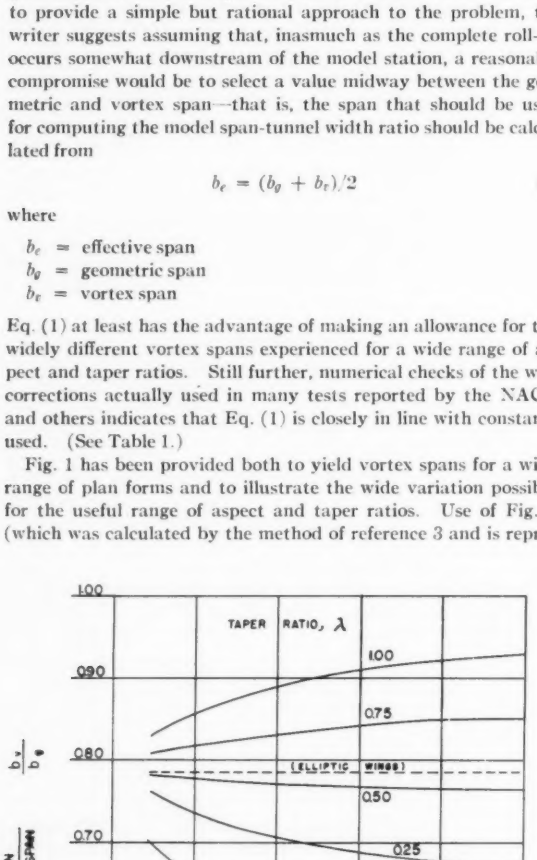

FIG. 1 EFFECT OF TAPER AND ASPECT RATIO ON THE VORTEX SPAN. (ELLIPTIC WINGS SHOWN DOTTED)

REFERENCES

[1] Silverstein, Abe, and White, James A., *Wind Tunnel Interference with Particular Reference to Off-Center Positions of the Wing and to the Downwash at the Tail*, TR 547, 1935.

[2] Swanson, Robert S., and Toll, Thomas A., *Jet Boundary Corrections for Reflection Plane Models in Rectangular Wind Tunnels*, TR 770, 1943.

[3] Glauert, H., *The Elements of Aerofoil and Airscrew Theory*, p. 167; Cambridge University Press, New York, 1926.

[4] Pope, Alan, *Basic Wing and Airfoil Theory*, p. 229; McGraw-Hill Book Company, Inc., New York, 1951.

Hypersonic Viscous Flow over an Inclined Wedge†

Lester Lees
Associate Professor of Aeronautics and Applied Mechanics, California Institute of Technology, Pasadena, Calif.
July 29, 1953

IN A RECENT NOTE,[1] Dr. Shih-I. Pai attempts to extend previous work on hypersonic viscous flow over a flat plate[2, 3] to the more general case of an inclined wedge. Unfortunately, his results for the compression side of the wedge at large angle of attack are incorrect. The present note tries to clarify the situation and to define the regions of "strong" and "weak" interaction for this problem.

Without going into detail, it turns out that the tangent-wedge approximation gives a good representation of the relation between pressure p^* and flow deflection angle θ along the surface of a body with an attached leading-edge shock in hypersonic, rotational, planar flow.[4] Therefore, in the viscous flow problem, p^* and θ at the outer edge of the viscous layer are connected by the usual oblique shock relations, where $\theta = \theta_B + (d\delta/dx^*)$. Here, $d\delta/dx^*$ is the "induced" flow deflection and θ_B is the slope of the body surface, equal to $\theta_W \pm \alpha$ for a wedge, where θ_W is the wedge half angle and α is angle of attack. In considering the compression side of a wedge at large angle of attack Pai[1] relates p^* to the corresponding shock angle θ_S, and represents θ_S as the sum of θ_0, the shock angle without induced effects, and θ_1, the viscous effect. In this problem the quadratic term involving $\theta_1^2 \cos^2 \theta_0$ is small in comparison with the other two terms in the

† This work was supported partly by the USAF Air Research and Development Command, under Contract AF-33(038)-250 (Princeton University) and partly by the Air Force and Army Ordnance under Contract DA-04-495-Ord-19 (GALCIT).

expression for $p^*/p_\infty{}^* = p$, or $\theta_1{}^2 \cos^2\theta_0 \ll \sin^2\theta_0$ [Eq. (19), reference 1]. But this condition rules out the possibility that the linear term involving $\theta_1 \sin 2\theta_0$ could ever be large compared with the inviscid term. In other words, the pressure can never be proportional to θ_1, or to $d\delta/dx^*$, and therefore the "similarity" condition for the velocity profiles and the associated relation $\delta \sim x^{*3/5}$ found by Pai do not, in fact, exist.

Actually, the hypersonic viscous flow on the compression side of a wedge at large angle of attack is a more general case of the weak interaction on a flat plate at $\alpha = 0°$ treated by Probstein and the present writer[5] and by Maslen.[6] Here it is not the pressure but the pressure perturbation, which is proportional to $d\delta/dx^*$. Although the flight Mach Number is high, the inviscid flow Mach Number is reduced considerably across the leading-edge shock, and the interaction effects are much smaller than for the flat plate at the same local Reynolds Number and Mach Number ahead of the body. Except possibly very near the leading edge (see below), $d\delta/dx^* < \theta_B$, and

$$\frac{p^*}{p_B{}^*} = 1 + \left(\frac{1}{p}\frac{dp}{d\theta}\right)_{\theta=\theta_B}\frac{d\delta}{dx^*} + \cdots$$

where the quantity $[(1/p)(dp/d\theta)]_{\theta=\theta_B}$ is obtained from the oblique shock relations, and $d\delta/dx^*$ is given by the usual boundary-layer solution for zero pressure gradient, or

$$\frac{d\delta}{dx^*} = d_B\sqrt{C_B}M_B{}^2/\sqrt{Re_{xB}}$$

The quantity d_B is a function of the gas properties, surface temperature, and Mach Number; C_B is the constant in the linear viscosity-temperature temperature relation; and M_B, Re_{xB} are Mach Number and Reynolds Number, respectively, based on inviscid flow quantites at the outer edge of the boundary layer "far" from the leading edge. In particular, if

$$M_\infty\theta_B = M_\infty(\theta_W + \alpha) > 2$$

(approx.) then

$$p^*/p_B{}^* = 1 + 2d_B(\chi_B/K_B) + \cdots,$$

where

$$\chi_B = \sqrt{C_B}\,(M_B{}^3/\sqrt{Re_{xB}})$$
$$K_B = M_B\theta_B$$

In this case solutions of the Prandtl boundary-layer equations are obtained in the form of asymptotic series in ascending powers of χ_B for any arbitrary thermal conditions at the wedge surface. In order to compare this result with the flat-plate case, we recognize that the viscosity ratio

$$\mu_B/\mu_\infty{}^* \to M_\infty{}^2\theta_B{}^2$$

if a linear viscosity-temperature relation is employed, and also $M_B\theta_B \to$ const., so that

$$\frac{\chi_B}{K_B} \to \frac{\bar{\chi}}{K^2} \text{ and } \frac{\Delta p^*}{p_B{}^*} \to 2\frac{d_B}{K^2}\bar{\chi}$$

where $\bar{\chi} = \sqrt{C}\,M_\infty{}^3/\sqrt{Re_x}$ and $K = M_\infty\theta_B$. As indicated by the factor $2/K^2$, the interaction effects are reduced considerably, and the solutions can be pushed to much lower local Reynolds Numbers than for the flat plate at zero angle of attack at the same flight Mach Number.†

For thin wedges at not too high angles of attack, when the Mach Number is sufficiently high ($M_\infty > 15$) and the local Reynolds Number is sufficiently low ($Re_x < 10^6$), then $d\delta/dx^* > \theta_B$ and $M_\infty\theta > 2$ simultaneously, and we are dealing with the opposite extreme case of "strong" interaction treated in references 2, 3, and 7. Except for the special case of the flat plate at $\alpha = 0°$ the geometric flow inclination θ_B cannot be completely neglected in comparison with $d\delta/dx^*$, as in the first approximation to the strong interaction region. For the more general case of the inclined wedge the generating parameter is suggested by considering the p^*-θ relation for $M_\infty\theta > 2$,

$$p = \frac{\gamma}{2}(\gamma+1)M_\infty{}^2\left(\frac{d\delta}{dx^*}\right)^2\left(1+\frac{\theta_B}{d\delta/dx^*}\right)^2 + \frac{3\gamma+1}{\gamma+1} - \frac{8\gamma}{(\gamma+1)^2}\frac{1}{M_\infty{}^2(d\delta/dx^*)^2}\frac{1}{\left(1+\dfrac{\theta_B}{d\delta/dx^*}\right)^2} + \cdots$$

But

$$\frac{\theta_B}{d\delta/dx^*} = \frac{M_\infty\theta_B}{M_\infty(d\delta/dx^*)} \approx \frac{K}{\sqrt{\bar{\chi}}}$$

where the flat-plate solution[3]

$$\frac{\delta}{x} = \delta_0 C^{1/4}\frac{\sqrt{M_\infty}}{(Re_{x^*})^{1/4}}$$

is utilized to evaluate $d\delta/dx^*$ approximately. Therefore analytical solutions of the Prandtl boundary-layer equations for the strong interaction region on an inclined wedge are obtained as asymptotic series of the following form:‡

$$p = p_0\bar{\chi}\left[1 + \frac{p_1K}{\sqrt{\bar{\chi}}} + \frac{p_2 + p_3K^2}{\bar{\chi}} + \cdots\right]$$

$$\frac{u^*(x,y)}{u_\infty{}^*} = u_0(\sigma) + \frac{K}{\sqrt{\bar{\chi}}}u_1(\sigma) + \cdots, \text{ etc.}$$

where $\sigma \sim y^*/(x^*)^{3/4}$, and p_1, p_2, p_3 are constants. The function $u_0(\sigma)$ (and the corresponding T_0) is the flat plate solution given in reference 3, while $u_1(\sigma)$, $T_1(\sigma)$, etc., each satisfies a linear second-order ordinary differential equation with coefficients depending only on the previous terms in the expansion. For Prandtl Number of unity the local heat transfer coefficient (for example) is expressed as

$$C_H = C_{H_0}\sqrt{\frac{p^{(0)}}{2}}\left[1 + \frac{a_1K}{\sqrt{\bar{\chi}}} + \frac{a_2 + a_3K^2}{\bar{\chi}} + \cdots\right]$$

where C_{H_0} is the classical value given by $0.332\sqrt{C}/\sqrt{Re_{x^*}}$, and $p^{(0)} = p_0\bar{\chi}$.

So far as the expansion side of a wedge at large angle of attack is concerned, preliminary experimental results, obtained by Nagamatsu and coworkers in the GALCIT 5-in. hypersonic tunnel at $M = 5.8$, show that the pressure rise across the trailing-edge shock is communicated upstream and causes separation of the laminar boundary layer almost from the leading edge. Thus it is doubtful that the usual boundary-layer theory can be applied to this problem.

All of the above results deal with the "direct problem" for a body of simple geometry. At the suggestion of Dr. H. S. Tsien, Ting-Yi Li and the present writer recently solved the "inverse problem" of determining the airfoil shape required to produce a prescribed pressure distribution including hypersonic viscous effects. An iterative scheme based on the von Kármán-Pohlhausen method is employed and numerical computations are now in progress.

It must be emphasized that practically all of the current theoretical work on this problem is based on the idealization of a mathematically sharp leading edge. Since the leading-edge

† In general, the weak interaction region is characterized by the condition $\chi_B = 0(1)$, and so it exists also on thin wedges at small angles of attack when the local Reynolds Number is sufficiently high. In this case $M_\infty\theta \leqq 1$, and $d\delta/dx^*$ can be less than, equal to, or greater than θ_B. These questions and others are discussed in a comprehensive monograph on hypersonic viscous flow by R. F. Probstein and the present writer, now in preparation.

‡ Shen's results for the insulated wedge obtained by the von Kármán-Pohlhausen method can also be expressed in the form of asymptotic series in ascending powers of $1/\sqrt{\bar{\chi}}$ [Eqs. (29) and (30) of reference 7, transformed].

radius is always small but finite in real life, the above results are expected to be valid when the Reynolds Number per linear foot along the body surface is not too high. Otherwise, the hypersonic viscous effects are submerged in the inviscid flow effects associated with a finite leading-edge radius of curvature. At high Mach Numbers, these effects may be propagated far downstream of the leading edge. Theoretical and experimental studies are now required to settle this problem.

References

[1] Pai, Shih-I., *A Note on Hypersonic Viscous Flow over a Flat Plate*, Readers' Forum, Journal of the Aeronautical Sciences, Vol. 20, No. 7, pp. 502–504, July, 1953.

[2] Li, Ting-Yi, and Nagamatsu, H. T., *Shock Wave Effects on the Laminar Skin Friction of an Insulated Flat Plate at Hypersonic Speeds*, Journal of the Aeronautical Sciences, Vol. 20, No. 5, pp. 345–355, May, 1953.

[3] Lees, L., *On the Boundary-Layer Equations in Hypersonic Flow and Their Approximate Solutions*, Readers' Forum, Journal of the Aeronautical Sciences, Vol. 20, No. 2, pp. 143–145, February, 1953.

[4] Munk, M. M., and Prim, R. C., *Surface Pressure Gradient and Shock Front Curvature at the Edge of a Plane Ogive with Attached Shock Front*, Journal of the Aeronautical Sciences, Vol. 15, No. 11, pp. 691–695, November, 1948. (More extensive calculations recently carried out by Elliott and Probstein at Princeton.)

[5] Lees, L., and Probstein, R. F., *Hypersonic Viscous Flow over a Flat Plate*, Princeton University, Aeronautical Engineering Laboratory Report No. 195, April 20, 1952.

[6] Maslen, S. H., *Second Approximation to Laminar Compressible Boundary-Layer on a Flat Plate in Slip Flow*, NACA TN No. 2818, November, 1952.

[7] Shen, S. F., *An Estimate of Viscosity Effect on the Hypersonic Flow over an Insulated Wedge*, Journal of Mathematics and Physics (M.I.T.), Vol. 3, No. 3, pp. 192–205, October, 1952.

On Strong Interaction for the Hypersonic Boundary Layer on an Inclined Wedge

Shih-I Pai

Associate Research Professor, Institute for Fluid Dynamics and Applied Mathematics, University of Maryland, College Park, Md.

August 13, 1953

IN THE PRECEDING NOTE,[1] Dr. Lester Lees criticizes my analysis for hypersonic viscous flow on the compression side of a wedge at large angle of attack.[2] Unfortunately, his criticism is based on his misunderstanding of my analysis, which was only briefly mentioned in reference 2. In this note, I give a little more detail of my analysis in order to clarify such a misunderstanding and to show the relative region of application of my results and of those of Dr. Lees.

For the compression side, the pressure is given by Eq. (19) of reference 2. Since the quadratic terms of Eq. (19) of reference 2 are in general negligible and θ_1 is proportional to $d\delta/dx$, we have for the compression side the following expression of pressure:

$$p^* \frac{p_{+\infty}}{p_{-\infty}} = \frac{p}{p_{-\infty}} = \frac{p_{+\infty}}{p_{-\infty}} + \gamma M_{-\infty}^2 \sin 2\theta_0 \cdot \frac{d\delta}{dx} \qquad (1)$$

For such a pressure distribution, I have shown in reference 2 that there is no similar solution. Dr. Lees' analysis of reference 1, strictly speaking, holds only very far downstream. For a strong interaction region where the term $M_{-\infty}^2(d\delta/dx)$ is not negligibly small, we cannot use the method of Lees. Some other suitable method should be used. One of the simplest methods, which would bring out the essential feature of the problem, is that given by Dr. Shen in his original analysis of the problem,[3] in which for first approximation the fundamental equation is as follows:

$$\eta^2 p^* = (2/m_1)\xi \qquad (2)$$

where $\eta = \delta/L$, $\xi = x/L$, $L = (M_{+\infty}^2\mu_w)/(\rho_{+\infty}u_{+\infty})$, $p^* = p \div p_{+\infty}$, and m_1 is a constant. Eq. (2) is the same as that given by Shen in reference 3, but the characteristic length L for the non-dimensional quantities η and ξ is different from that given by Shen. Eq. (2) may be solved for any pressure distribution. For the compression side of a wedge at an angle of attack, the expression of Eq. (1) may be used to calculate p^*.

Substituting Eq. (1) into Eq. (2), we have

$$\eta^2[(d\eta/d\xi) + A] = B\xi \qquad (3)$$

where A and B are constants for a given problem.

Eq. (3) has a singularity at the origin. Near the origin we have

$$\eta \sim \xi^{3/2} \qquad (4)$$

A change of variable may now be made. Let

$$\zeta = \xi^{1/2} \qquad (5)$$

The solution of Eq. (3) may be written as follows:

$$\eta = \zeta^2 \sum_{n=0}^{\infty} a_n \zeta^n \qquad (6)$$

The coefficients may be determined by substituting Eq. (6) into Eq. (3). Further improvements may be obtained by the procedure outlined by Shen in reference 3. We will omit them here.

It is easy to show that all the examples of similar solutions which I gave in reference 2 are the corresponding leading terms of the series similar to Eq. (6) for the corresponding expressions of p^*. It shows the behavior of the singularity at the origin for the corresponding problems. That is why I mentioned briefly the similar solution for the compression side in reference 2. Mathematically speaking, these solutions belong in the same category. Unfortunately, Dr. Lees erroneously assumed that such a solution is applicable for the whole region of strong interaction. All of his criticisms are based on an assumption that I did not make! In fact I do not think that any of the leading terms are good enough to be used for the whole region of strong interaction, including the case of a flat plate at zero angle of attack for which Dr. Lees made such an assumption in his analysis.[4] According to my analysis [Eq. (11) of reference 2], the second term of the pressure is proportional to $M_{-\infty}(d\delta/dx)$, which is not negligibly small in that analysis. Further investigation of the effect of such a term should be made.

In conclusion, my analysis is correct, and it discusses the case of strong interaction, while Dr. Lees' results apply for the case of weak interaction. It is interesting to notice that Dr. Lees' impression of my analysis is the same as his impression of Dr. Shen's original analysis[3] of this problem in the earlier stage of the investigation. Since the investigation of hypersonic viscous flow is still in a relatively early stage, I think that as time goes on all of the misunderstanding will be cleared up.

References

[1] Lees, Lester, *Hypersonic Viscous Flow over an Inclined Wedge*, see page 794 of this issue of the JOURNAL.

[2] Pai, Shih-I, *A Note on Hypersonic Viscous Flow over a Flat Plate*, Readers' Forum, Journal of the Aeronautical Sciences, Vol. 20, No. 7, pp. 502–503, July, 1953.

[3] Shen, S. F., *An Estimate of Viscosity Effect on the Hypersonic Flow over an Insulated Wedge*, Jour. of Math. and Physics, Vol. 31, No. 3, pp. 192–205, October, 1952 (also M.I.T. Thesis, 1949).

[4] Lees, Lester, *On the Boundary Layer Equations in Hypersonic Flow and Their Approximate Solutions*, Readers' Forum, Journal of the Aeronautical Sciences, Vol. 20, No. 2, pp. 143–145, February, 1953.

Effect of a Turbojet Engine on the Dynamic Stability of an Aircraft

Hans C. Vetter
El Segundo Division, Douglas Aircraft Company, Inc., El Segundo, Calif.

July 6, 1953

SUMMARY

It has been frequently noted that the calculated lateral damping of a turbojet-powered airplane is not always in complete agreement with flight tests. This paper gives a summary of three major effects of a turbojet engine on the dynamic stability of an aircraft. These three effects are: (a) thrust component in the direction of wing lift; (b) "Coriolis" reaction of air and exhaust gases in jet duct; and (c) coupling of lateral and longitudinal modes due to gyroscopic action of the turbine and compressor. All these are essentially low-speed effects.

(I) NOTATION

x, y, z	=	Cartesian coordinates
ϕ, θ, ψ	=	disturbances and angle of roll, pitch, and yaw
α, β	=	disturbances in angle of attack and sideslip
γ	=	flight-path angle
α_{CL}	=	angle between jet duct centerline and rolling axis
α_T	=	angle between gross thrust line and rolling axis ($\alpha_T = \alpha_{CL}$ if tailpipe is undeflected)
q	=	free-stream dynamic pressure
S	=	wing area
b	=	wing span
l_w	=	mean aerodynamic chord of wing
I	=	moment of inertia tensor
J	=	polar moment of inertia of turbine and compressor
W	=	weight of airplane
V	=	true air speed
C_L	=	lift coefficient
C_D	=	drag coefficient
C_l	=	rolling moment coefficient
C_m	=	pitching moment coefficient
C_n	=	yawing moment coefficient
C_R	=	ram drag coefficient (ram drag = $C_R q S$)
C_T	=	gross thrust coefficient (gross thrust = $C_T q S$)
v	=	velocity of air in jet duct
ω	=	engine r.p.m.
$\vec{R}$	=	$xi + yj + zk$ = position vector
$\vec{\Omega}$	=	$\phi i + \theta j + \psi k$ = angular velocity vector
$\vec{G}$	=	moment vector
$\vec{H}$	=	angular momentum vector
i, j, k	=	unit vectors
ρ	=	density of air
A	=	cross-sectional area of jet duct
ζ	=	distance measure (along jet duct axis)
Δ_T	=	increment due to thrust
$u( )$	=	unit step function

Subscripts

p	=	partial differentiation with respect to $b\dot{\phi}/2V$
q	=	partial differentiation with respect to $l_w\dot{\theta}/2V$
r	=	partial differentiation with respect to $b\dot{\psi}/2V$
1	=	static, trimmed condition

The airplane axes used throughout are the conventional NACA stability axes.

(II) POWER-ON LIFT

THIS EFFECT HAS, in the past, been generally passed off as insignificant. This is not so for aircraft with no flaps and relatively small lift-curve slopes. This effect amounts to a correction of the trimmed lift coefficient calculated from

$$C_{L_1} = (W \cos \gamma_1)/q_1 S \tag{1}$$

By considering the thrust in the force geometry of the airplane (see Fig. 1), we get

$$\left.\begin{aligned} \frac{W \cos \gamma_1}{q_1 S} &= C_{L_1} + C_{T_1} \sin \alpha_T \\ \frac{W \sin \gamma_1}{q_1 S} &= C_{T_1} \cos \alpha_T - C_{R_1} - C_{D_1} \end{aligned}\right\} \tag{2}$$

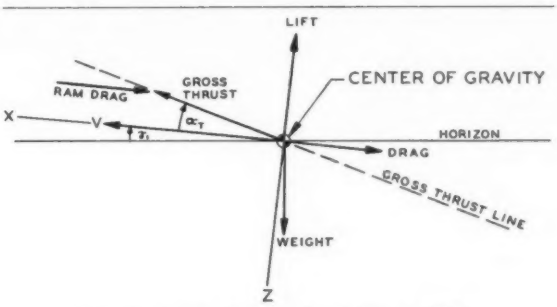

FIG. 1. Force diagram for trimmed flight.

A solution of Eq. (2) for α_T for a power-approach condition can show as much as a 2° discrepancy with the value of α_T calculated from Eq. (1). This means a change in the flight-path inertias and in the stability derivatives.

(III) "CORIOLIS" DAMPING

Those who have recognized the presence of this effect have probably ignored it and, in most cases, rightfully so. This effect can be significant only in airplanes with poor damping in yaw when flying at low indicated airspeeds.

"Coriolis" damping occurs because the air in the jet duct is traveling in a radial path with respect to the center of gravity of the airplane when the airplane is performing rotational oscillations. By using the coordinate system of Fig. 2 and the formulas

$$\text{"Coriolis" moment} = -2 \int_{\zeta=-h}^{\zeta=d} \vec{R} \times (\vec{\Omega} \times \dot{\vec{R}}) \rho A \, d\zeta \tag{3}$$

$$\text{"Coriolis" force} = -2 \int_{\zeta=-h}^{\zeta=d} (\vec{\Omega} \times \dot{\vec{R}}) \rho A \, d\zeta \tag{4}$$

$$\rho(\zeta)\, A(\zeta)\, v(\zeta) = (\text{rate of airflow}) \times [1 + \tau u(\zeta + l)] \tag{5}$$

we get

$$\left.\begin{aligned} \Delta_T C_{l_p} &= -2C_R \frac{\Lambda^2}{b^2} \sin^2 \alpha_{CL} + 2C_R \frac{\lambda^2}{b^2} \sin 2\alpha_{CL} \\ \Delta_T C_{l_r} &= -C_R \frac{\Lambda^2}{b^2} \sin 2\alpha_{CL} + 4C_R \frac{\lambda^2}{b^2} \cos^2 \alpha_{CL} \\ \Delta_T C_{n_p} &= -C_R \frac{\Lambda^2}{b^2} \sin 2\alpha_{CL} - 4C_R \frac{\lambda^2}{b^2} \sin^2 \alpha_{CL} \\ \Delta_T C_{n_r} &= -2C_R \frac{\Lambda^2}{b^2} \cos^2 \alpha_{CL} - 2C_R \frac{\lambda^2}{b^2} \sin 2\alpha_{CL} \\ \Delta_T C_{y_p} &= 4C_R(\lambda^2/ab) \sin \alpha_{CL} \\ \Delta_T C_{y_r} &= 4C_R(\lambda^2/ab) \cos \alpha_{CL} \\ \Delta_T C_{m_q} &= -2C_R(\Lambda^2/l_w^2) \\ \Delta_T C_{L_q} &= 4C_R(\lambda^2/al_w) \cos \alpha_{CL} \\ \Delta_T C_{D_q} &= 4C_R(\lambda^2/al_w) \sin \alpha_{CL} \end{aligned}\right\} \tag{6}$$

where

$$\begin{aligned} \Lambda^2 &= (h^2 - d^2) + \tau(h^2 - l^2) \\ \lambda^2 &= a[(h + d) + \tau(h - l)] \\ \tau &= \frac{\text{rate of fuel flow (lbs. per sec.)}}{\text{rate of airflow (lbs. per sec.)}} \end{aligned}$$

The most important one of these is $\Delta_T C_{n_r}$. $\Delta_T C_{n_r}$ has been known to amount to as much as 12 per cent of the aerodynamic value of C_{n_r} at high lift coefficients.

(IV) GYRO-COUPLING

This is another effect, such as the first mentioned, which has in all probability been recognized but passed off as insignificant.

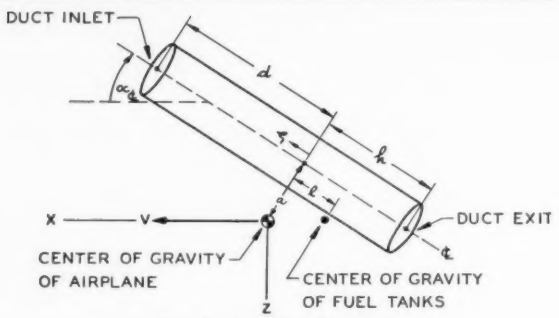

FIG. 2. Jet duct geometry.

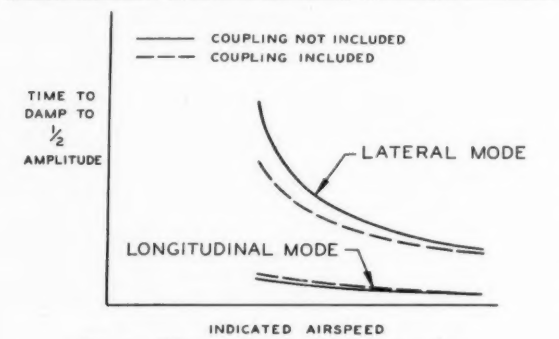

FIG. 3. Effect of gyro-coupling on damping.

However, with the trend toward larger and heavier jet engines, this effect is making itself felt more and more, especially in lighter type aircraft.

In order to include the gyroscopic terms in the equations of motion, we return to the basic equations of dynamics—namely,

$$\left.\begin{aligned} \vec{DH}/Dt &= \dot{\vec{H}} + \vec{\Omega} \times \vec{H} = \vec{G} \\ \vec{H} &= I\vec{\Omega} + J\vec{\omega} \end{aligned}\right\} \tag{7}$$

$$\left.\begin{aligned} H_x &= I_{xx}\dot{\phi} - I_{xz}\dot{\psi} + J\omega \cos \alpha_{CL} \\ H_y &= I_{yy}\dot{\theta} \\ H_z &= I_{zz}\dot{\psi} - I_{xz}\dot{\phi} - J\omega \sin \alpha_{CL} \\ & (I_{xy} = I_{yz} = 0) \end{aligned}\right\} \tag{8}$$

By substituting Eqs. (8) into Eqs. (7) and neglecting all products of angular rates (perturbation method), we get

$$\left.\begin{aligned} G_x &= I_{xx}\ddot{\phi} - I_{xz}\ddot{\psi} - J\omega \sin \alpha_{CL}\dot{\theta} = C_l qSb \\ G_y &= I_{yy}\ddot{\theta} + J\omega \cos \alpha_{CL}\dot{\psi} + J\omega \sin \alpha_{CL}\dot{\phi} = C_m qS\bar{l}_w \\ G_z &= I_{zz}\ddot{\psi} - I_{xz}\ddot{\phi} - J\omega \cos \alpha_{CL}\dot{\theta} = C_n qSb \end{aligned}\right\} \tag{9}$$

If we consider the quantity $J\omega \cos \alpha_{CL}$, which appears in the yawing equation of motion, as a yawing moment per unit pitch rate—i.e., C_{n_q}—then the value of C_{n_q} for one of the modern jet airplanes at low indicated air speeds is twice as large as C_{n_r}. This is a definite indication of a sizeable coupling between the lateral and longitudinal modes of motion. This coupling, when included in the equations of motion, leads to the following general results: (a) an increase in the calculated lateral damping at low indicated air speeds; (b) a small decrease in the calculated longitudinal damping; (c) an insignificant change in the frequency of both modes; (d) small excitation of either mode when the other is disturbed—small enough, in fact, that a pilot seldom if ever notices it; (e) a small difference in the first few seconds of a calculated rolling time history. Fig. 3 shows the relative effects of coupling on the calculated damping for a modern jet airplane.

Note on Nonstationary Slender-Body Theory

J. D. Cole
Guggenheim Aeronautical Laboratory, California Institute of Technology, Pasadena, Calif.
July 14, 1953

A BODY OF REVOLUTION performing arbitrary motion along its axis can be represented within linearized (acoustic) theory by a distribution of sources that vary in time along the axis of flight. It has been shown by Frankl[1] that for very slender bodies the instantaneous source strength is equal to the velocity times the rate of change of cross-sectional area along the body. In this note an asymptotic expansion of the potential near the axis is given, and the results for a special case are presented.

The potential is represented by an integral of the retarded values of the source strength $S(x, t)$,

$$\Phi(x, r, t) = -\frac{1}{4\pi}\int_{-\infty}^{\infty} \frac{S\left(\tau, t - \frac{\sqrt{(x-\xi)^2 + r^2}}{c}\right) d\xi}{\sqrt{(x-\xi)^2 + r^2}} \tag{1}$$

in coordinates where the air is at rest at infinity (reference 2, p. 524). The source strength is zero outside the body so that the integral in Eq. (1) is carried out over only those values of ξ which are common to the flight path and the surface of the upstream Mach cone

$$\tau = t - [\sqrt{(x-\xi)^2 + r^2}/c]$$

as shown in Fig. 1. There are integrals for the recent past x_1 to x_2 and the distant past x_3 to x_4, etc.

The integral for the recent past can be analyzed for small r by splitting it into

$$\int_{x_1}^{x-\epsilon(r)}, \qquad \int_{x-\epsilon(r)}^{x+\epsilon(r)}, \qquad \int_{x+\epsilon(r)}^{x_2}$$

since most of the contribution near the body comes from $\xi = x$. For the middle integral, S can be approximated by its value at $(\xi = x, r = 0)$; for the others, expansions of S and the square root can be made in powers of r. The integrals for the distant past can easily be approximated by putting $r = 0$, so that they represent waves that are plane at the body. This procedure results in an asymptotic formula valid near the body for small r,

$$\begin{aligned} \Phi(x, r, t) = {} & \frac{1}{2\pi} S(x, t) \log \frac{r}{2} - \frac{1}{4\pi}\left[S\left(x_1, t - \frac{x - x_1}{c}\right) \times \right. \\ & \left. \log (x - x_1) + S\left(x_2, t - \frac{x_2 - x}{c}\right) \log (x_2 - x) \right] - \\ & \frac{1}{4\pi}\int_{x_1}^{x_2} \left[\frac{1}{c} S_t\left(\xi, t - \frac{|x-\xi|}{c}\right) + \operatorname{sign}(x - \xi) \times \right. \\ & \left. S_x\left(\xi, t - \frac{|x-\xi|}{c}\right) \right] \log|x - \xi| d\xi - \\ & \frac{1}{4\pi}\int_{x_3}^{x_4} \frac{S\left(\xi, t - \frac{|x-\xi|}{c}\right)}{|x-\xi|} d\xi, \text{ etc., } + O(\epsilon \log \epsilon) \end{aligned} \tag{2}$$

where $x_1(x, t)$ and $x_2(x, t)$ are the values of ξ in the recent past at which $\tau = t \mp [(x - \xi)/c]$, respectively, intersects the boundaries of the flight path (Fig. 1); x_3 and x_4 are similar values in the distant past; and $\epsilon = \epsilon(r)$ such that $\sqrt{r} > \epsilon > r$ as $r \to 0$.

It follows from Eq. (2) and the boundary condition $\Phi_r = U \times$ slope that

$$S(x, t) = U(t) \frac{\partial A}{\partial x}(x, t) = U(t) A'\left[x + \int_0^t U(\tau) d\tau\right] \tag{3}$$

where

$U(t)$ = velocity of body in negative x-direction
$A(x)$ = cross-sectional area distribution of body at $t = 0$

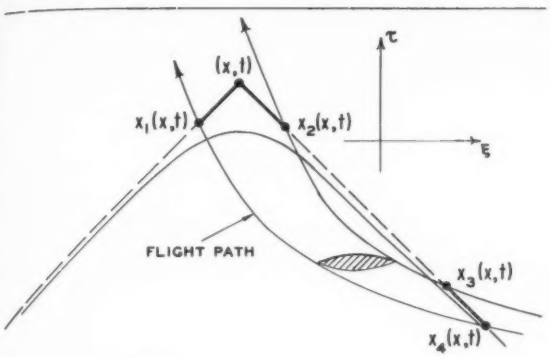

Fig. 1.
SPACE - TIME DIAGRAM

Just as Eq. (1) includes the source distribution for steady subsonic or supersonic flow as special cases, given by a translation of axes, Eq. (2) includes the usual steady slender-body results (for example, Eqs. (10) and (21) in reference 3).

As a simple application of Eq. (2), consider a cone decelerating uniformly from supersonic to sonic velocity. Taking the equation of the leading edge as $\xi = -c\tau + b\tau^2$, we have $U(t) = c - 2bt$; the velocity is sonic at $t = 0$. $A(x) = \pi\delta^2x^2$, where δ = semiangle of cone.

For $\sqrt{b} \times$ body length$/c << 1$, an approximation is easily found

$$S(x, t) \doteq 2\pi\delta^2 c(x + ct)$$
$$x_1(x, t) \doteq (1/2)(x - ct)$$
$$x_2(x, t) = c\sqrt{(x + ct)/b} + x + ct$$

At sonic velocity the nose is at $x = 0$, and the pressure coefficient including square terms is

$$C_p = 2\delta^2 \log [\sqrt{2c}/\delta(bx)^{1/4}] - (\delta^2) \qquad (4)$$

The logarithmic singularity as the deceleration $b \to 0$ corresponds to the growth of pressure proportional to log time, a result of linearized theory at $M = 1$. For any $b \neq 0$ linearized theory gives a finite resistance at $M = 1$.

REFERENCES

[1] Frankl, F. I., *Effect of the Acceleration of Elongated Bodies of Revolution upon the Resistance in Compressible Flow*, NACA TM No. 1230, 1949. (Translation from the Russian paper in Prikl. Mat. i. Mekh., Vol. 10, No. 4, 1946.)

[2] Lamb, *Hydrodynamics;* Dover Press, 1945.

[3] Sears, W., and Adams, M., *Slender-Body Theory—Review and Extension*, Journal of the Aeronautical Sciences, Vol. 20, No. 2, pp. 85–98, February, 1953.

Remarks on "Shock-Wave Effects on the Laminar Skin Friction of an Insulated Flat Plate at Hypersonic Speeds"[1]

M. Z. v. Krzywoblocki
Professor of Gasdynamics and Theoretical Aerodynamics, University of Illinois, Urbana, Ill.

July 2, 1953

EACH PROBLEM IN ENGINEERING IN PARTICULAR, and in mathematical physics in general, may and can be reduced to the fundamental problems in these two fields: mathematics and theoretical physics. As the writer has shown,[2] the problem of the boundary layer reduces to the two fundamental problems: in mathematics (existence and, possibly, uniqueness theorem) and in theoretical physics (the proper equations describing adequately the physical phenomenon in question). There is not much advantage in going into details such as the interaction between a shock and the boundary layer without first solving the fundamentals. The problem of interaction will technically introduce only some changes in the boundary conditions, since, from the mathematical standpoint, in a boundary value problem with a fixed differential system (partial or ordinary), the only changes that can occur are in the boundary conditions. If these boundary conditions are consistent with the boundary value problem in this or in that case, mathematically there will be no changes and the question reduces to some formal calculations.

If they are inconsistent then a completely new boundary value problem must be attacked and solved. It is also known that, at the present status of knowledge in mathematics, one may be able to prove some existence theorems but not that of uniqueness with respect to the particular differential system and boundary value problem in the paper in question. Hence, the speculations of the authors on the uniqueness of the solutions (page 353)[1] simply cannot be seriously accepted. Turning to the fundamental problem in theoretical physics; any statement that we can accept the Navier-Stokes equations as the universal system able to solve all of our problems of the boundary layer from zero altitude up to an arbitrary distance above the earth simply leads to an absurdum. The solution of the problem of validity of various forms of equations of motion and energy on various levels in various intensities of density of a gas is the most urgent problem of today. The kinetic theory of gases of a monatomic gas, even with all its deficiencies, applied to rarefied air may give errors of a smaller order than the Navier-Stokes equations of continuum mechanics applied to that range of rarefied gases. Of course, all such statements must be accepted cautiously, up to the moment when more data are available. Even now some results from the theory of shocks seem to indicate that such statements are true.

The authors[1] presented some considerations on hypersonic flow without going into the fundamentals. Hence some remarks seem to be in order. The fundamental equations are the Navier-Stokes equations. Hence, logically, the results are valid only in the domain where these equations are valid. Some cases may be discussed: (a) Certainly they are valid in the range of high density gases, but in this range there is no sense in talking about Mach Numbers of the order of 15, say. (b) Since the possibility of reaching such high Mach Numbers is in the range of rarefied gases, there may be a level at which the Navier-Stokes equations are approximately valid; but to show that, one has to show that any other system of equations, based on the kinetic theory of gases, say, containing higher order terms, gives an error greater than that of the Navier-Stokes equations. (c) There may be an altitude at which the equations based upon the kinetic theory of gases of a monatomic gas will give less error due to higher order terms than Navier-Stokes equations; in this case one has to use the kinetic theory of gases as the fundamental concept. (d) There may be the region in which the kinetic theory of polyatomic gases must be used. As is seen, to understand the results derived by the authors, a thorough discussion, perhaps beyond present possibilities due to the lack of sufficient data and information, must be presented. This is completely lacking. Of course, the higher order terms due to the kinetic theory of gases, if taken into account, may significantly change the numerical results of the authors. Another question is the thickness of the shock wave. In their discussion the authors use the calculations by A. E. Puckett and H. J. Stewart based upon the Navier-Stokes equations. But it is well known that the equations of continuum mechanics are not adequate enough to supply information on the thickness of a shock wave. The only results comparable with tests were obtained by means of the kinetic theory of gases.[3]

Since, moreover, the thickness of a shock wave increases considerably in the range of hypersonics, it seems that again this

problem was presented superficially in the paper in question. One has to understand deeply that the problem of the boundary layer in hypersonics cannot be solved merely by a simple extension of Prandtl's 50-year-old boundary-layer notion. A thorough construction of new fundamentals must be accomplished, and from this standpoint the address given by Professor Hirschfelder during the Third Midwestern Conference on Fluid Mechanics in Minneapolis was of great significance.

REFERENCES

[1] Li, T. Y., and Nagamatsu, H. T., *Shock-Wave Effects on the Laminar Skin Friction of an Insulated Flat Plate at Hypersonic Speeds*, Journal of the Aeronautical Sciences, Vol. 20, No. 5, pp. 345-355, May, 1953.

[2] Krzywoblocki, M. Z. v., *On the Fundamentals of the Boundary Layer Theory*, J. Franklin Institute, Vol. 255, No. 4, pp. 289-299, 1953.

[3] Mott-Smith, H. M., *The Solution of the Boltzmann Equation for a Shock Wave*, Phys. Rev., Vol. 82, pp. 885-892, 1951.

Similarity Theory of Isotropic Turbulence

(*Concluded from page 778*)

REFERENCES

[1] von Kármán, Th., and Howarth, L., *On the Statistical Theory of Isotropic Turbulence*, Proc. Roy. Soc., Vol. A 164, p. 192, 1938.

[2] Rotta, J., *Das Spektrum isotroper Turbulenz im statistischen Gleichgewicht*, Ing.-Arch., Vol. 18, p. 60, 1950.

[3] Batchelor, G. K., *The Role of Big Eddies in Homogeneous Turbulence*, Proc. Roy. Soc., Vol. A 195, p. 513, 1949.

[4] Rotta, J., *Neue Rechnungen zur statistischen isotropen Turbulenz*, ZAMM, Vol. 29, p. 12, 1949.

[5] Heisenberg, W., *Zur statistischen Theorie der Turbulenz*, Z. Physik, Vol. 124, p. 628, 1948.

[6] Heisenberg, W., *On the Theory of Statistical and Isotropic Turbulence*, Proc. Roy. Soc., Vol. A 195, p. 402, 1948.

[7] Batchelor, G. K., and Townsend, A. A., *Decay of Turbulence in the Final Period*, Proc. Roy. Soc., Vol. A 194, p. 524, 1948.

[8] Kolmogoroff, K. N., *On Degeneration of Isotropic Turbulence in an Incompressible Viscous Liquid*, C. R. Acad. Sci., U.R.S.S., Vol. 31, p. 538, 1941.

[9] Batchelor, G. K., and Townsend, A. A., *Decay of Isotropic Turbulence in the Initial Period*, Proc. Roy. Soc., Vol. A 193, p. 539, 1948.

[10] Baines, W. D., and Peterson, E. G., *An Investigation of Flow through Screens*, Trans. A.S.M.E., Vol. 73, p. 467, 1951.

[11] Frenkiel, F. N., *The Decay of Isotropic Turbulence*, Journ. Appl. Mech., Vol. 15, p. 311, 1948.

[12] Simmons, L. F. G., and Salter, C., *An Experimental Determination of the Spectrum of Turbulence*, Proc. Roy. Soc., Vol. A 165, p. 73, 1938.

[13] Liepmann, H. W., Laufer, J., and Liepmann, K., *On the Spectrum of Isotropic Turbulence*, NACA TN No. 2473, 1951.

[14] Goldstein, S., *On the Law of Decay of Homogeneous Isotropic Turbulence and the Theories of Equilibrium and Similarity Spectra*, Proc. Camb. Phil. Soc., Vol. 47, p. 554, 1951.

[15] Kovasznay, L. S. G., *Spectrum of Locally Isotropic Turbulence*, Journal of the Aeronautical Sciences, Vol. 15, No. 12, p. 745, December, 1948.

Ludwig Prandtl, 1875–1953

(*Concluded from page 779*)

Of his other major contributions, we have space only to mention his mixing length theory of turbulence, his work on heat transfer in moving fluids, his pioneer wind-tunnel designs, the Prandtl soap-film analogy for the study of torsional deflections and stresses in prismatic bodies, and his papers on creep and flow, on the theory of failure, and on the penetration of rigid bodies in a plastic medium.

Those who had the privilege of friendship with Prandtl knew him as a modest, friendly, unassuming man, far from one's preconceived notion of a great leader of men. It is said that his lectures were not suitable for beginners and that he was always surprised that others did not see the relationships so clearly as he. He taught by association and example. He gave much credit to his coworkers and deprecated his own contributions to aeronautical practice. His work will live long not only in the impress of his concepts on aeronautical practice but in the ever widening influence of the scientists and engineers who have felt the challenge of his personality and work.

HUGH L. DRYDEN
Director, NACA